

IMPURITY PROFILING AND DEGRADATION STUDY OF PIDOTIMOD

3.1. SELECTION OF DRUG

At the end of 1990s, ARTIs (Acute respiratory tract infections) were called the ‘forgotten pandemic’, after the introduction of new and safe vaccines and antibiotics that has contributed to some extent in controlling the most life-threatening ARTIs. This definition still applies after 20 years due to less impact of these therapies in pediatric age group especially for treatment of viral ARTIs. To prevent and cure ARTIs in children several immune stimulants with different mode of action from natural and synthetic origins have been introduced, that act by strengthening the children’s innate defense mechanisms. One of these compound, Pidotimod (PDM), has attempted to prove its mechanisms of action both *in vitro* and *in vivo* (1) . It was developed by the Italian company, Poli Industria Chimica and marketed for clinical treatment in the year 1993. PDM was the first compound that comes under the class of biological response modifiers with a peptide-like structure that can stimulate both primary and acquired immune responses to bacteria and virus (2). Most of the studies related to PDM were published approximately 25 years ago but PDM is still used today to prevent ARTIs. Despite the availability of publications during approval of PDM, a gap exists in the literature concerning comprehensive pharmacological and analytical studies. Some recent findings on PDM investigated the new mechanisms of induction of primary and secondary immune responses (3-5). Also PDM underwent reappraisal (6) after several years and new synthetic route was published (7).

In spite of its remarkable use and efficacy in preventing ARTIs, there have been no reports on impurity profiling, stress degradation and structural characterization of the degradation products (DPs) of PDM up to our knowledge. Hence, the investigation was undertaken to study the impurity profiling and degradation study of the drug PDM under different stress conditions. Two major degradation products formed under acid degradation condition were isolated and its structures were proposed by IR, Mass and NMR spectra. Structure of other degradation products were proposed by LC-MS/MS study and mechanistic degradation pathways were outlined.

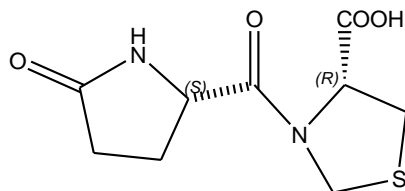
3.2 DRUG PROFILE

General Properties (8, 9):

IUPAC Name: (R)-3-[(S)-(5-oxo-2-pyrrolidiny)carbonyl]-thiazolidine-4-carboxylic acid.

Molecular Formula: C₉H₁₂N₂O₄S

Molecular Weight: 244.27



Chemical Structure:

Figure 3.1: Structure of Pidotimod

Appearance: White or slightly ivory, odorless microcrystalline powder

Melting point: 194-198°C

pKa: 3.03

Solubility: Freely soluble in water; methanol; ethanol; sparingly soluble in dimethylformamide and practically insoluble in chloroform and hexane.

Drug Category: Immuno-modulator

Mechanism of action: Pidotimod induces dendritic cell (DC) maturation, up-regulates the HLA-DR expression and CD83 and CD86, a co-stimulatory molecules and stimulates DCs to release pro-inflammatory molecules, drives T cell proliferation and differentiation towards a Th-1 phenotype, enhances the function of natural killer cells, promotes phagocytosis and inhibits thymocyte apoptosis (10-12). Also Pidotimod seemed to modulate airway epithelial cell functions that is involved in host-virus interactions, probably through NF-kB activation (13).

Uses: In prevention and treatment of ARTIs in children.

Marketed Formulation: Axil (Boehringer, Mann.)

Pigitil (Fidia)

Onaka (Max Pharma)

Polimod (Poli)

3.3 LITERATURE REVIEW

An extensive literature survey revealed that few analytical methods have been established and reported for the estimation and quantification of PDM, these include HPLC-UV (14), HPLC-MS (15), HPLC-MS/MS (16), HILIC-MS/MS (17). Bioequivalence evaluation of two formulations of PDM has been reported (18). There is one published report for the determination of residual organic solvents in PDM by GC (19). Synthesis and preliminary pharmacological evaluation of PDM, its enantiomer, diastereomers, carboxamido derivatives (20) and analytical and chemical profile of PDM has been described in the year 1994 (21) by Crimella T. They reported presence of two process related impurity and two other impurity besides process related impurity in industrial lot of PDM. Chiral separation of PDM and its enantiomers was reported on CHIRALPAK stationary phase (22). Recently study on thermodynamic parameters, crystal structure and molecular docking of PDM enantiomers was published (23).

3.4. SECTION –A

DEVELOPMENT AND VALIDATION OF QbD BASED STABILITY INDICATING HPLC METHOD

3.4.1 EXPERIMENTAL

3.4.1.1 Chemicals and Reagents

The PDM bulk drug was purchased from Swapnaroop drugs, Aurangabad, India. HPLC grade Methanol (MeOH) and Acetonitrile (ACN) were procured from Spectrochem Pvt. Ltd., Mumbai. Ammonium acetate was purchased from Loba Chemicals Pvt. Ltd. (Mumbai, India). Unless otherwise specified, all solutions were filtered through a 0.2 µm Nylon 6, 6 membrane filter, Ultipor[®] N66[®] from Pall Life Sciences, USA; prior to use. Analytical grade hydrochloric acid (HCl) and sodium hydroxide (NaOH) were procured from SD Fine chem. Ltd., Mumbai, India. Hydrogen peroxide (H₂O₂) was procured from Fischer Ltd., India.

3.4.1.2 Equipments and Chromatographic Conditions

Precision water/oil baths equipped with temperature controller were used for degradation studies for acidic, basic, neutral hydrolysis and oxidative degradation conditions.

Photolytic degradation study was carried out in a photo-stability chamber (Thermolab Scientific Equipments Pvt Ltd, Vadodara) equipped with a light bank consisting of four UV (OSRAM L73) and fluorescent (OSRAM L20) lamps, that complied with specifications prescribed in the ICH guideline Q1B. The system is capable of controlling specific temperature and humidity ($\pm 2^{\circ}\text{C}$ and $\pm 5\%$ RH). For thermal and humidity study; thermal-humidity chamber (S. R. Labs Instruments, Thane, Maharashtra) was used and set at accelerated condition of $40^{\circ}\text{C}/75\%$ RH.

Other equipments used were an ultrasonic bath (Analab Scientific Instruments Pvt Ltd, Vadodara), precision analytical balance (A X 120, by Shimatzu Corporation analytical and measuring Instruments division, Kyoto, Japan), pH Meter (Labindia Instruments Pvt Ltd, Navi Mumbai). For DOE and statistical analysis Design-Expert[®] software; version 9 (Stat-Ease, Inc., Minneapolis, MN, USA) and SPSS- Minitab version 16.1.2 were used. Other calculations were done by Microsoft Excel 2010.

UV Spectrophotometer: The suitable wavelengths for estimation of drugs were identified by scanning over the range of 200–400 nm with a Shimadzu UV-1700 double beam spectrophotometer (Shimadzu, Japan).

Liquid Chromatographic system: The HPLC (high performance liquid chromatographic) system consisted of manual injector, low pressure gradient flow control valve, column oven, solvent delivery module, photodiode array (PDA) detector and system controller with Empower-2 software (all from Waters Acquity Corporation, Milford, MA, USA).

For stability indicating assay method the separation was accomplished on a Phenomenex RP- C18 column (250 \times 4.6 mm, 5 μm) at wavelength of 215 nm. The mobile phase consisted of a mixture of ammonium acetate buffer (10 mM, pH 4.5 adjusted with glacial acetic acid) and MeOH/ACN (90:10) in the ratio 97:03, v/v at a flow-rate of 1.0 ml/min with isocratic elution. The analysis was performed at 39°C using column oven with injection volume of 20 μL .

For enantiomeric separation and stability indicating chiral assay method separation was accomplished on a CHIRADEX RP- C18 column (150 \times 4.6 mm, 5 μm) at wavelength of 215 nm. The mobile phase consisted of a mixture of 10 mM ammonium acetate buffer (pH adjusted to 5.5 with glacial acetic acid) and MeOH in the ratio 80:20, v/v at a flow-rate of

0.8 ml/min with isocratic elution. The analysis was performed at ambient temperature with injection volume of 20 μ L. The mobile phase was filtered through 0.2 μ m disposable filters from Ultipore[®], PALL lifesciences (40 mm) and degassed by ultrasonic vibrations prior to use.

Mass spectroscopy: The LC-MS/MS studies were carried out on LCQ fleet, Thermo Fisher scientific instrument coupled with quaternary system delivery module in positive and negative ESI (electro spray ionization) mode. The nebulizer pressure was set at 20 psi using nitrogen gas; the gas temperature was set at 250⁰C using drying gas nitrogen at 30 psi pressure and capillary voltage 5500 V. For data acquisition and processing Xcalibur software was used.

FT-IR Spectroscopy: The IR spectra of PDM and degradation products were recorded using Bruker IR Affinity-1, FT-IR instrument coupled with IR solution software. Approximately 1mg of sample was thoroughly mixed with 100 mg of potassium bromide (KBr, finely powdered and dried) to prepare KBr disc. The diffuse reflectance spectra were recorded using DRS assembly.

NMR Spectroscopy: ¹H and ¹³C-NMR spectra of PDM and its degradation products were recorded by using Bruker Advance II 400 NMR spectrometer that consisted of dual broad band probe and z-axis gradients. The spectra were recorded using D₂O as a solvent and tetramethylsilane as an internal standard.

3.4.1.3 Preparation of Stock, Sample and Buffer solutions

Stock solutions of PDM were prepared in double distilled water to produce a concentration of 1 mg/ml. The working standards were prepared in mobile phase to produce 50 – 300 μ g/ml of PDM. To analyze the stressed samples suitable dilutions were made in mobile phase to obtain the final concentration of 200 μ g/ml with respect to PDM. Same aliquots i.e. 50 – 300 μ g/ml of PDM were prepared for recovery studies and assay of synthetic mixture.

Acetate buffer (10 mM) was prepared by dissolving 0.35 gm of anhydrous ammonium acetate in 500 mL of double distilled water and adjusted to pH 4.5 using glacial acetic acid which was finally filtered with 0.2 μ m Nylon membrane filter and degassed by ultrasonication for 5 minutes.

3.4.1.4 Preparation of Degradation Products (DPs)

Stress degradation studies were carried out as per ICH guidelines. A preliminary degradation study was performed to gather some basic information about the stability of the API and to determine number of DPs formed under different stress conditions. Four samples were generated for every stress condition for API, i) the blank solution stored at normal conditions ii) the blank solution subjected to stress condition in the same manner as the drug iii) zero time sample containing the API which was stored at normal conditions and iv) the drug solution subjected to stress treatment. Then in the final study, PDM was stressed to maximum condition where 05-80% decrease in peak area of API occurred. Degradation samples generated for each stress condition were mixed to optimize and develop quality by design based stability indicating assay method.

The same stress degradation study was performed on synthetic mixture of PDM prepared in laboratory as the formulation is not available in Indian market to determine formation of any DPs due to drug-excipient interaction.

The specific stress conditions applied were as follows:

Hydrolytic Degradation (Acid/Base/Neutral hydrolysis):

Hydrolytic degradation studies were performed in acidic, basic and neutral conditions by heating or refluxing API in HCl, NaOH and H₂O. For acid hydrolysis 1 mg/ml of PDM in freshly prepared 0.8 N HCl was prepared and solution was refluxed at 80⁰C in dark for 3 hrs. For base hydrolysis 1 mg/ml of PDM in freshly prepared 0.1 N NaOH was prepared and solution was refluxed at 80⁰C in dark for 3 hrs. For neutral hydrolysis 1 mg/ml of PDM was prepared in distilled water and refluxed at 80⁰C in dark for 6 hrs. Aliquot of 2 mL of these samples were withdrawn neutralized with NaOH/HCl in case of acid/base hydrolysis and stored in freezer before analysis.

Oxidative (Peroxide- induced) Degradation:

For oxidative degradation study 1 mg/ml of PDM was prepared in 0.01% H₂O₂. The solution was refluxed at 80⁰C in dark for 1.5 hrs.

Photolytic Degradation:

For the photochemical stability, solid drug (API) was spread in 1mm thickness on a petridish and exposed to 5382 LUX and 144UW/cm² in photo-stability chamber for 21 days.

Thermal (Dry heat induced) Degradation:

For preparing dry heat induced degradation product, solid drugs (API) was spread on a petridish with approximately 1mm thickness and placed in oven at 80°C for 21 days under dry heat condition in the dark.

Thermal-Humidity induced Degradation:

Solid drug (API) was placed in stability chamber at 40°C±2° C and 75±5 % RH for 21 days.

All the degradation samples were suitably diluted with mobile phase to make final concentration of 200 ppm with respect to PDM and filtered through 0.2 µm nylon membrane syringe filter prior to injection in HPLC.

3.4.1.5 Preparation of synthetic mixture

Synthetic mixture for recovery and degradation study was prepared by formula prescribed in patent (24) and is shown in table 3.1 as the PDM formulation is not available in Indian market.

Table 3.1: Preparation of Laboratory sample (synthetic mixture)

Excipient	Quantity (%)
Pidotimod	72.70
MCC	17.65
PVP	4.55
Mannitol	4.00
Mag. Stearate	1.00

3.4.1.6 Method Development

3.4.1.6.1 Analytical target profile

The ATP (Analytical Target Profile) (25-27) was defined for method which is analogous to the QTPP (Quality Target Product Profile) for pharmaceutical process according to the ICH Q8 (R2) guideline (28). These are

- 1) To develop stability indicating liquid chromatographic method that shows well resolved, sharp and asymmetric peak of PDM.
- 2) The drug peaks should be separated with peaks of DPs.
- 3) The resolved peaks should be acquired in shorter run time.

The defined ATP will lay down the basis for determining CQAs.

3.4.1.6.2 Preliminary investigations

Preliminary investigations were executed to study the effect of critical method parameters on chromatographic separation.

Detection wavelength and polarity

PDM and DPs show better sensitivity at 215 nm hence detection was carried out at this wavelength. Due to its dipeptide structure PDM is highly polar in nature with pKa value 3.03. DPs were even more polar than PDM (except 1), so higher ratio of buffer was used to increase retention time (Rt) and resolve the DPs.

Buffer pH

The pH of the buffer showed high impact on Rt of PDM while it showed moderate effect on resolution of DPs. Lower buffer pH i.e. 3.8 delayed the Rt of PDM and also resolved DP-1, DP-2 and DP-3. By increasing the pH to 5.8 the Rt of PDM decreased and DP-2 and DP-3 were co eluted. It also decreases the resolution of DP-1 and DP-2. DP-4 was well resolved at all pH.

Evaluation of solvent type and temperature

Although ACN was better in terms of sensitivity and number of theoretical plates, it gives very short Rt of PDM. Also DP-1, DP-2 and DP-3 were co-eluted and were difficult to resolve at higher buffer ratio. MeOH increases the Rt of PDM and resolve DPs at higher buffer ratio, but it decreases the sensitivity. So, mixture of MeOH and ACN was chosen to optimize Rt, resolution, sensitivity and number of theoretical plates. The column

temperature has fairly good impact on R_t and peak symmetry of PDM and DPs while it has moderate effect on resolution.

3.4.1.6.3 Risk assessment by cause- effect relationship and CNX approach

The method development was then assessed by risk assessment (29). The Ishikawa /fishbone diagram was constructed to identify possible factors and to relate them to the requirements included in the ATP (30). This allowed identification of factors that should be studied during risk assessment. (31). These are column age, mobile phase composition, flow rate of mobile phase, column oven temperature, column equilibrium time, detection wavelength and buffer strength. The risk factors were defined and ranked using Cause-Effect Risk Assessment Matrix with Control-Noise-Experimentation (CNX) approach (32). High-risk factors were then assessed experimentally using statistical based approach, Design of Experiments (DoE). These parameters are the critical process parameters (CPPs).

3.4.1.6.4 Design of Experiments

Full Factorial design (FFD): A 4^2 FFD requiring 16 experimental runs was utilized to estimate the main and interaction effects of four high risk factors selected after CNX risk assessment. The purpose of the FFD design was to identify the effects of factors on the selected responses and to obtain the optimized solutions and design space of the analytical method.

3.4.1.7 Method Validation using ICH Q2(R1) guideline and total error approach

The present method was validated according to the ICH Q2(R1) (33) and the ISO-17025 guidelines (34) applying accuracy profiles, which is based on the “total error” approach. In order to estimate the difference between the observed and true value, this approach determines the total error by combining the intermediate precision (random error) and trueness (systemic error). In the present method response function, trueness, precision and accuracy were determined by total error approach and linearity and range, LOD (limit of detection), LOQ (limit of quantification) and robustness were determined as per ICH guidelines.

3.4.1.8 Uncertainty of Measurements (UM)

Since few factors were not included in the validation such as errors during mass of sample taken there may be some doubts in the results, although the method was validated. So uncertainty estimation was carried out and compiled up with the Expanded Uncertainty (EU) and Relative Expanded Uncertainty (REU) results.

3.4.1.9 Application of developed HPLC method

The developed SIAM was applied for the analysis of PDM in synthetic mixture. Stress degradation was carried out in synthetic mixture and % degradation was calculated.

3.4.2 RESULTS AND DISCUSSION

3.4.2.1 Determination of suitable wavelength

The UV spectrum of PDM is presented in figure 3.2. The spectrum indicates that λ_{\max} of PDM is 206 nm but in order to avoid solvent interferences chromatograms were recorded at 215 nm as PDM gives sufficient absorption at this wavelength also.

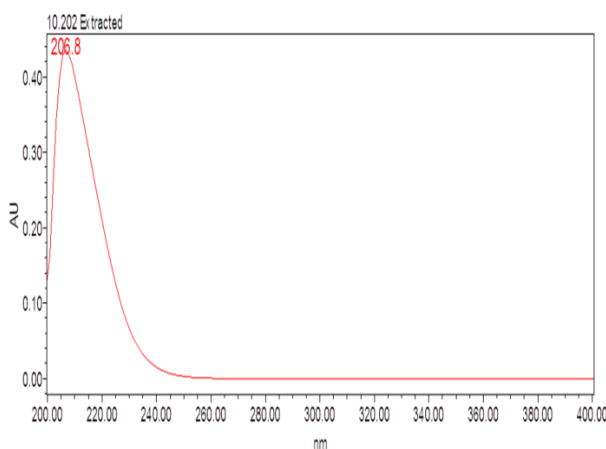


Figure 3.2: UV Spectra of PDM

The UV spectra of PDM and its impurities were extracted in PDA detector from 200-400 nm and is illustrated in figure 3.3. The spectrum indicates that 202- 206 nm gives a good sensitivity for the DPs and PDM but chromatograms were recorded at 215 nm to avoid solvent interferences at this wavelength as DPs and PDM gives sufficient absorption at this wavelength also.

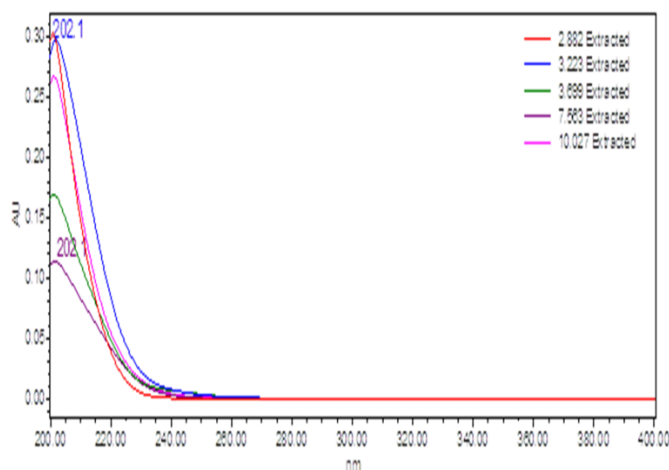


Figure 3.3: UV spectra of PDM and DPs extracted from PDA detector

3.4.2.2 Method optimization and development

3.4.2.2.1 ATP

Based on preliminary investigation, the parameters that will be focused in our method development were selected and enlisted as ATP.

3.4.2.2.2 Risk assessment by cause- effect relationship and CNX approach

The Cause effect or Ishikawa diagram is shown in Figure 3.4 that may influence the method performance criteria. Table 3.2 enlists the factors and their score that were considered in method development. Based on CNX risk assessment the contributing method parameters were divided into primary (High Risk, score ≥ 200) and secondary (Marginal Risk, score < 200) factors. % organic in mobile phase, pH of mobile phase, flow rate of mobile phase, % ACN in organic phase and column oven temperature were considered as primary factors due to high and marginal risk. Among primary factors % ACN in organic phase was fixed at 10% based on preliminary trials and previous experience and rest four variables were optimized by DoE to determine significant factors affecting method performance. Among secondary factors the column equilibrium time was fixed at 20 min, wavelength at 215 nm and buffer strength at 10 mM based on preliminary trials and experience.

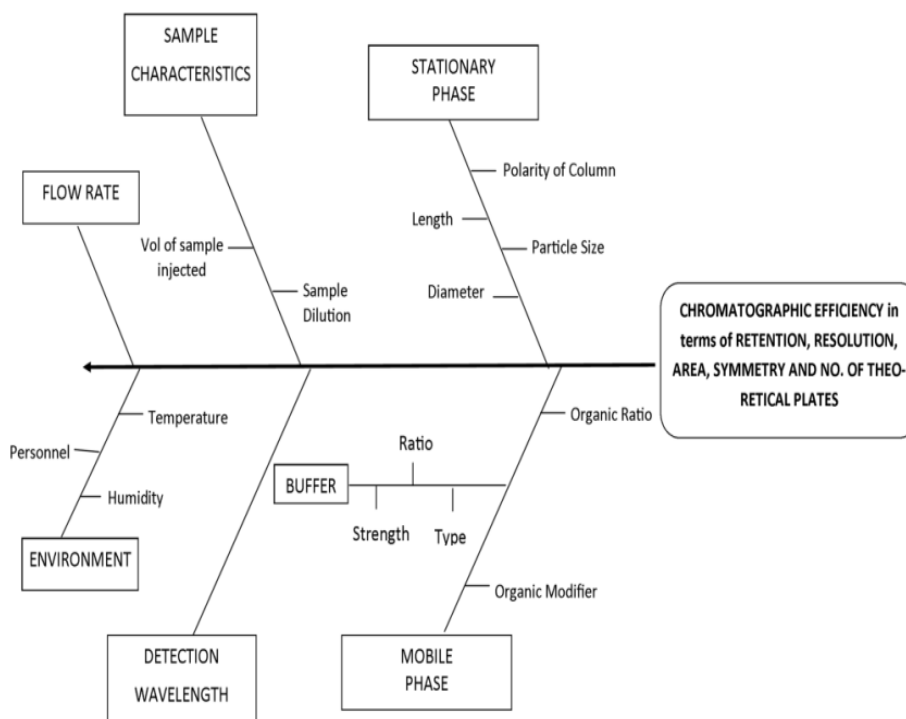


Figure 3.4: Ishikawa or cause effect diagram

Table 3.2: CNX risk assessment for chromatographic separation

Method parameter	Cause	Component attributes			Total score	C, N, X	Strategy
		Resolution	Retention time	Tailing			
	Attribute Score	10	10	10			
Column	Column age, of injection	10	10	10	300	N	New column
Column	Stationary phase type	10	10	10	300	C	C-18
Mobile Phase	% organic	10	10	10	300	X	DoE

Mobile Phase	pH	10	10	10	300	X	DoE
Pump	Flow Rate	5	10	5	200	X	DoE
Mobile Phase	% ACN	5	10	5	200	C	Fixed (10%)
Heater	Column Temp	5	5	10	200	X	DoE
Column	Equillibration	5	5	1	110	C	Fixed (20 min)
Instrumental	Wavelength	5	5	1	110	C	Fixed (215)
Mobile Phase	Buffer strength	1	5	1	70	C	Fixed (10 mM)

Notes: C – controlled, N = Noise, E = Experimental; Scoring: 1 – negligible risk, 5 – low risk (potential impact), 10 – high risk (proven impact) Final score is the summation of each component attribute times the parameter score (10x10+10x10+10x10=300)

3.4.2.2.3 DoE-4² Full Factorial Design (FFD)

During preliminary stress degradation study it was observed that DP-1, DP -2 and DP -3 were formed in almost all degradation conditions. DP-4 was not formed in oxidative degradation while it was formed under acid, base, neutral and photolytic degradation. The chromatographic conditions utilized during preliminary trials described that DP-1 and DP-2 were co eluted and resolution of DP-2 and DP-3 was low while PDM and DP-4 were well resolved. So, considering the above observations, DOE was applied to resolve the Pair of peaks (RS1: DP-1and DP-2, RS2: DP-2 and DP-3) and to reduce the Rt of last eluting peak (DP-4) i. e. chromatographic run time. The 4² FFD comprising 16 runs was utilized for method optimization and development. Based on CNX risk assessment, the independent variables (factors) were chosen, these are flow rate (A), Buffer pH (B), ratio (%) of organic in mobile phase (C) and column temperature (D) while the dependent variables (Responses) were RS1, RS2 and Rt (of last eluting peak). Factors and their levels for FFD are shown in table 3.3. The matrix of FFD with their measured responses is shown in table 3.4. Some of the chromatograms of FFD trials are shown in figure 3.5.

Table 3.3: Variables and their levels for Full Factorial Design

Factors	Coded Levels	Actual Levels
A: Flow Rate	-1	0.6
	1	1.2
B: pH of Mobile Phase	-1	4.0
	1	5.8
C: Ratio (%) Organic in Mobile Phase	-1	1
	1	8
D: Column oven temperature	-1	25
	1	40
Responses		Constraints
R1: resolution between peak pair 1 (RS1)		$2 \leq R1 \leq 4$
R2: : resolution between peak pair 2 (RS2)		$1.5 \leq R2 \leq 2.5$
R3: Retention time of last eluting peak (Rt)		minimize

Table 3.4: Matrix of experiments for Full Factorial Design and results of their responses

RU N	Independent Variable				Dependent Variable		
	FR (ml/min) [A]	pH [B]	% ORG [C]	Temp. [D]	RS1 [R1]	RS2 [R2]	Rt [R3]
1	0.6	5.8	8	40	1.9	0.45	7.01
2	0.6	5.8	1	40	4.2	1.6	11.92
3	1.2	5.8	8	40	1.7	0	5.188
4	0.6	4	8	25	1.5	1.5	12.5
5	1.2	4	8	25	1.1	2	10.83
6	0.6	4	1	25	4	2.6	25.9
7	0.6	4	1	40	2.5	2.4	18.2

8	1.2	4	1	25	2.8	2.3	26.42
9	1.2	5.8	1	25	3.56	1.62	31
10	0.6	5.8	1	25	6.56	2.3	23.03
11	1.2	5.8	1	40	3.9	1.6	11.5
12	1.2	4	8	40	1	1.6	7.5
13	0.6	5.8	8	25	2	0.9	13.79
14	1.2	5.8	8	25	1.8	0	9.52
15	0.6	4	8	40	1.2	1.8	8.59
16	1.2	4	1	40	2.4	2.2	14.5

FR= Flow rate of mobile phase; pH= pH of mobile phase; % ORG= Organic % in mobile phase; Temp= Column temperature; RS1= Resolution between peak pair 1; RS2= Resolution between peak pair 2; Rt= Retention time of last eluting peak

Effect of factors on responses

Three models were generated with respect to responses RS1, RS2 and Rt. The half normal plots were used for choosing statistically significant effects. The pareto chart is useful for checking the significance of next largest unselected effect. The half normal plot and pareto charts for RS1, RS2 and Rt are shown in figure 3.6.

RS1

Regression coefficients of responses and ANOVA results are presented in table 3.5 and 3.6. From regression analysis of reduced quadratic model (RQM) it can be concluded that C was most influencing factor affecting negatively response RS1. B was the next contributing factor that contributes positively. Factor A and D were contributing negatively the method performance. Factor D had least contribution. The same can be inferred from main and interaction plot for RS1 (figure 3.7) and contour and 3D plots (figure 3.10). There is interaction effect between AD and BC; other terms were included in model to support hierarchy although they are not significant.

The quadratic equation in terms of coded factors for reduced model is as follows:

$$RS1 = +2.63 - 0.35 * A + 0.57 * B - 1.11 * C - 0.28 * D + 0.23 * AC + 0.25 * AD - 0.25 * BC + 0.21 * CD - 0.23 * ACD$$

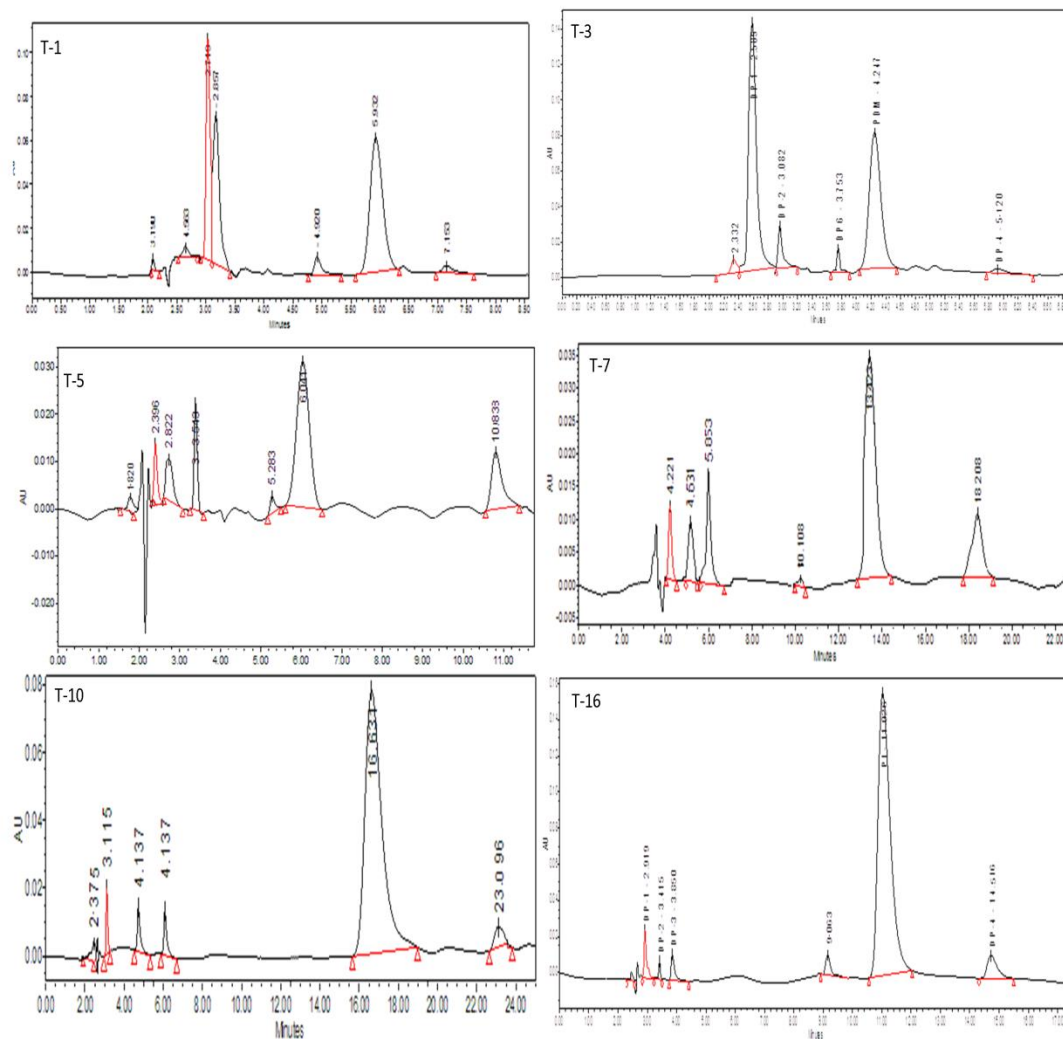


Figure 5.5: Some chromatograms of FFD Trials

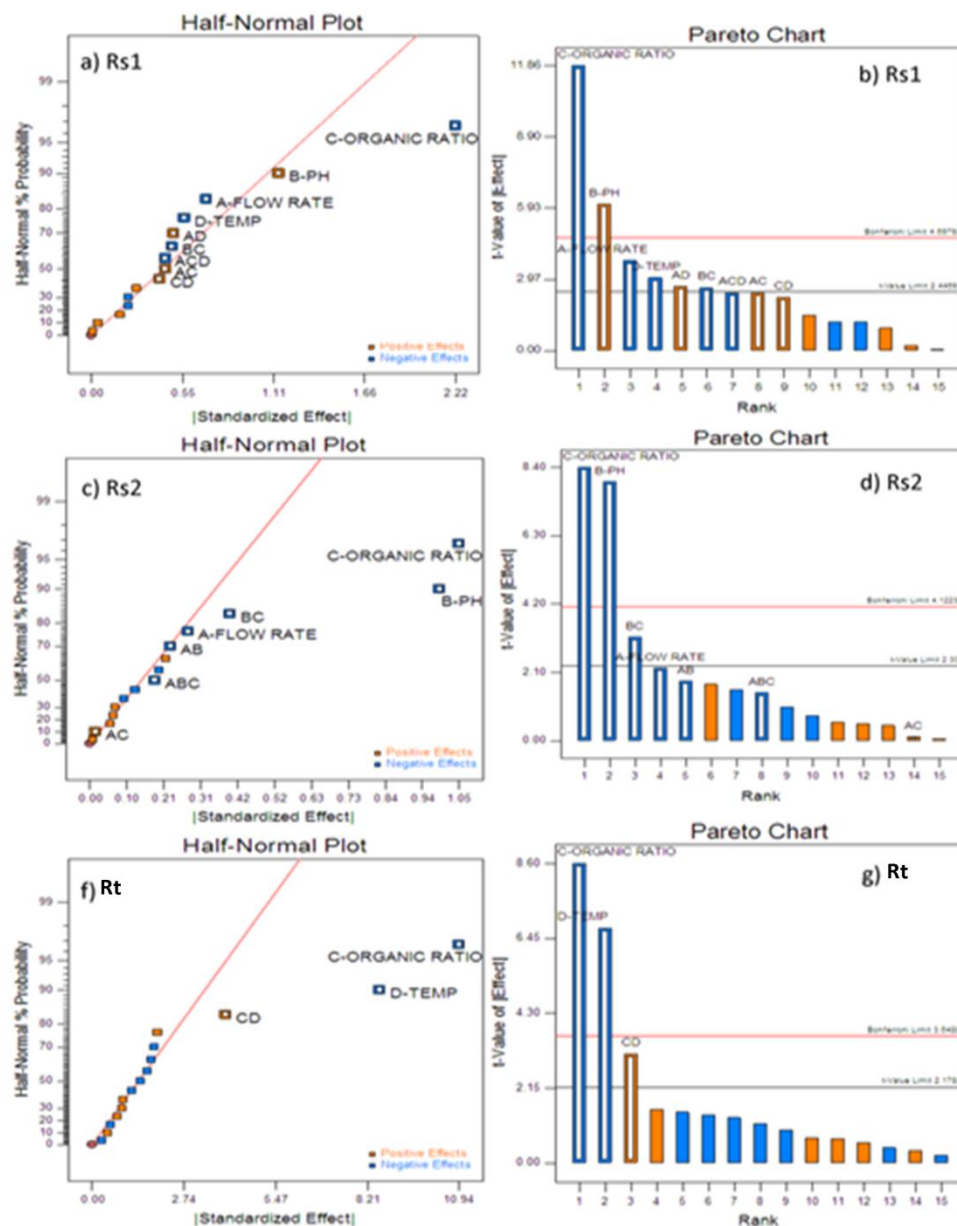


Figure 3.6: a) Half normal plot for RS1, b) Pareto chart for RS1, c) Half normal plot for RS2, d) Pareto chart for RS2, e) Half normal plot for Rt, f) Pareto chart for Rt

RS2

From table 3.5 and figure 3.8 it can be concluded that B and C were most influencing factors, contributing equally (as the associated p-value is <0.0001) and affecting negatively response RS2. Factor A was also contributing significantly and negatively. The response RS2 was not effected by factor D. There was significant interaction effect between B and

C, while other terms were included in model to support hierarchy although they are not significant.

The quadratic equation in terms of coded factors for full model is as follows:

$$RS2 = +1.55 - 0.14 * A - 0.50 * B - 0.52 * C - 0.11 * AB + 8.125E-003 * AC - 0.20 * BC - 0.092 * ABC$$

Rt

As shown in table 3.5 and figure 3.9 it can be concluded that C and D were most influencing factors as the associated p-values are equal (<0.0001). Both the factors were negatively affecting response Rt. The factors A and B were not contributing significantly. There was significant interaction effect between C and D.

The quadratic equation in terms of coded factors for reduced model is as follows:

$$RT = +14.84 - 5.47 * C - 4.29 * D + 1.99 * CD$$

Table 3.5: Regression analysis results

Factors	RS1 coefficient	p value (prob>F)	RS2 coefficient	p value (prob>F)	Rt coefficient	p value (prob>F)
Intercept	2.63	0.0004*	1.55	0.0001*	14.84	< 0.0001*
A	-0.35	0.0095*	-0.14	0.0500*	--	--
B	0.57	0.0009*	-0.50	< 0.0001*	--	--
C	-1.11	< 0.0001*	-0.52	< 0.0001*	-5.47	< 0.0001*
D	-0.28	0.0232*	--	--	-4.29	< 0.0001*
AB	--	--	-0.11	0.1036	--	--
AC	0.23	0.0526	8.125E-003	0.8994	--	--
AD	0.25	0.0366*	--	--	--	--
BC	-0.25	0.0394*	-0.20	0.0130*	--	--
BD	--	--	--	--	--	--

CD	0.21	0.0680	--	--	1.99	0.0086*
ABC	--	--	-0.092	0.1784	--	--
ACD	-0.23	0.0526	--	--	--	--
A ²	--	--	--	--	--	--
B ²	--	--	--	--	--	--
C ²	--	--	--	--	--	--
D ²	--	--	--	--	--	--

Regression coefficients are in coded values, *Statistically significant (p<0.05)

Model Fitting and Statistics

Statistically, high values of the r^2 for all dependent variables indicate a good fit. Adjusted- r^2 and Predicted- r^2 values were also in reasonable agreement, particularly for reduced models signifying good model fit (table 3.6). Better p-value and predicted- r^2 value obtained for reduced model might be due to elimination of insignificant terms. Further all models, showed adequate precision value more than 4, indicating adequate model discrimination.

Table 3.6: ANOVA results showing the effect of independent variables on the responses

Resp onse	Mod el	SS	D F	MS	F- value	p- value	PRES S	r^2	Adj- r^2	Pred- r^2	AP
RS1	RQM	32.33	9	3.59	25.76	0.0004	5.95	0.974	0.936	0.820	17.17
RS2	RQM	9.59	7	1.37	22.08	0.0001	1.99	0.950	0.907	0.803	14.19
Rt	RQM	83.46	3	27.8 2	43.09	< 0.0001	13.03	0.915	0.893	0.849	15.34

RQM=reduced quadratic model, RLM= reduced linear model, SS= Sum of Squares, DF= Degrees of freedom, PRESS= prediction error sum of squares, Adj- r^2 = Adjusted r^2 , Pred- r^2 = Predicted r^2 , AP= Adequate Precision.

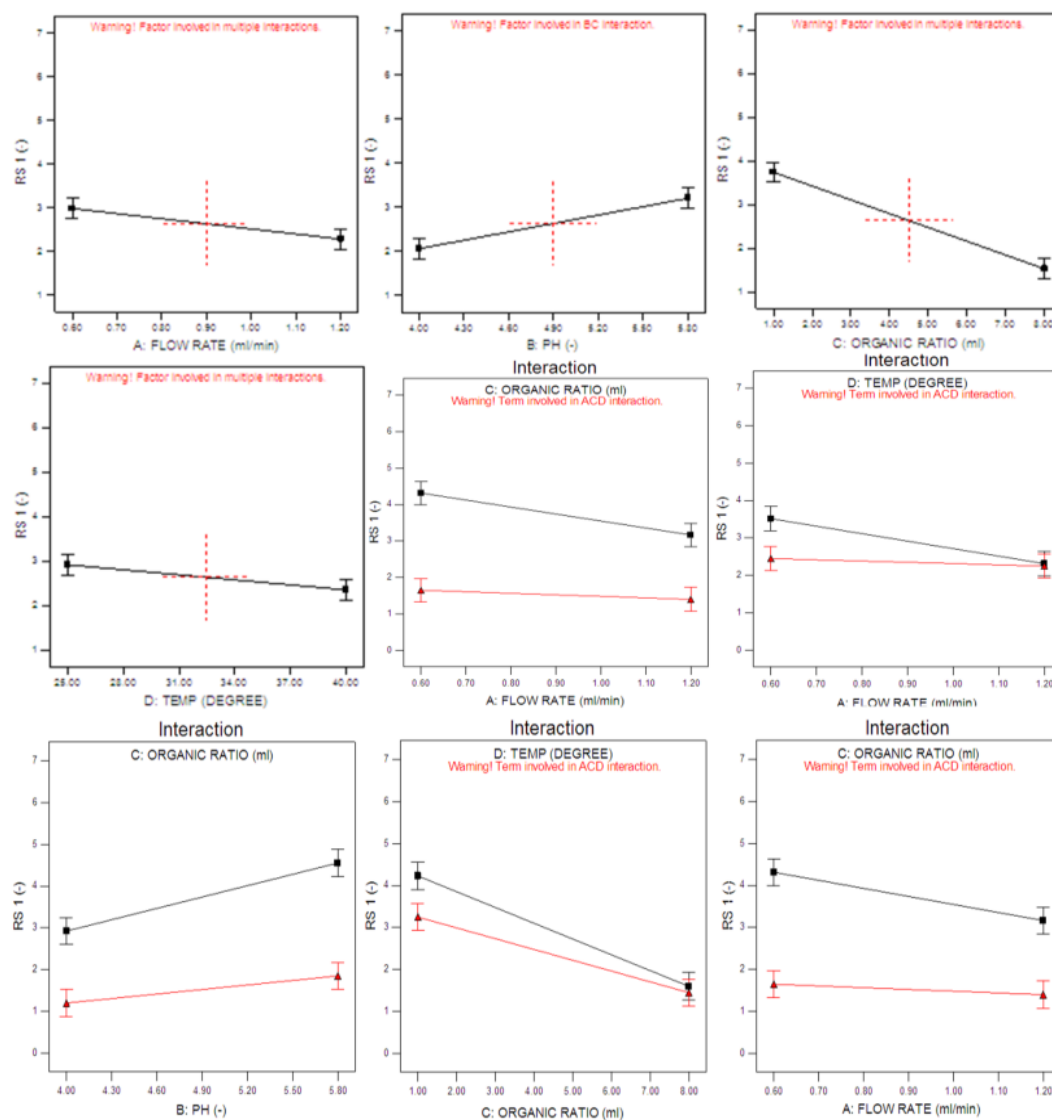


Figure 3.7: Main and interaction effect plots for RS1

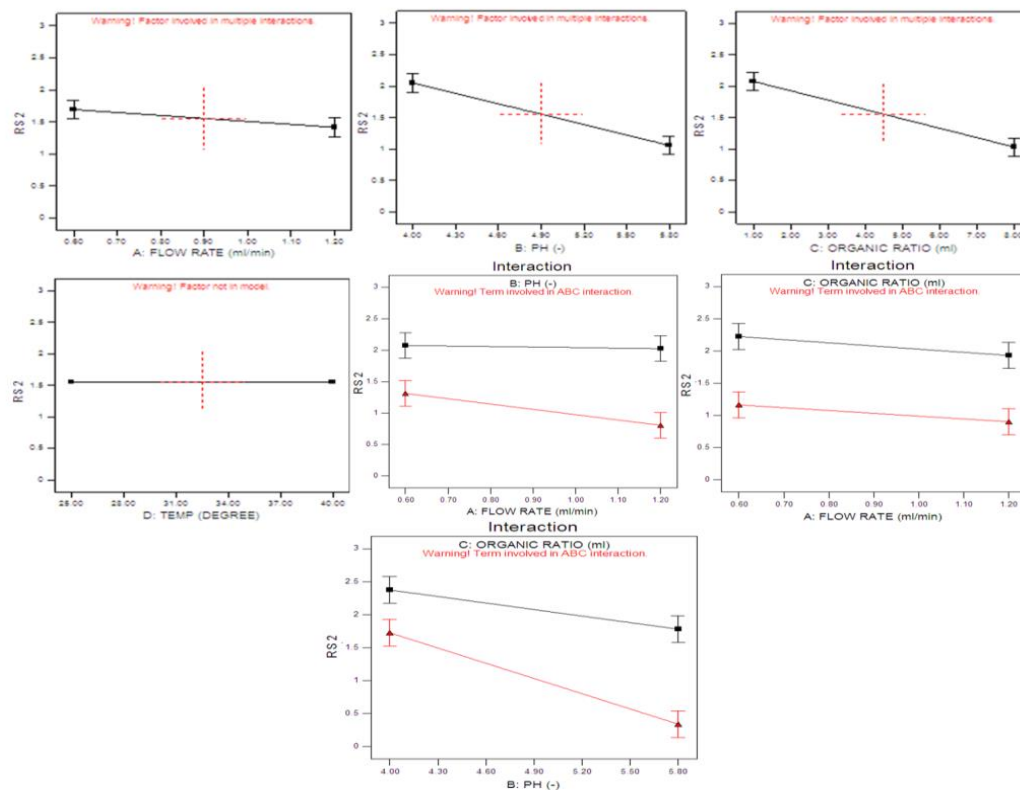


Figure 3.8: Main and interaction effect plots for RS2

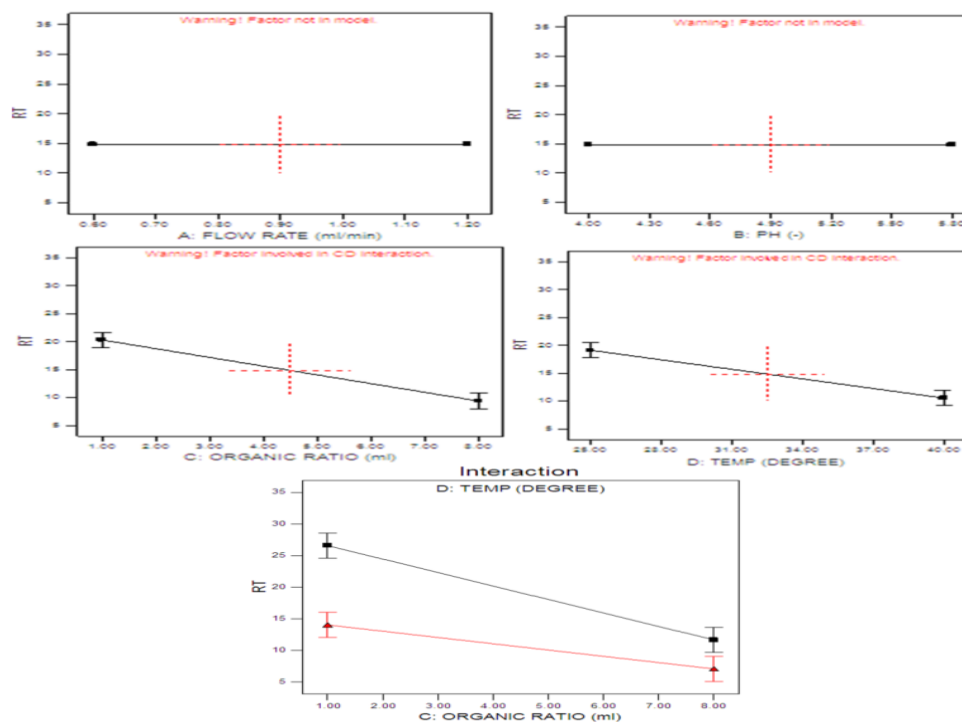


Figure 3.9: Main and interaction effect plots for Rt

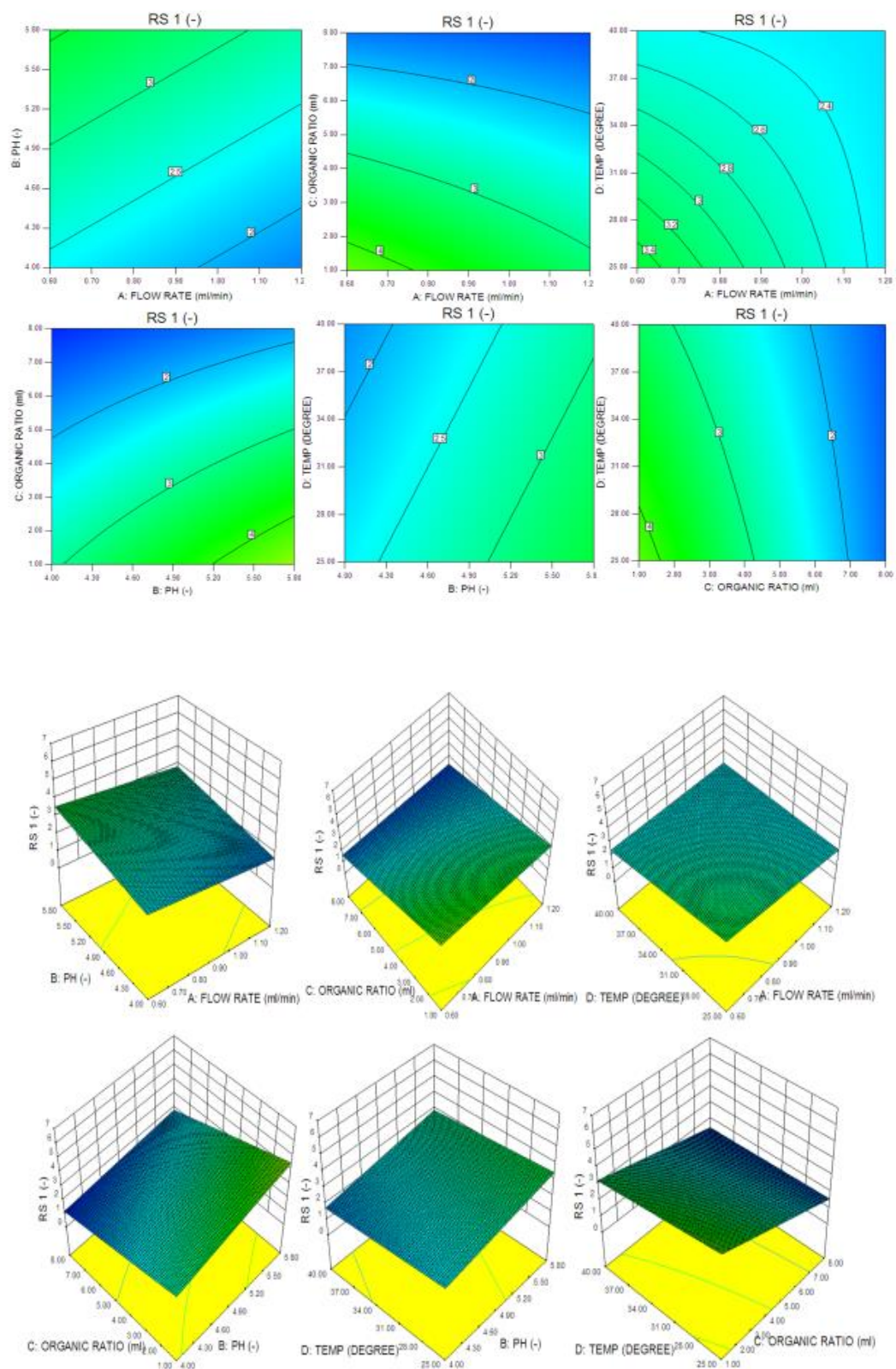


Figure 3.10: Contour and 3D Plots for RS1 (value increases from blue to green)

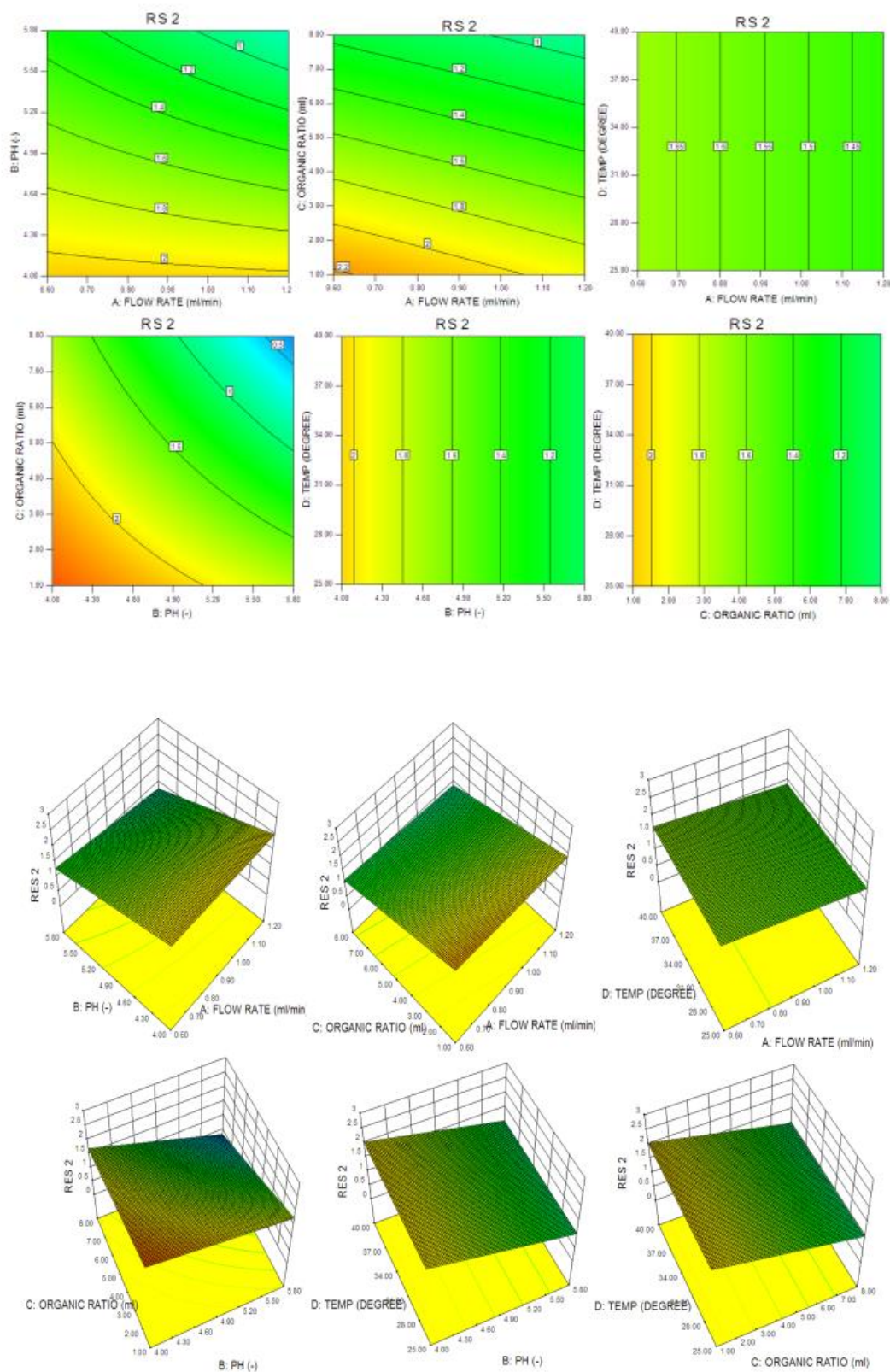


Figure 3.11: Contour and 3D Plots for RS2 (value increases from blue to red)

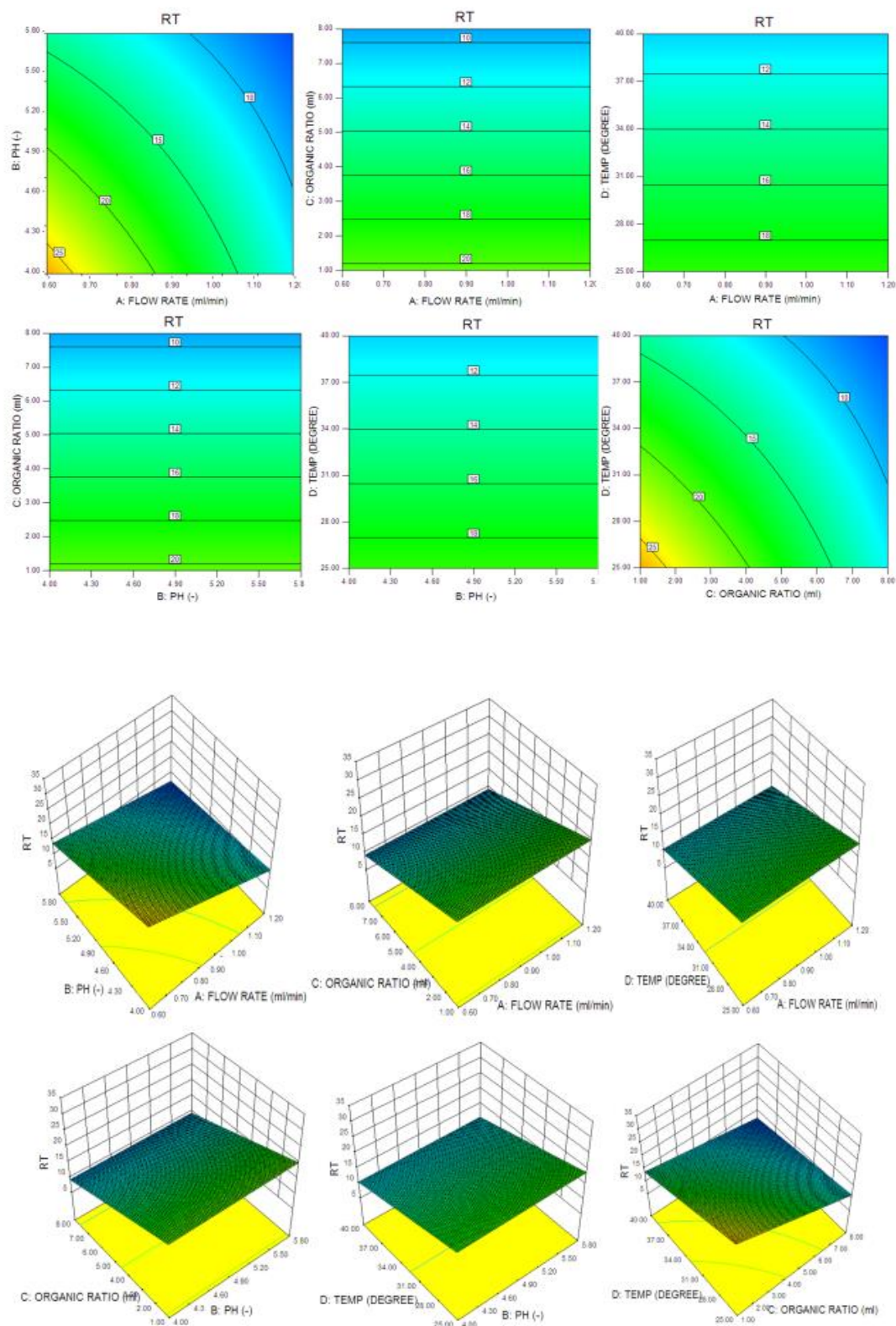


Figure 3.12: Contour and 3D Plots for Rt (value increases from blue to red)

Interaction between the factors and residual plots

Due to interaction a particular factor could not produce the same effect on the response at the different levels of the other factor. The ANOVA results (table 3.6) and figure 3.7-3.9 depicts the interaction effects amongst the factors. The p-value indicates that there is significant interaction effect among AD and BC for response RS1, BC for response RS2 and CD for response Rt, as the associated p-value for interactions are less than 0.05. The residual plots viz., normal probability plot of residuals, residuals versus predicted and residual versus run for RS1, RS2 and Rt are depicted in figure 3.13

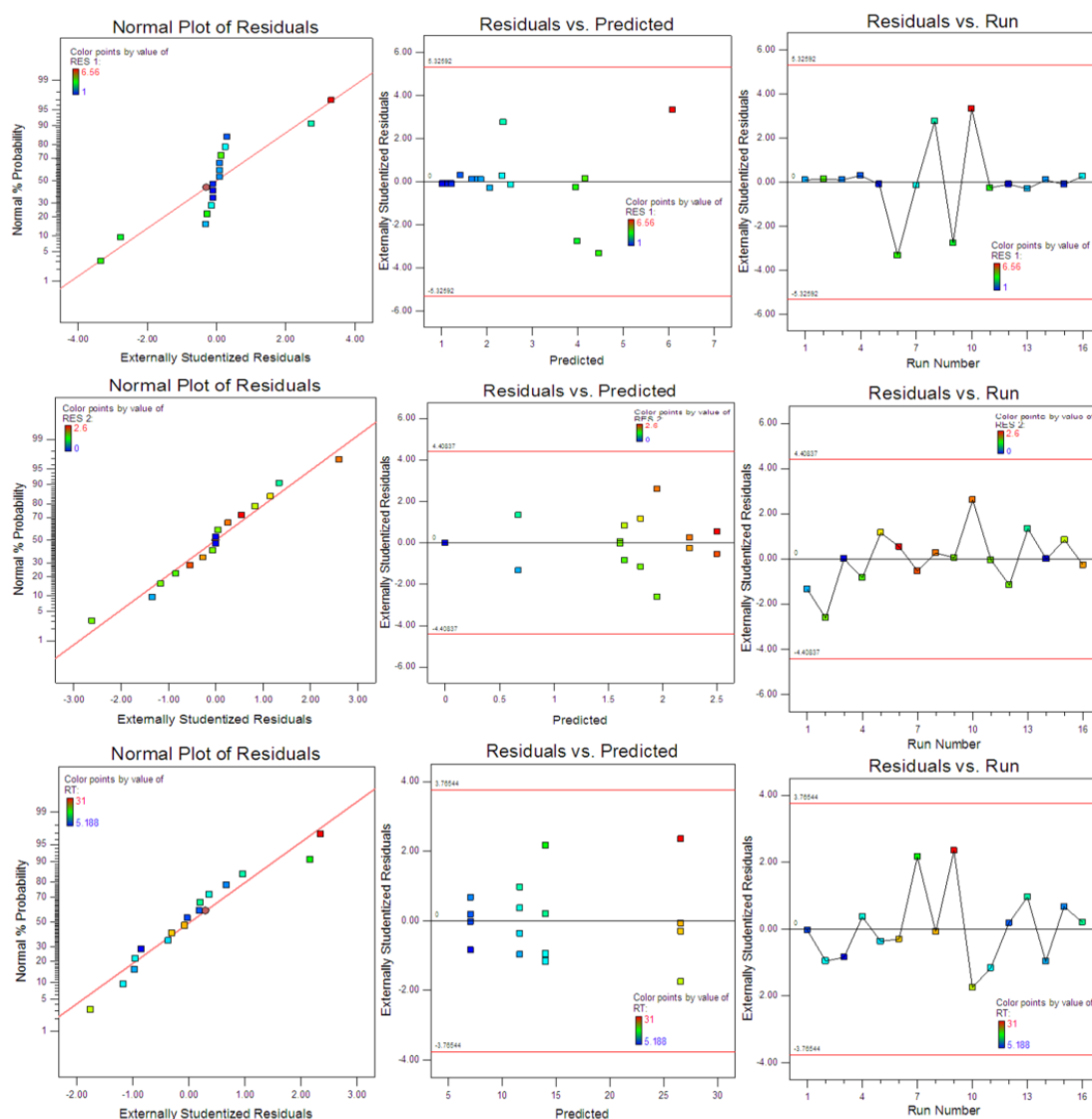


Figure 3.13: Residual plots for RS1, RS2 and Rt

The residuals appear to follow almost straight line as indicated by the normal probability plot of residuals for responses and thus non-normality, outliers, skewness/ unidentified variables did not exist. From the plot of residual versus predicted and residual versus run of responses, it was observed that residuals were randomly scattered about zero and hence existence of missing terms, non-constant variance and outliers can be ruled out.

Evaluation of model using cross-validation

Five experiments were conducted to evaluate the reliability of the selected model, by varying the variables at values other than that of the model. Lower values of % bias for all responses prove the reliability of selected model. Table 3.7 shows the predicted, experimental values and % bias for responses. Percent relative error or bias between predicted and experimental values for responses were calculated by the equation:

$$\text{Bias} = \frac{(\text{Predicted Value} - \text{Experimental Value})}{\text{Predicted value}}$$

Table 3.7: % Bias of responses for the cross validation set

Responses	Test	Factors/Levels				Predicted values	Experimental Values	Bias (%)
		A	B	C	D			
RS1	1	0.6	4.67 (4.65)	4.81 (4.8)	35.33 (35)	2.54	2.66	-0.0476
	2	0.81 (0.8)	5.31 (5.30)	3.77 (3.8)	39.56 (39)	2.87	2.73	0.0494
	3	0.91	5.22 (5.20)	3.63 (3.6)	38.16 (38)	2.87	2.7	0.0602
	4	1.06 (1.0)	4.99 (5.0)	3.87 (3.9)	39.75 (40)	2.52	2.5	0.0099
	5	1.10 (1.1)	4.76 (4.75)	2.75 (2.8)	39.45 (39.5)	2.64	2.5	0.0515
RS2	1	0.6	4.67 (4.65)	4.81 (4.8)	35.33 (35)	1.74	1.8	-0.0321
	2	0.81 (0.8)	5.31 (5.30)	3.77 (3.8)	39.56 (39)	1.51	1.4	0.0716

	3	0.91	5.22 (5.20)	3.63 (3.6)	38.16 (38)	1.52	1.35	0.1118
	4	1.06 (1.0)	4.99 (5.0)	3.87 (3.9)	39.75 (40)	1.52	1.5	0.0138
	5	1.10 (1.1)	4.76 (4.75)	2.75 (2.8)	39.45 (39.5)	1.78	1.65	0.0756
	1	0.6	4.67 (4.65)	4.81 (4.8)	35.33 (35)	12.80	13.1	-0.0237
	2	0.81 (0.8)	5.31 (5.30)	3.77 (3.8)	39.56 (39)	11.55	11.34	0.0178
Rt	3	0.91	5.22 (5.20)	3.63 (3.6)	38.16 (38)	12.58	12.41	0.0136
	4	1.06 (1.0)	4.99 (5.0)	3.87 (3.9)	39.75 (40)	11.33	11.1	0.0206
	5	1.10 (1.1)	4.76 (4.75)	2.75 (2.8)	39.45 (39.5)	12.67	12.55	0.0098

Note: The value in bracket indicates actual experimental values taken for experiment

A= Flow rate of mobile phase; B= pH of mobile phase; C= Organic % in mobile phase; D= Column temperature; RS1= Resolution between peak pair 1; RS2= Resolution between peak pair 2; Rt= Retention time of last eluting peak

Optimization using desirability function

The information obtained from desirability function can be useful for predicting optimum level of individual variable. The desirability value 1 indicates that the response is at optimum or on target while for totally unacceptable response the desirability value was given 0. The optimized methods with acceptable ranges for responses were determined by setting the goals of the critical responses. Response RS1 was selected to be in between 2-4, Response RS2 was set to maximize (1.5-2.2) and Rt of the last eluting peak was set to minimize in order to reduce the total run time of method. Desirability function was calculated for the responses. Several optimized solutions for the specified criteria were generated by the software; out of which 4 solutions were used for checkpoint analysis (n=4) as shown in table 3.8. One of the solutions with % of organic in mobile phase 3, pH 4.5 at flow rate of 1 ml/min was chosen as the optimized working point. The contour and 3D desirability plots for optimized working point is shown in figure 3.14 and overlay plot

is shown in figure 3.15. The observed responses values (table 3.9) lie within 95% confidence interval of the predicted response values.

Table 3.8: Point Verification and working point selection

Optimized solution	Pred	Obs	Pred	Obs	Pred	Obs
	RS1	RS1	RS2	RS2	Rt	Rt
FR-1.17 (1.2), pH-4.84 (4.9), Org Ratio- 2.48 (2.5), Temp.-39.78 (40)	2.73	2.65	1.75	1.7	12.71	12.54
FR-0.60, pH-4.97 (4.8), Org Ratio- 5.33 (5), Temp.-35.24 (35)	2.54	2.5	1.53	1.5	12.13	12.0
FR-0.90, pH-4.78 (4.8), Org Ratio- 3.68 (4), Temp.-39.27 (39)	2.50	2.5	1.73	1.7	11.82	11.64
FR-0.98 (1), pH-4.54 (4.5), Org Ratio- 2.90 (3), Temp.-38.83 (39)	2.50	2.79	1.92	1.69	12.93	12.20

Pred= predicted value, Obs= Observed value

Table 3.9: Observed versus. Predicted responses for optimized working point

Response	Predicted mean	Observed	SE Mean	95% CI low	95% CI high
R1	2.77	2.79	0.1367	2.44	3.11
R2	1.55691	1.69	0.0713	1.39	1.7
Rt	12.498	12.20	0.8602	10.62	14.37

CI= confidence interval

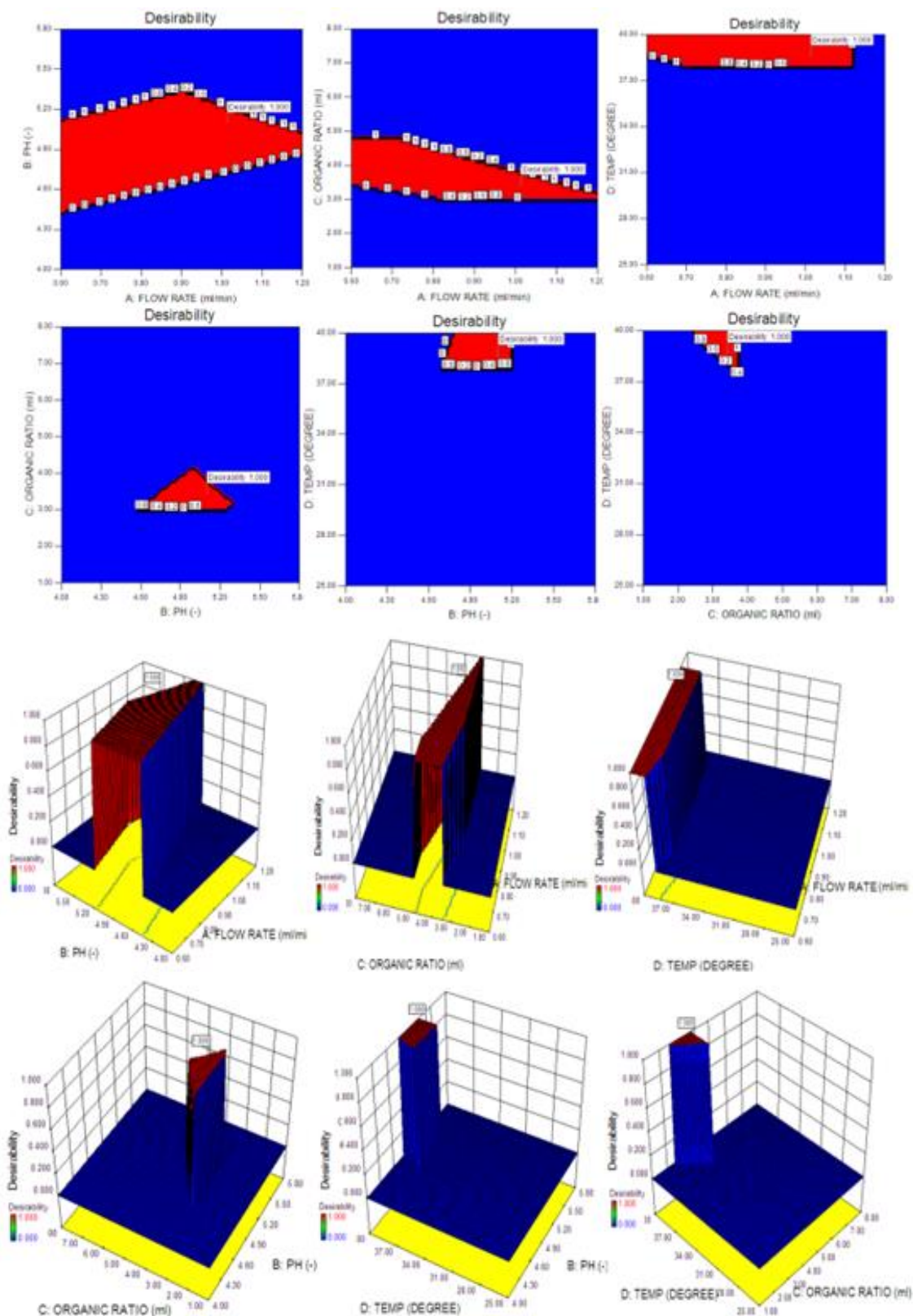


Figure 3.14: contour and 3D-Desirability plot for optimized chromatogram (desirability increases from blue to red region; blue region indicates 0 and red region indicates 1 desirability)

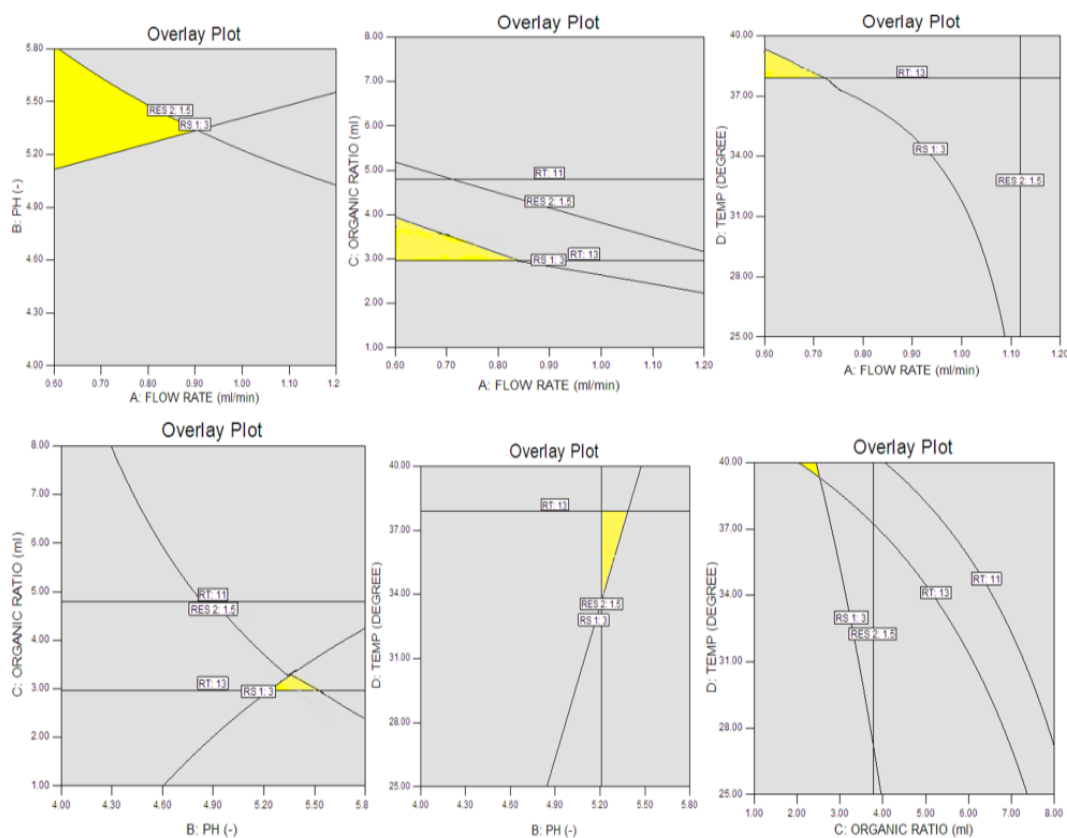


Figure 3.15: Overlay plot for optimized chromatogram (yellow region: design space, gray region: undesirable region)

The final optimized chromatogram obtained with the selected working point is depicted in figure 3.16 that comprises of well resolved peaks of PDM and DPs. The peak purity studies of resolved peaks in mixture of degradants are shown in table 3.10 and figure 3.17.

It was observed during peak purity studies that peaks for DP-1, DP-2 and DP-3 were not pure while other peaks in the chromatogram i.e. peaks of DP-6, DP-5, PDM and DP-4 were pure. Later on LC-MS/MS studies revealed that the peaks of DP-1, DP-2, and DP-3 had different masses for oxidative and neutral degradation while had same masses for acid, base, photolytic and thermal-humidity degradation condition, though it gives peaks at same Rt in LC-PDA. Also the peak purity studies of individual degradation conditions showed that the all peaks were pure and are illustrated in figure 3.24-3.29 and table 3.21-3.26.

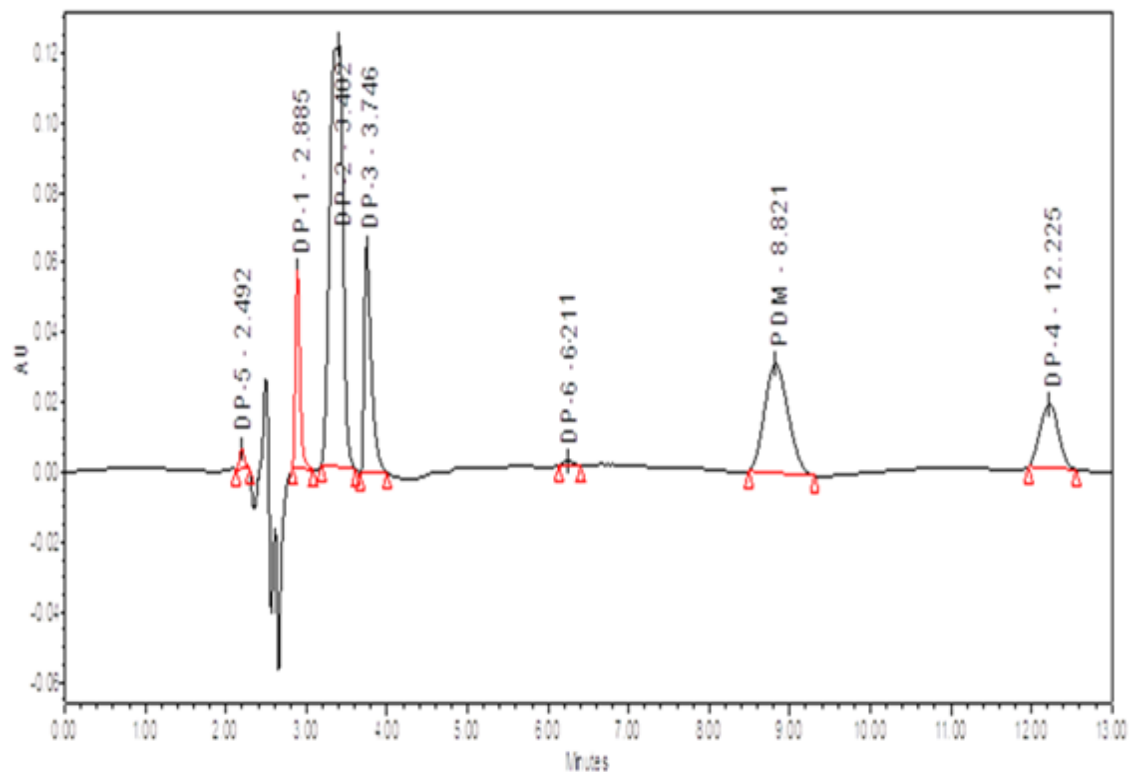
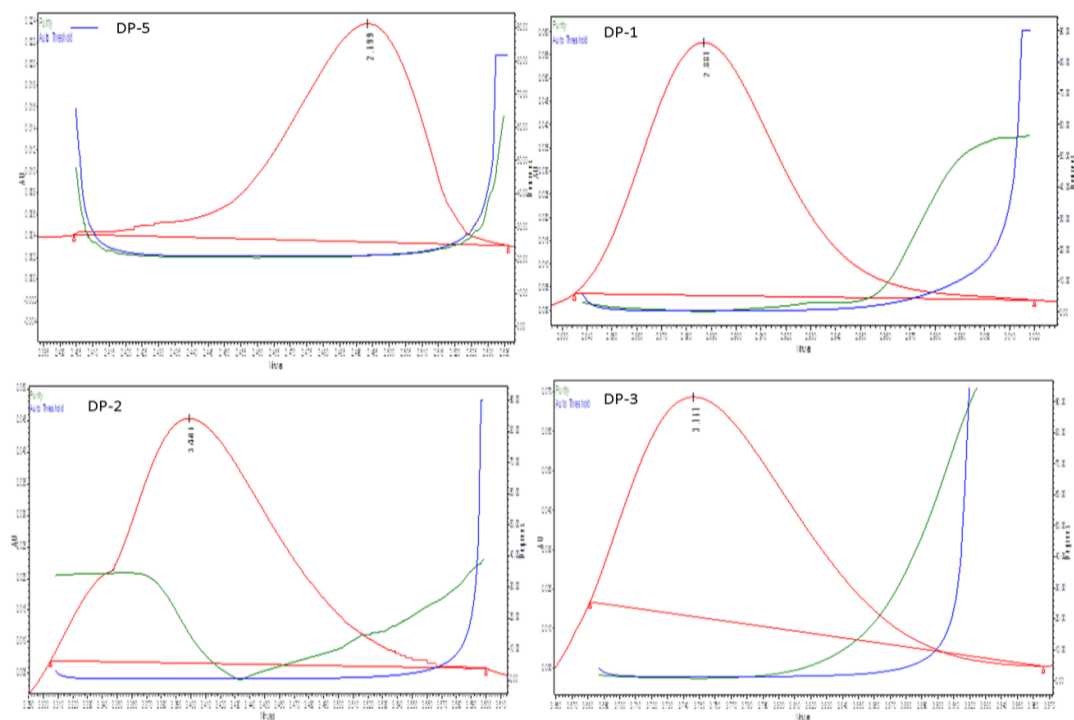


Figure 3.16: Chromatogram showing resolved peaks in mixture of degradants



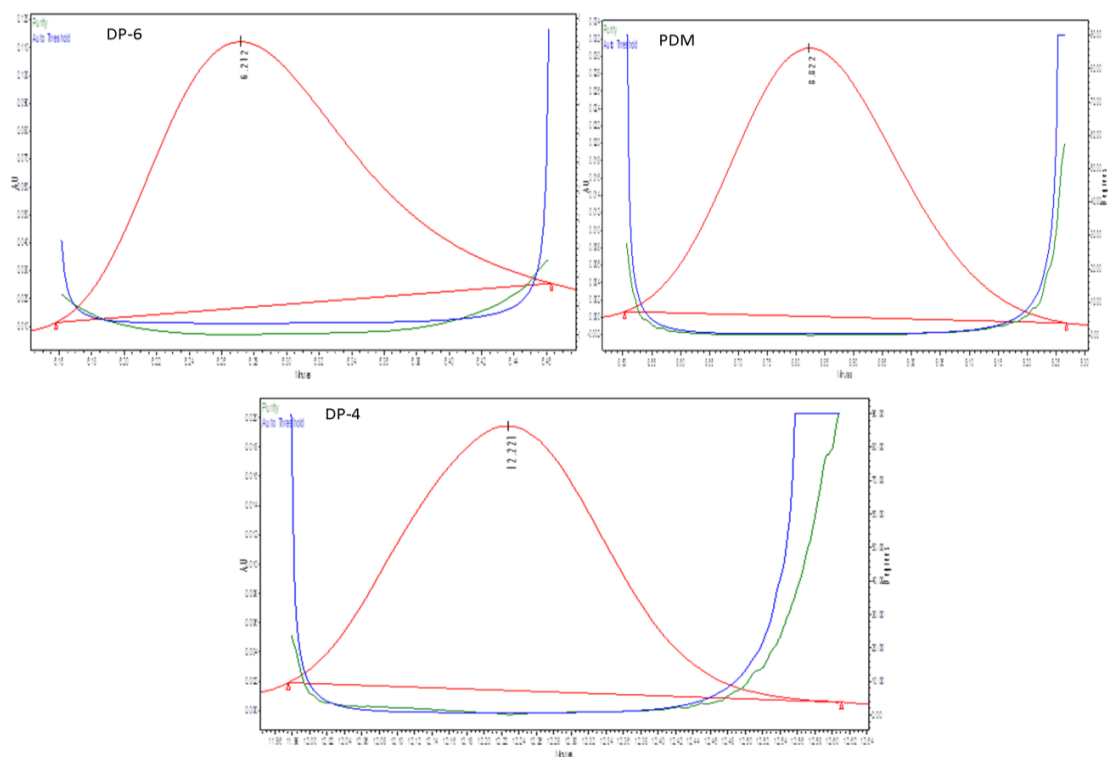


Figure 3.17: Peak purity plots for optimized chromatographic condition

Table 3.10: Peak purity studies for peaks of optimized chromatographic condition

S. No.	Peaks	Rt	Peak purity Angle	Peak purity Threshold
1.	DP-5	2.49	3.158	3.484
2.	DP-1*	2.88	7.248	1.714
3.	DP-2*	3.40	2.287	1.264
4.	DP-3*	3.74	1.761	1.692
5.	DP-6	6.21	1.841	1.974
6.	PDM	8.82	0.414	0.635
7.	DP-4	12.22	0.240	0.397

Note: *indicates peaks are not pure; peaks at Rt 2.88, 3.40 and 3.74 showed different masses in LC-MS for neutral and oxidative degradation.

3.4.2.3 Method Validation using ICH Q2(R1) guideline and total error approach

3.4.2.3.1 Linearity and Range

Linearity test solutions for PDM assay method were prepared from drug stock solution of 1 mg/ml in mobile phase at concentration levels of 50-250 µg/ml in triplicate. The calibration curve was constructed by plotting concentrations versus peak areas of PDM. The regression equation was calculated and was found to be linear in the selected concentration range with r^2 value 0.9994 and regression equation $Y = 0.22695X - 361608$. The linearity of the method was established in accordance with ICH Q2(R1) guideline. Overlay chromatogram and calibration curve showing linearity of PDM is shown in figure 3.18.

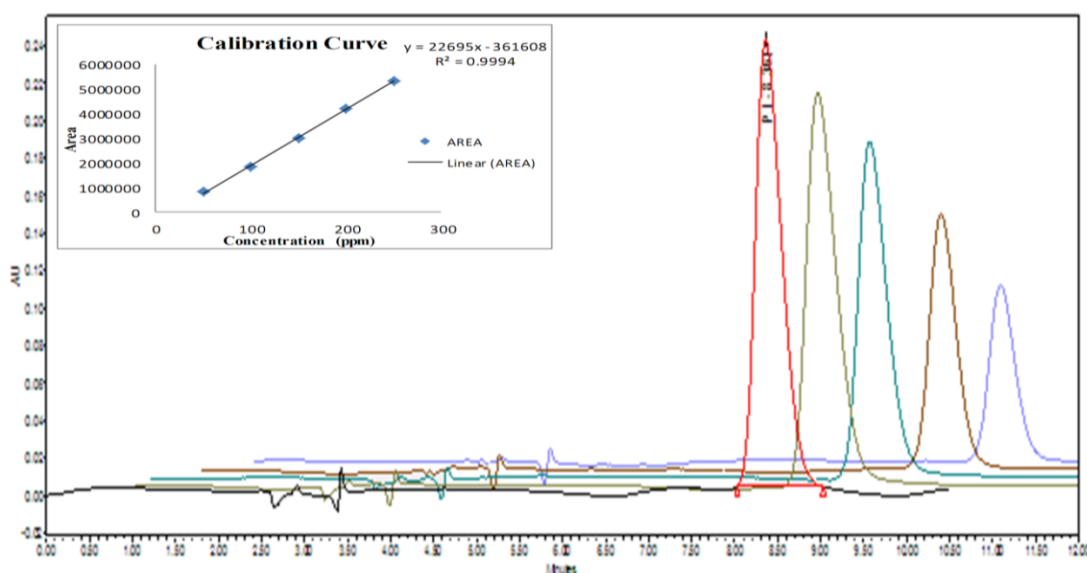


Figure 3.18: Overlay plot and calibration curve showing linearity of method

3.4.2.3.2 Response function (calibration curve)

Linear regression model was used to prepare calibration curves in the present method. The Validation and calibration sets (table 3.11 and 3.12) were prepared for generating models. To study response function three different sets were prepared within the concentration range of 50-250 µg/ml. All three sets followed the linear regression model as indicated by their regression analysis parameters. Series 2 showed the best coefficient of determination with r^2 value 0.9999 and regression equation $Y = 4385 + 1.6566E+04 X$, which was selected for further computation.

Table 3.11: validation standards

Sample ID	Series	Conc. Level (µg/ml)	Introduced conc. (µg/ml)	Analytical response (Area)
A1	1	1	50	829163
A10	1	4	200	3306412
A11	1	4	200	3329996
A12	1	4	200	3326544
A13	1	5	250	4142475
A14	1	5	250	4161545
A15	1	5	250	4145640
A2	1	1	50	831749
A3	1	1	50	830236
A4	1	2	100	1668206
A5	1	2	100	1665498
A6	1	2	100	1664172
A7	1	3	150	2487309
A8	1	3	150	2496247
A9	1	3	150	2492408
B1	2	1	50	826917
B10	2	4	200	3301668
B11	2	4	200	3303760
B12	2	4	200	3296828
B13	2	5	250	4125473
B14	2	5	250	4149264
B15	2	5	250	4141035
B2	2	1	50	830125
B3	2	1	50	829237

B4	2	2	100	1665834
B5	2	2	100	1662130
B6	2	2	100	1658414
B7	2	3	150	2473751
B8	2	3	150	2490345
B9	2	3	150	2477621
C1	3	1	50	831127
C10	3	4	200	3324148
C11	3	4	200	3297140
C12	3	4	200	3319984
C13	3	5	250	4147135
C14	3	5	250	4136725
C15	3	5	250	4147610
C2	3	1	50	826785
C3	3	1	50	829996
C4	3	2	100	1662054
C5	3	2	100	1657570
C6	3	2	100	1659962
C7	3	3	150	2493081
C8	3	3	150	2483355
C9	3	3	150	2479988

Table 3.12: Calibration standards

Sample ID	Series	Conc. Level (µg/ml)	Introduced conc. (µg/ml)	Analytical response (Area)
A1	1	1	50	829773

A2	1	1	50	832571
A3	1	2	150	2475719
A4	1	2	150	2494613
A5	1	3	250	4128987
A6	1	3	250	4157975
B1	2	1	50	833701
B2	2	1	50	836131
B3	2	2	150	2480142
B4	2	2	150	2489393
B5	2	3	250	4138970
B6	2	3	250	4157175
C1	3	1	50	827993
C2	3	1	50	833851
C3	3	2	150	2480679
C4	3	2	150	2492553
C5	3	3	250	4134785
C6	3	3	250	4154975

Furthermore in order to check the adequacy of the regression model for calibration, a test of lack of fit (LOF) and Levene's test i. e. evaluation of homogeneity of variance was performed. As demonstrated in table 3.13 outliers were not found in calibration curve, since the p-values were found to be higher than 0.05. Standard residual plot was also plotted as shown in table 3.14 and figure 3.19. Back calculation was done to confirm the chosen regression equation. Linear plot (figure 3.20) based upon absolute β -expectation

limit was constructed between introduced and back calculated concentrations. The r^2 value was 0.9998 with regression equation $Y = 0.02221 + 0.9995 X$ [where Y = Back calculated concentrations ($\mu\text{g/ml}$) and X = Introduced concentration ($\mu\text{g/ml}$)], which indicates that the calibration lines adequately describe the observed relationship.

Table 3.13: Lack of Fit and Levene's test for linear regression model

Test	Error	SS	df	MS	F_{calc}	$F_{\text{crit}}, 95\%$	p-value
Lack of Fit	LOF error	6.8758E+07	3	2.2919E+07	0.1866	3.863	0.9029
	Pure error	1.1055E+09	9	1.2283E+08			
Levene's test	Model	2.6418E+08	2	1.3209E+08	32.30	36.82	0.3660
	Error	6.1336E+07	15	4.0891E+06			

Table 3.14: Standardized residual from the selected calibration model

Sample ID	Series	Conc. level	Introduced conc.	Analytical response	Fitted value	Standardized residual
A1	1	1	50	829773.0	8.3045E+05	-0.05503
A2	1	1	50	832571.0	8.3045E+05	0.1718
A3	1	2	150	2475719.0	2.4866E+06	-0.8825
A4	1	2	150	2494613.0	2.4866E+06	0.6490
A5	1	3	250	4128987.0	4.1428E+06	-1.116
A6	1	3	250	4157975.0	4.1428E+06	1.233
B1	2	1	50	833701.0	8.3267E+05	0.1246
B2	2	1	50	836131.0	8.3267E+05	0.4194
B3	2	2	150	2480142.0	2.4893E+06	-1.105
B4	2	2	150	2489393.0	2.4893E+06	0.01711
B5	2	3	250	4138970.0	4.1458E+06	-0.8323
B6	2	3	250	4157175.0	4.1458E+06	1.376

C1	3	1	50	827993.0	8.3049E+05	0.2918
C2	3	1	50	833851.0	8.3049E+05	0.3918
C3	3	2	150	2480679.0	2.4875E+06	-0.7929
C4	3	2	150	2492553.0	2.4875E+06	0.5929
C5	3	3	250	4134785.0	4.1445E+06	-1.128
C6	3	3	250	4154975.0	4.1445E+06	1.228

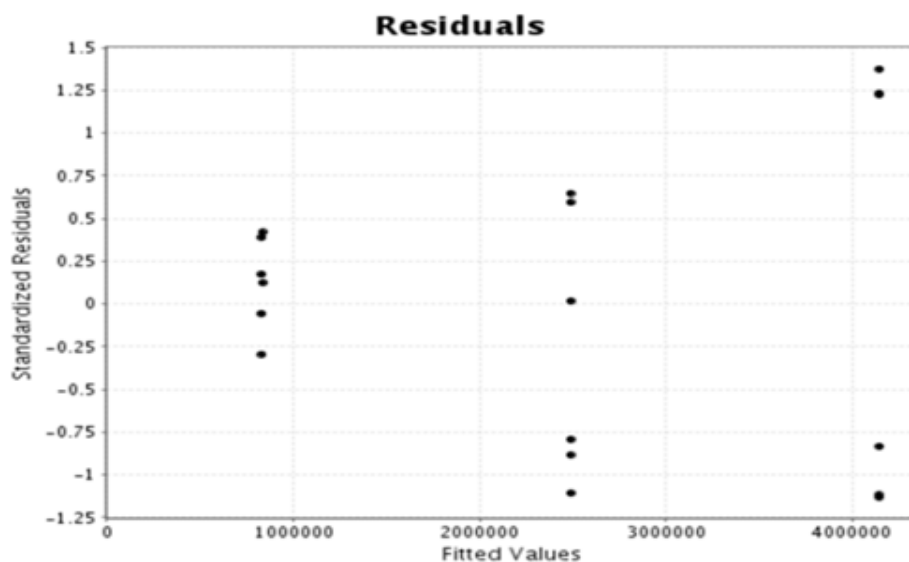


Figure 3.19: Standard residual plot of three different series representing absence of outliers

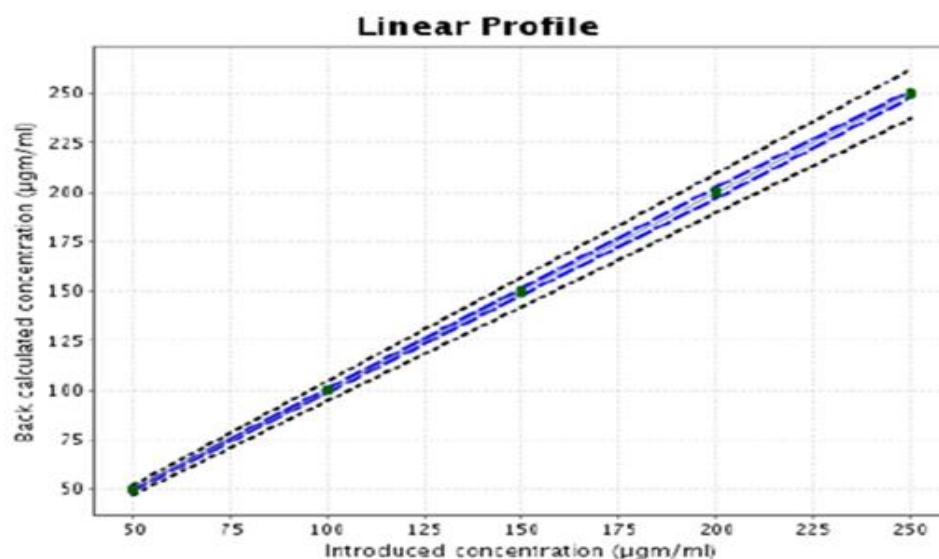


Figure 3.20: Plot of linear regression model of back calculated concentrations versus the introduced concentrations. (plain line = identity line ($Y = X$); Dashed line = Accuracy Profile; dotted curves = the acceptance limits. The method is considered to be valid within the range for which the dashed curves lie within dotted acceptance limits)

3.4.2.3.3 Trueness

The percentage relative bias of the method was calculated to justify the trueness of the method. As shown in table 3.15 it can be concluded that the trueness for all concentrations is acceptable, since the percentage relative bias is limited between -0.0059 % to 0.1906 %, furthermore its percentage recovery lies within 95% confidence interval.

Table 3.15: Results of trueness study

Conc. Level	Mean introduced conc. (µg/ml)	Mean Back calculated conc. (µg/ml)	Absolute Bias (µg/ml)	Relative Bias (%)	Recocery (%)	95% confidence interval of recovery (%)
1	50	49.90	- 0.1041	- 0.2082	99.79	[99.58 , 100.0]
2	100	100.2	0.1906	0.1906	100.2	[100.0 , 100.4]
3	150	149.9	- 0.1065	- 0.0710	99.93	[99.67 , 100.2]
4	200	199.7	- 0.2554	- 0.1277	99.87	[99.55 , 100.2]
5	250	250.0	- 0.01489	- 0.0059	99.99	[99.80 , 100.2]

3.4.2.3.4 Precision

The results of precision for both intermediate precision and repeatability were less than 2% (in terms of %RSD), which suggested that the developed chromatographic method was reproducible and precise. Table 3.16 represent the results of relative and absolute intermediate precision and repeatability which justifies the reproducibility of the method. Further 95% confidence upper limit have also been demonstrated.

Table 3.16: Results of absolute and relative intermediate precision and repeatability

Conc. (µg/ml)	Relative intermediate precision and repeatability			Absolute intermediate precision and repeatability		
	Rep (%RSD)	IP (%RSD)	95% Upper confidence limit	Rep (SD)	IP (SD)	Ratio of variance

			Rep (SD) (µg/ml)	IP (%R SD)			component s (Between/ within)
50	0.214	0.296	0.205	0.535	0.107	0.148	0.9008
100	0.167	0.262	0.320	0.997	0.167	0.262	1.454
150	0.276	0.362	0.794	1.909	0.414	0.543	0.7143
200	0.342	0.449	1.312	3.168	0.685	0.899	0.7258
250	0.236	0.259	1.133	1.991	0.591	0.649	0.2048

Rep= repeatability, IP= intermediate precision, RSD= relative standard deviation, SD= standard deviation

3.4.2.3.5 Accuracy

Standard addition method was utilized to evaluate the accuracy of the method using matrix of synthetic mixture. Accuracy takes into account the total error of the test results and is represented by the β -expectation tolerance limits. The accuracy obtained by considering linear regression model has been presented in table 3.17. It was also found that the β -expectation tolerance limits did not exceed the acceptance limits, which indicates that tolerance limits included the β -percent (95%) of the future measurement of unknown samples and is shown by accuracy profile illustrated in figure 3.21. Risk profile (figure 3.22) justified the accuracy profile of the method by choosing maximum risk level at 5.0%. It was concluded that the risk of outliers are within limits and future analysis of unknown sample will fall within the range.

Table 3.17: Result of accuracy study in terms of relative beta-expectation tolerance limits and risk assessment obtained by linear regression model

Matrix	Conc. (µg/ml)	Beta expectation tolerance limits (µg/ml)	Relative beta expectation tolerance limits (%)	Risk (%)
Synthetic mixture	50	[49.46,50.34]	[1.089, 0.6728]	0.00638
	150	[148.3,151.5]	[1.111, 0.9689]	0.00827

250

[248.3,251.7]

[0.6720, 0.6600]

0.00007

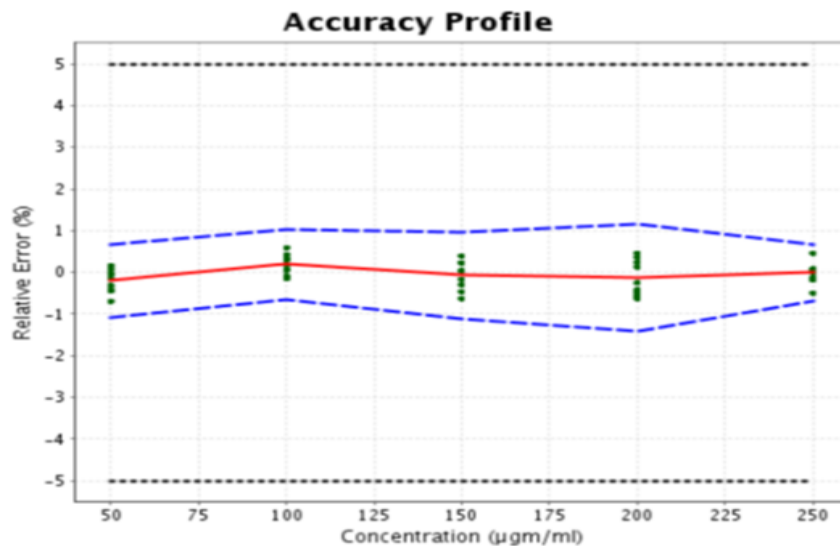


Figure 3.21: Accuracy profile obtained by considering Linear Regression Model (plain red line = the relative bias, dashed lines = β -expectation tolerance limits; dotted lines = the acceptance limits; dots = relative error of the back calculated concentrations plotted against targeted concentration)

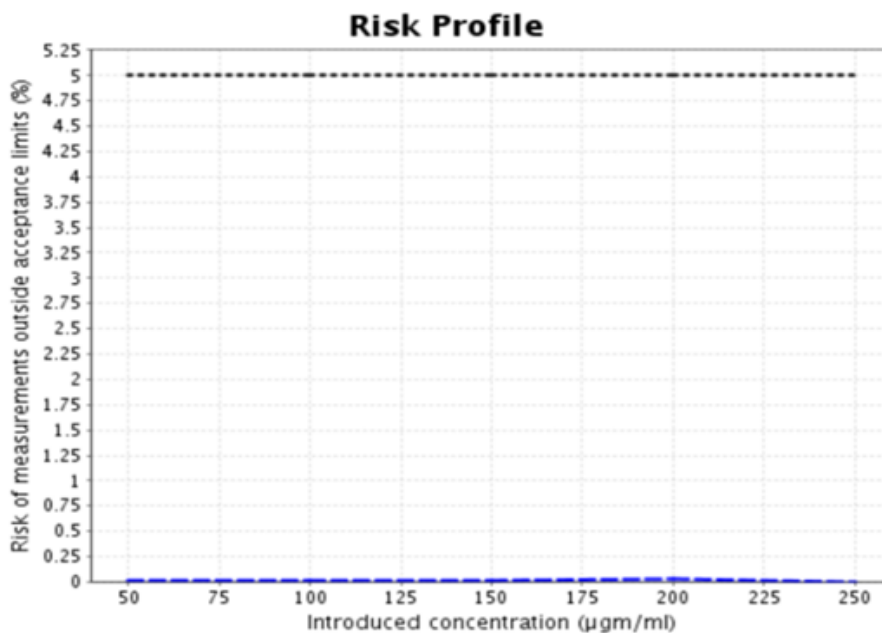


Figure 3.22: Risk profile obtained by considering Linear Regression Model (dotted line represents the 5.0 % risk level)

3.4.2.3.6 LOD and LOQ

The LOD and LOQ for developed method were found to be 1.422 and 4.309 µg/ml, respectively. This indicates that the developed method had enough sensitivity to analyze the marketed formulations.

3.4.2.3.7 Robustness studies

Small but deliberate changes in the flow rate, column oven temperature, organic ratio in mobile phase, pH and detection wavelength were made to study the robustness of the developed method and were determined in the form of % RSD. Table 3.18 represents the results of robustness study, showing the effect of variation on area of analyte, Rt, tailing factor and number of theoretical plates. From these results it is concluded that the method has capacity to withstand some extent of human or system errors.

Table 3.18: Results of robustness study

Chromatographic changes	Observation			
	Area (% RSD)	Rt (% RSD)	Tailing Factor (% RSD)	Theoretical plates (% RSD)
Flow Rate (ml/min)				
0.9	0.48	0.66	0.59	0.35
1.0	0.40	0.59	0.55	0.30
1.1	0.45	0.61	0.54	0.32
Column oven temperature (°C)				
37	0.51	0.59	0.44	0.29
40	0.49	0.6	0.41	0.25
43	0.54	0.63	0.43	0.21
Organic Ratio				
2	0.99	0.98	0.85	0.76
4	1.00	1.2	0.81	0.75
5	0.98	1.2	0.80	0.71
pH				

4.3	0.89	0.99	0.53	0.66
4.6	0.87	0.97	0.51	0.60
4.8	0.88	0.90	0.50	0.65
Detection wavelength (nm)				
210	0.70	0.58	0.44	0.47
220	0.67	0.62	0.39	0.43

3.4.2.4 Uncertainty of Measurement

The uncertainty; expanded uncertainty; relative expanded uncertainty and uncertainty of bias; were calculated for the present method. From table 3.19 it can be concluded that the uncertainty values fall within limit so, there is no doubt that the developed method is robust.

Table 3.19: Results of uncertainty of measurements

Conc. (µg/ml)	Uncertainty (µg/ml)	Uncertainty of the Bias (µg/ml)	Expanded Uncertainty (µg/ml)	Relative Expanded Uncertainty (µg/ml)
50	0.06891	0.1634	0.3268	0.6535
100	0.1291	0.2921	0.5841	0.5841
150	0.2452	0.5959	1.192	0.7946
200	0.4070	0.9876	1.975	0.9876
250	0.2506	0.6962	1.392	0.5570

3.4.2.5 Stress degradation studies

As presented in figure 3.16 six DPs were formed under stress conditions when mixture of DPs was analyzed in LC-PDA. The summary of forced degradation condition with % degradation (% Deg), DPs formed with Rt in various stress conditions is presented in table 3.20. The % Deg is calculated by the formula:

$$\% \text{ Deg} = \frac{\left[\begin{array}{l} \text{(Initial area of untreated stock solution} \\ \text{– reduced area of treated stock solution)} \end{array} \right]}{\text{Actual initial area of untreated stock solution}} \times 100$$

PDM was most sensitive towards oxidative degradation. It undergoes significant degradation under base and acid degradation. Slight degradation was observed under neutral, photolytic and thermal-humidity degradation condition. The drug is most stable under dry heat induced degradation. The chromatograms of individual stressed samples are shown in figure 3.23. Also peak purity plot for individual stress degradation condition of acid, base, neutral, oxidative, photolytic and thermal-humidity induced degradation are presented in figure 3.24-3.29 respectively along with peak purity studies in table 3.21-3.26.

Table 3.20: Summary of stress degradation of PDM API and synthetic mixture

Stressor Type	Stressor Conc.	Time	DPs formed with Rt	% Deg (API)	% Deg (synthetic mixture)
Acid degradation	0.8 N, 80 ⁰ C	3 Hrs	DP-1(2.88), DP-2(3.40), DP-3(3.74), DP-4(12.22)	46.44	46.21
Base degradation	0.1 N, 80 ⁰ C	3 Hrs	DP-5(2.36) DP-1(3.01), DP-2(3.43), DP-3(3.82), DP-4(12.86)	61.25	60.99
Neutral degradation	80 ⁰ C	6 Hrs	DP-5(2.48), DP-1(2.91), DP-4(12.22)	10.4	10.1
Oxidative degradation	0.01 %, 80 ⁰ C	1.5 Hrs	DP-1(2.94), DP-2(3.24), DP-3(3.79), DP-6(6.19)	75.38	74.14

Photolytic degradation	--	21 days	DP-1(2.90), DP-2(3.28), DP-3(3.86), DP-4(12.36)	8.25	8.0
Dry Heat induced degradation	80 ⁰ C	21 days		No degradation	
Thermal Humidity induced degradation	40 ⁰ C±2 ⁰ C and 75 ⁰ C±5 ⁰ C	21 days	DP-1(2.91), DP-3(3.84), DP-4(11.98)	5.2	5.0

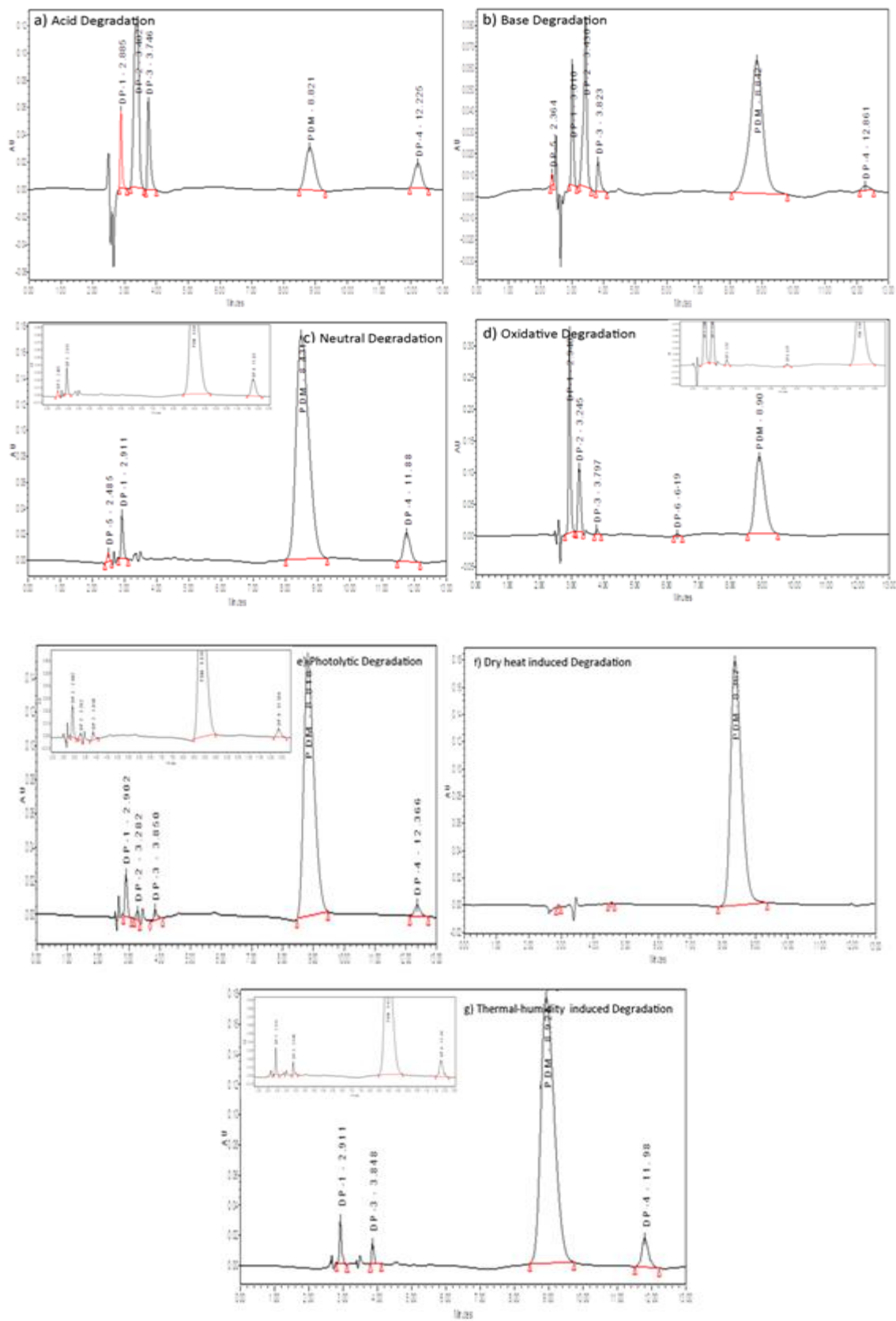


Figure 3.23: Chromatograms of a) Acid degradation, b) Base degradation, c) Neutral degradation, d) Oxidative degradation e) Photolytic degradation, f) Dry heat induced degradation and d) Thermal-humidity induced degradation

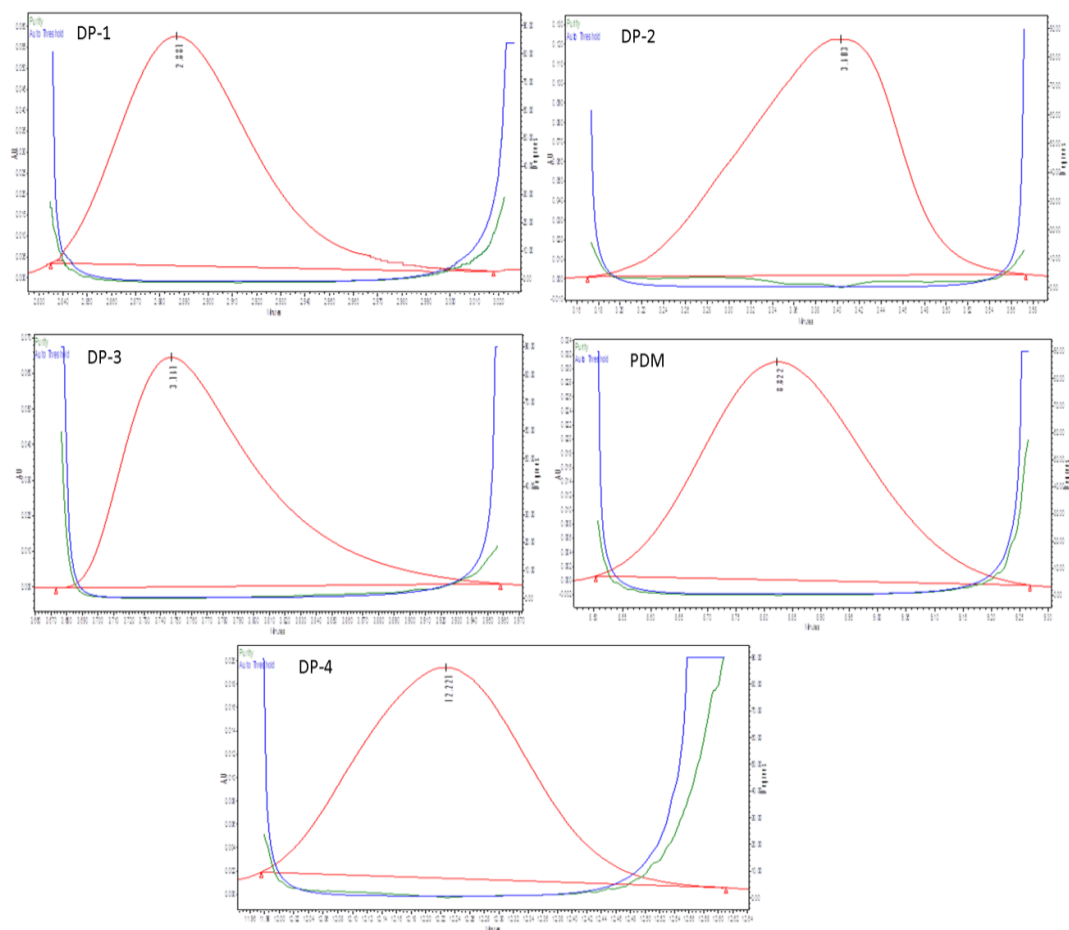


Figure 3.24: Peak purity plots for acid degradation

Table 3.21: Peak purity studies for acid degradation

S. No.	Peaks	Rt	Peak purity angle	Peak purity threshold
1.	DP-1	2.885	0.289	0.387
2.	DP-2	3.402	0.227	0.275
3.	DP-3	3.746	0.401	0.453
4.	PDM	8.821	0.390	0.561

5.	DP-4	12.225	0.956	1.130
----	------	--------	-------	-------

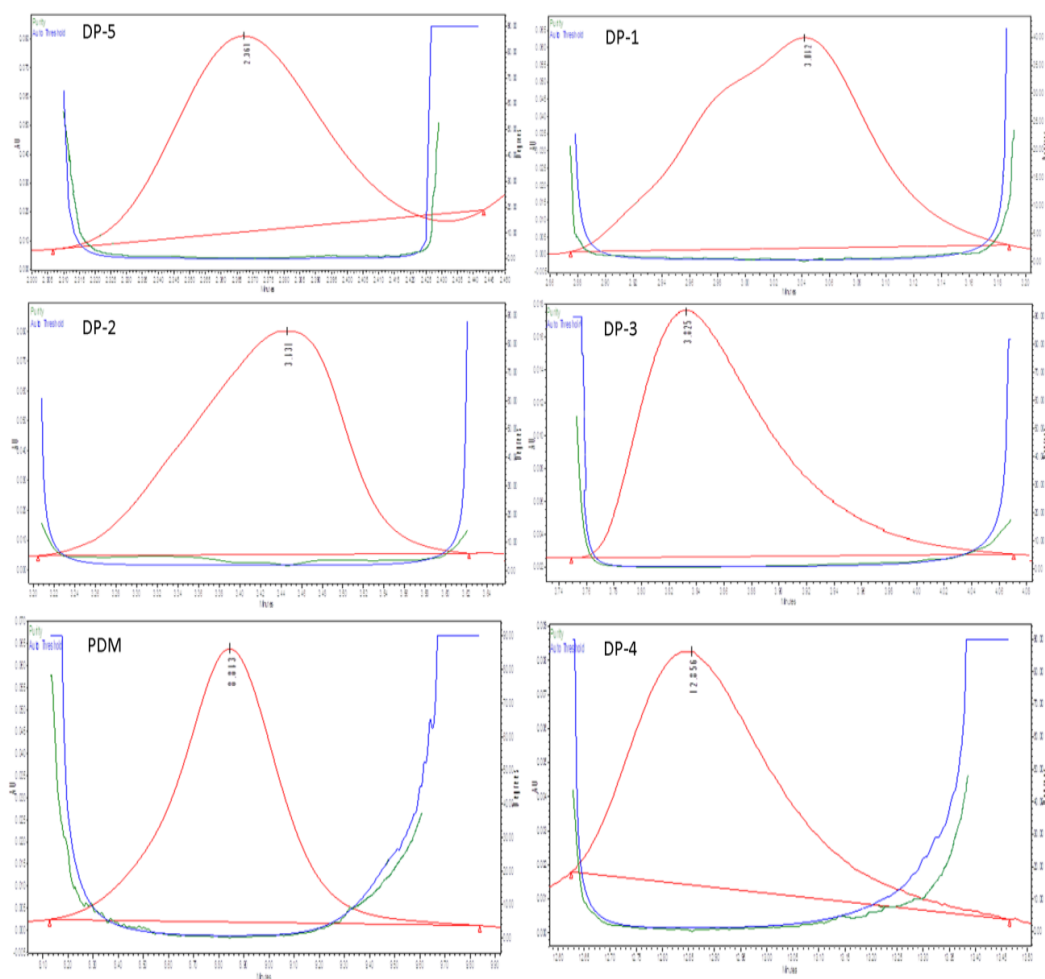


Figure 3.25: Peak purity plots for base degradation

Table 3.22: Peak purity studies for base degradation

S. No.	Peaks	Rt	Peak purity angle	Peak purity threshold
1.	DP-5	2.364	3.050	4.176
2.	DP-1	3.010	0.555	0.606
3.	DP-2	3.430	0.546	0.816
4.	DP-3	3.823	0.333	0.407
5.	PDM	8.842	0.421	0.522
6.	DP-4	12.861	0.433	0.479

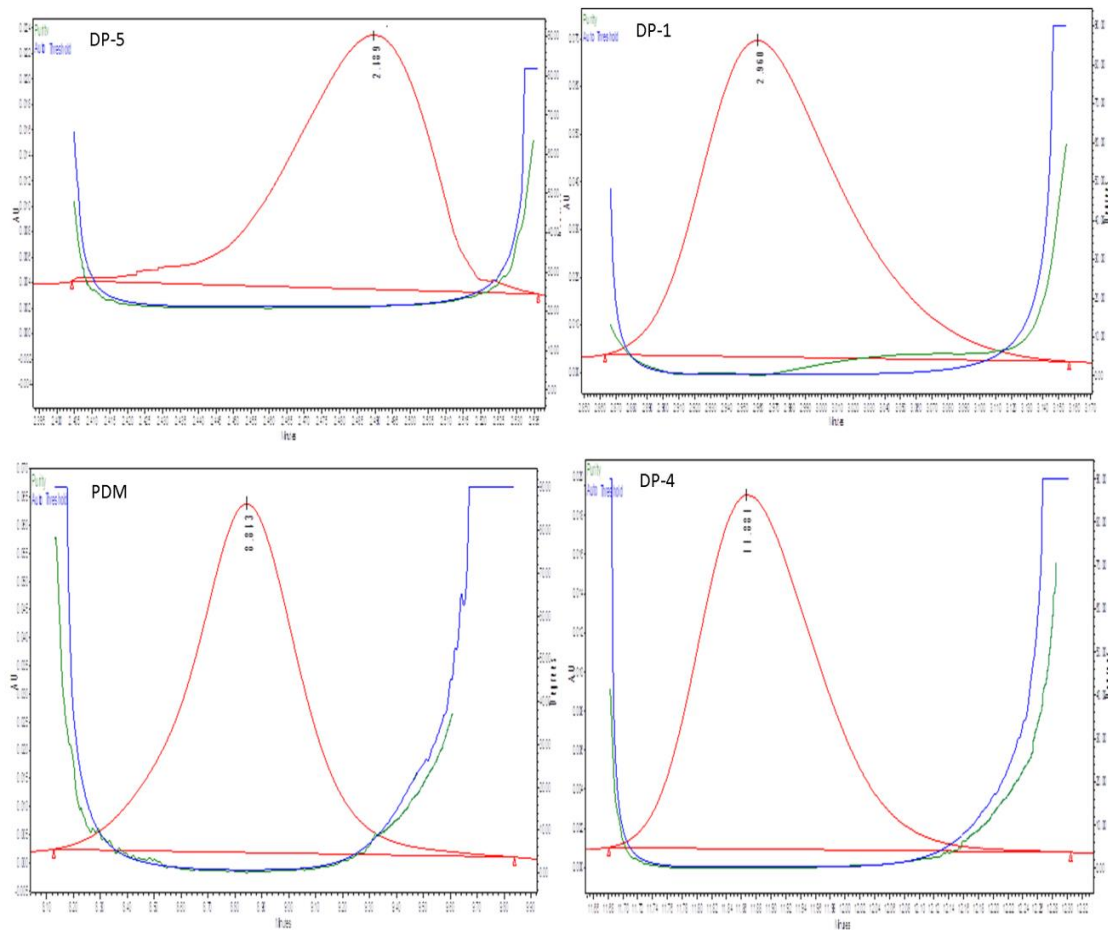


Figure 3.26: Peak purity plots for neutral degradation

Table 3.23: Peak purity studies for neutral degradation

S. No.	Peaks	Rt	Peak purity angle	Peak purity threshold
1.	DP-5	2.485	3.158	3.484
2.	DP-1	2.911	0.436	0.641
3.	PDM	8.816	0.276	0.351
4.	DP-4	12.366	0.416	0.597

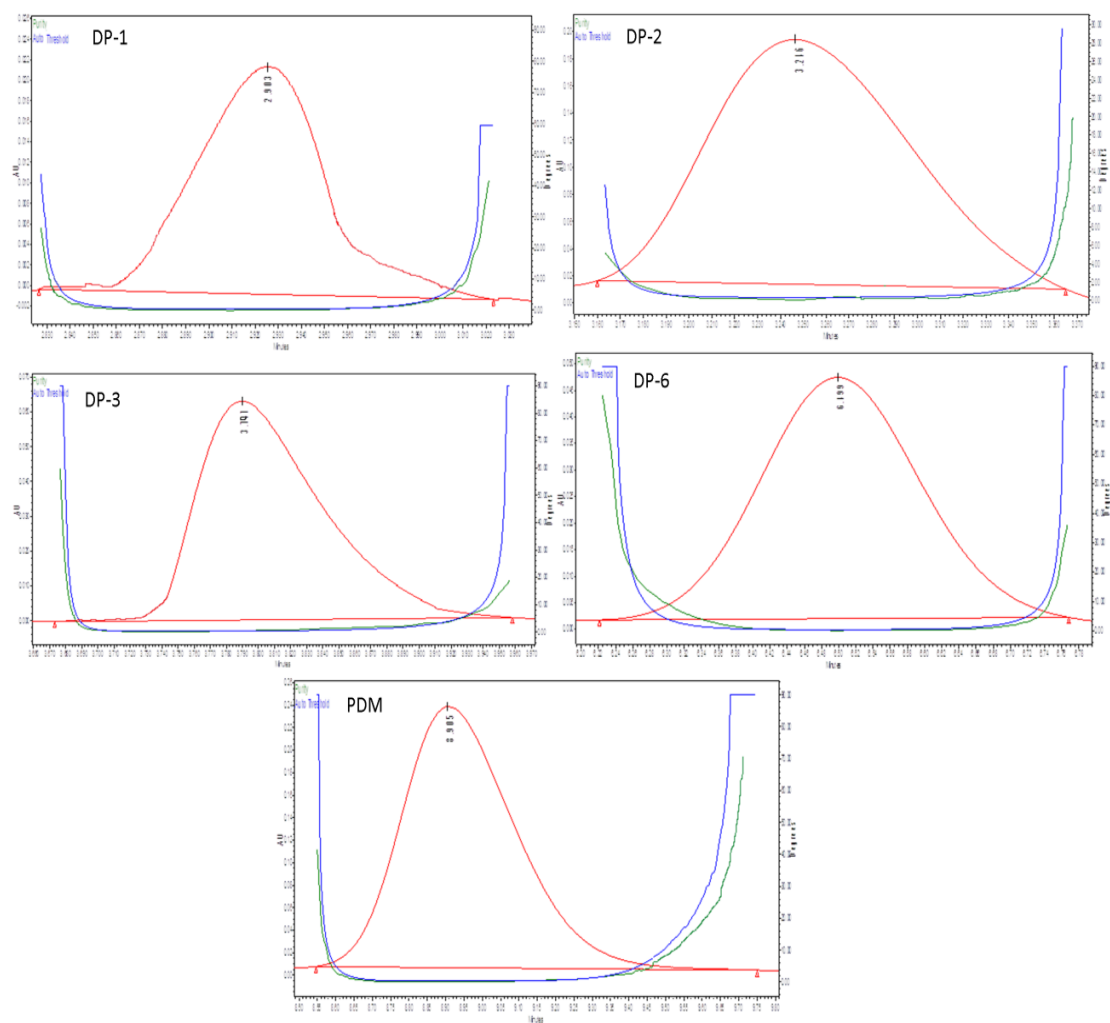


Figure 3.27: Peak purity plots for oxidative degradation

Table 3.24: Peak purity studies for oxidative degradation

S. No.	Peaks	Rt	Peak purity angle	Peak purity threshold
1.	DP-1	2.940	0.289	0.387
2.	DP-2	3.245	0.511	1.870
3.	DP-3	3.797	0.453	0.401
4.	DP-6	6.190	0.161	0.215
5.	PDM	8.907	0.390	0.561

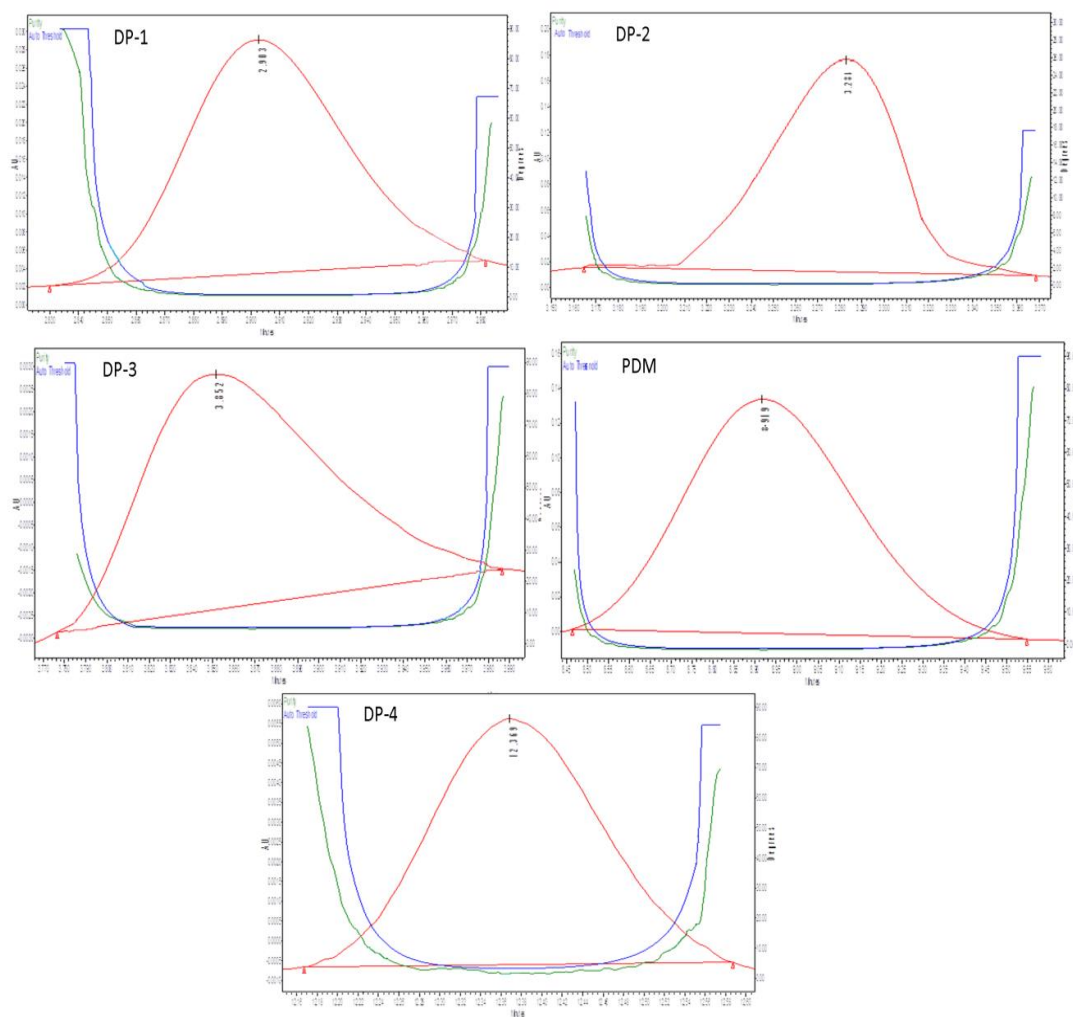


Figure 3.28: Peak purity plots for photolytic degradation

Table 3.25: Peak purity studies for photolytic degradation

S. No.	Peaks	Rt	Peak purity angle	Peak purity threshold
1.	DP-1	2.902	1.524	1.892
2.	DP-2	3.282	0.303	0.888
3.	DP-3	3.850	0.385	0.841
4.	PDM	8.810	0.436	0.641
5.	DP-4	12.366	0.240	0.397

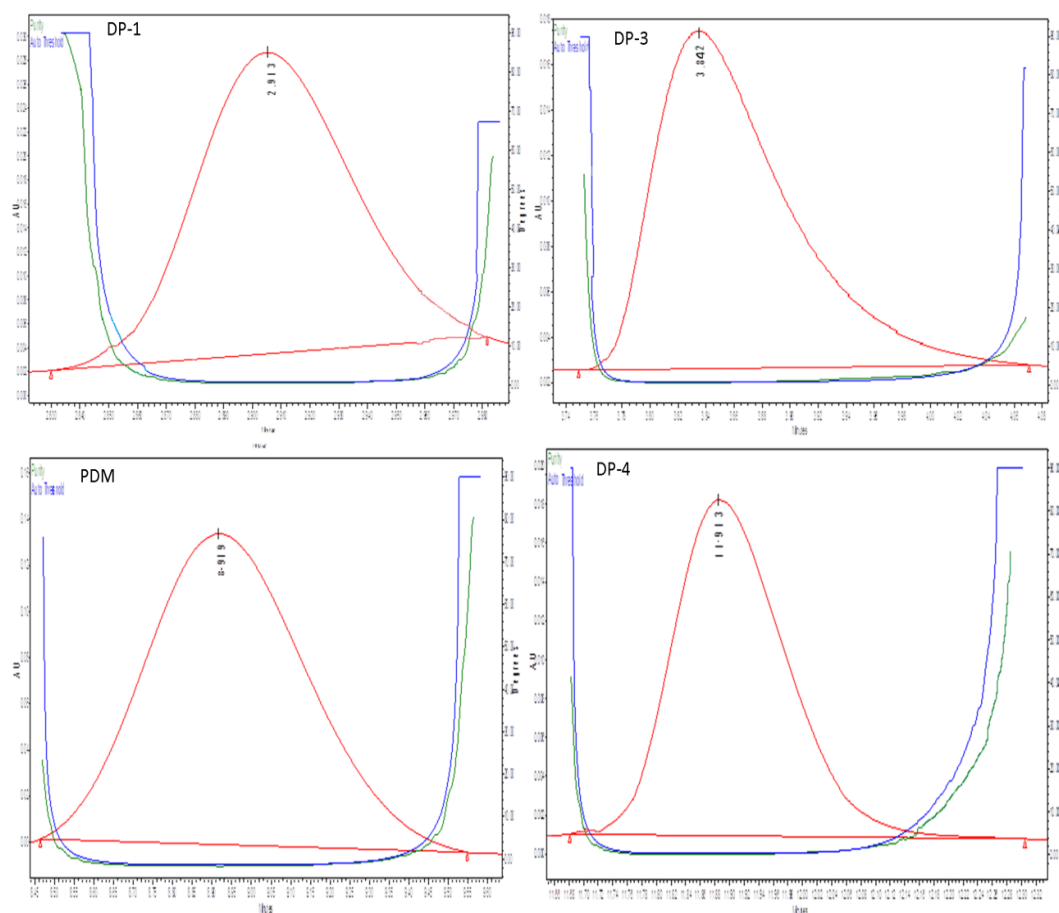


Figure 3.29: Peak purity plots for thermal-humidity induced degradation

Table 3.26: Peak purity studies for thermal-humidity induced degradation

S. No.	Peaks	Rt	Peak purity angle	Peak purity threshold
1.	DP-1	2.911	1.974	2.048
2.	DP-3	3.848	0.254	0.565
3.	PDM	8.921	0.269	0.412
4.	DP-4	11.98	3.263	4.441

3.4.2.6 Applicability of developed stability indicating assay method for analysis of formulation (Synthetic mixture)

The developed method was used to analyze stress degraded samples of a formulation containing PDM prepared in laboratory (synthetic mixture). The composition of synthetic mixture is shown in table 3.1. Stress degradation were carried out under same condition as specified for API and analyzed in the same way by same chromatographic condition. The degradation products were discernible and well separated. As presented in table 3.20 minor variation was observed in degradation of API and formulation.

3.5. SECTION –B

DEGRADATION KINETIC STUDY OF PIDOTIMOD BY HPLC METHOD

The degradation kinetics were studied for acid, base, neutral, oxidative and photolytic degradation, as Pidotimod (PDM) was susceptible to these degradation conditions.

3.5.1 EXPERIMENTAL

3.5.1.1 Chemicals and Reagents

The chemicals and reagents utilized in present section were same as described in section 3.4.1.1.

3.5.1.2 Equipments and Chromatographic Conditions

Same instruments and chromatographic conditions were utilized as described in section 3.4.1.2 for degradation kinetic study.

3.5.1.3 Preparation of Stock, Sample and Buffer solutions

Standard and stock solutions were prepared in same solvent with same dilutions as described in section 3.4.1.3. For preparation of sample solutions for kinetic study 5 mL of the sample solutions were withdrawn at different time intervals, placed into a 10 mL volumetric flask, neutralized with equivalent strength of NaOH/HCl, in case of acid and base degradation. The volume was completed with mobile phase and filtered through 0.2 μm membrane filter before HPLC analysis. The solutions (initial concentration $C_0 = 200 \mu\text{g/ml}$) were injected using the chromatographic conditions of the HPLC method described in section 3.4.1.2 using same column.

The % of drug degradation (% Deg) was calculated from the formula:

$$\% \text{ Deg} = \frac{\left[\begin{array}{l} \text{(Initial area of untreated stock solution} \\ \text{– reduced area of treated stock solution)} \end{array} \right]}{\text{Actual initial area of untreated stock solution}} \times 100$$

3.5.2 RESULTS AND DISCUSSION

The degradation rate kinetics were determined using linear regression analysis by plotting % of drug degradation (% Deg) versus time (for zero-order process), log of % Deg versus time (for first-order process) and $1/\% \text{ Deg}$ versus time (for second-order process). Experiments were done in triplicate and average values were considered for the analysis. Also, the arrhenius plots were constructed to study the effect of temperature on the rate of hydrolysis and oxidation. The rate constant (K_{obs}), half-life ($t_{1/2}$) and activation energy (E_a) were also calculated from the slope of lines at each temperature for acid, base, neutral and oxidative degradation conditions.

3.5.2.1 Kinetics of acid, base and oxidative degradation

The r^2 values for acid, base and oxidative degradation indicates that these conditions followed first order kinetics as r^2 values are highest (almost near to 1) for first order reaction. The regression equation and r^2 value for zero, first and second order reaction for acid, base and oxidative degradation conditions are presented in table 3.27-3.29 respectively. Finally after studying different parameters that affected the rate of the degradation it was concluded that the degradation rate is directly proportional to temperature and strength of stressor.

In order to demonstrate the effect of temperature on the rate constant the arrhenius plots were constructed (plot of log of the rate constant versus the reciprocal of the temperature). The first order reaction kinetic plots and arrhenius plot along with residual plots for acid degradation are presented in figure 3.30 and 3.31 respectively. Similarly first order reaction kinetic plots and arrhenius plot along with residual plots for base degradation are presented in figure 3.32 and 3.33 and first order reaction kinetic plots and arrhenius plot

along with residual plots for oxidative degradation are presented in figure 3.34 and 3.35 respectively.

The half- life and activation energy at different concentration and temperature were also calculated and are shown in table 3.30-3.32 for acid, base and oxidative degradation respectively.

Table 3.27: Regression equation and r^2 value for zero, first and second order reaction for acid degradation

S. No	Conc. (HCl)	Te mp.	r^2 Value			Regression Equation		
			Zero Order	First Order	Second Order	Zero Order	First Order	Second Order
1	1.5 N	60	0.9614	0.9884	0.9384	$8.1878x + 6.8815$	$0.1047x + 1.1482$	$-0.0079x + 0.0609$
		70	0.9585	0.985	0.9577	$8.6539x + 17.273$	$0.0807x + 1.3727$	$-0.0043x + 0.0382$
		80	0.9507	0.9898	0.984	$11.13x + 23.969$	$0.0771x + 1.5085$	$-0.003x + 0.027$
2	0.8 N	60	0.9804	0.9855	0.8981	$7.7629x + 4.0022$	$0.1164x + 1.0429$	$-0.0106x + 0.0765$
		70	0.9813	0.9886	0.9222	$10.519x + 9.4383$	$0.1045x + 1.2637$	$-0.0061x + 0.047$
		80	0.9626	0.9907	0.9639	$13.831x + 9.3183$	$0.1086x + 1.3423$	$-0.005x + 0.0382$
3	0.1 N	60	0.9563	0.9888	0.9342	$9.2442x - 5.7189$	$0.1684x + 0.7458$	$-0.0204x + 0.1285$
		70	0.9782	0.988	0.8755	$11.447x - 4.2125$	$0.1571x + 0.9282$	$-0.0143x + 0.0904$
		80	0.9684	0.9893	0.8922	$13.855x - 5.5735$	$0.1576x + 1.0031$	$-0.0118x + 0.0752$

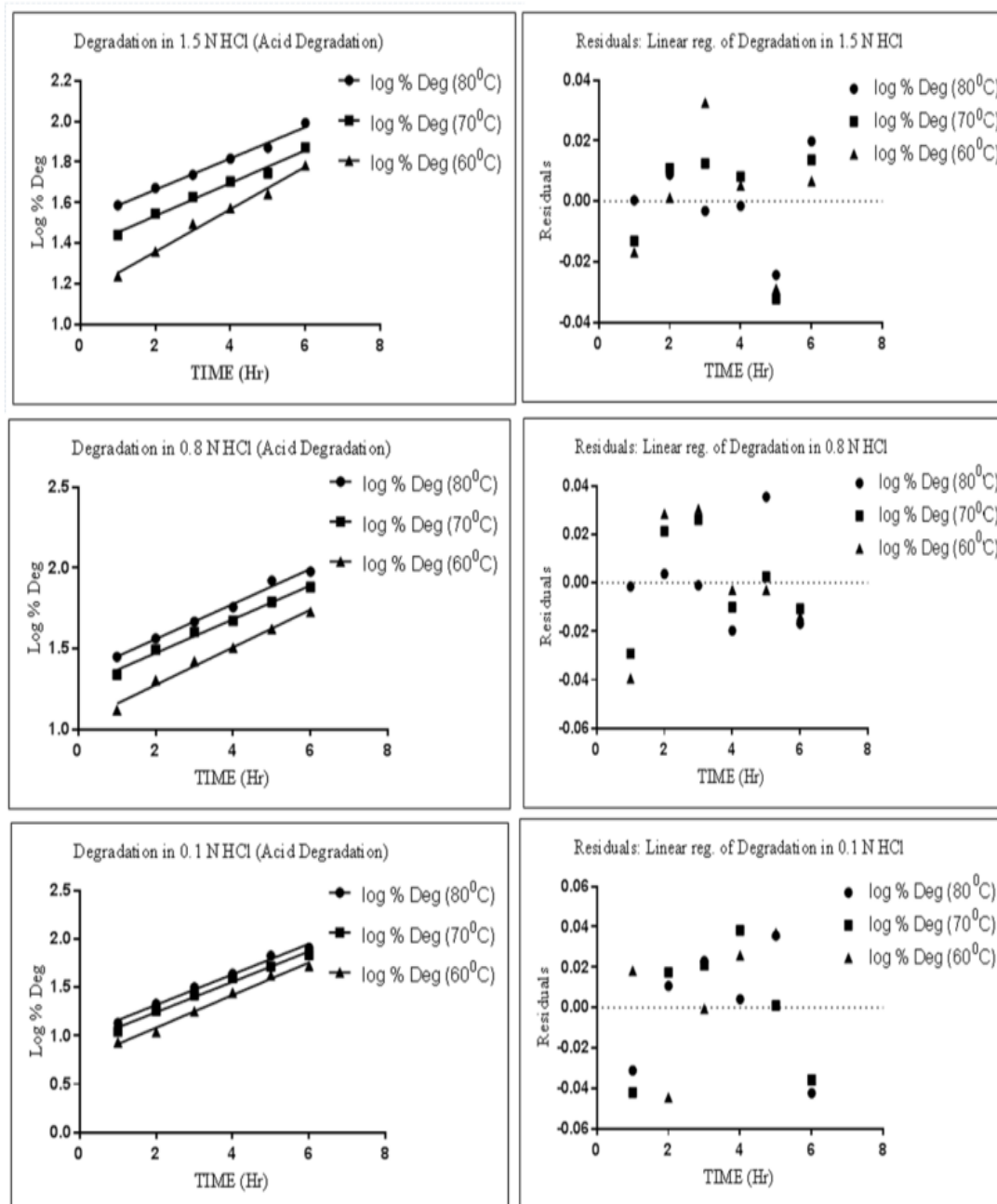


Figure 3.30: First order reaction kinetic and Residual plots for acid degradation

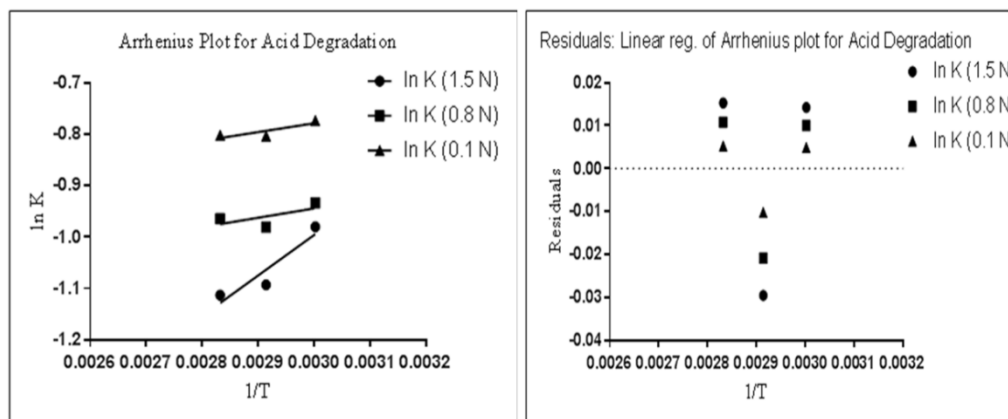


Figure 3.31: Arrhenius plot and residual plot for acid degradation

Table 3.28: Regression equation and r^2 value for zero, first and second order reaction for base Degradation

S. No	Conc. (NaOH)	Te mp.	r^2 Value			Regression Equation		
			Zero Order	First Order	Second Order	Zero Order	First Order	Second Order
1	0.2 N	60	0.9583	0.9901	0.9765	$10.441x + 20.982$	$0.0797x + 1.4592$	$-0.0034x + 0.0312$
		70	0.9819	0.9901	0.9802	$8.7526x + 32.087$	$0.0617x + 1.5689$	$-0.0024x + 0.0252$
		80	0.979	0.9889	0.9856	$9.2455x + 41.866$	$0.0543x + 1.6706$	$-0.0017x + 0.0202$
2	0.1 N	60	0.978	0.9897	0.9583	$10.824x + 6.4813$	$0.1123x + 1.2125$	$-0.0068x + 0.0513$
		70	0.9779	0.9903	0.9708	$9.4806x + 19.452$	$0.0804x + 1.4183$	$-0.0038x + 0.0344$
		80	0.9861	0.99	0.976	$8.877x + 34.573$	$0.0597x + 1.5962$	$-0.0022x + 0.0238$
3	0.02 N	60	0.9755	0.9892	0.8793	$5.6048x - 3.0235$	$0.1683x + 0.5435$	$-0.0343x + 0.212$
		70	0.9601	0.9889	0.93	$5.7076x + 4.1373$	$0.1072x + 0.9691$	$-0.012x + 0.0914$
		80	0.9434	0.9884	0.966	$6.9557x + 6.8471$	$0.0992x + 1.1138$	$-0.0082x + 0.0661$

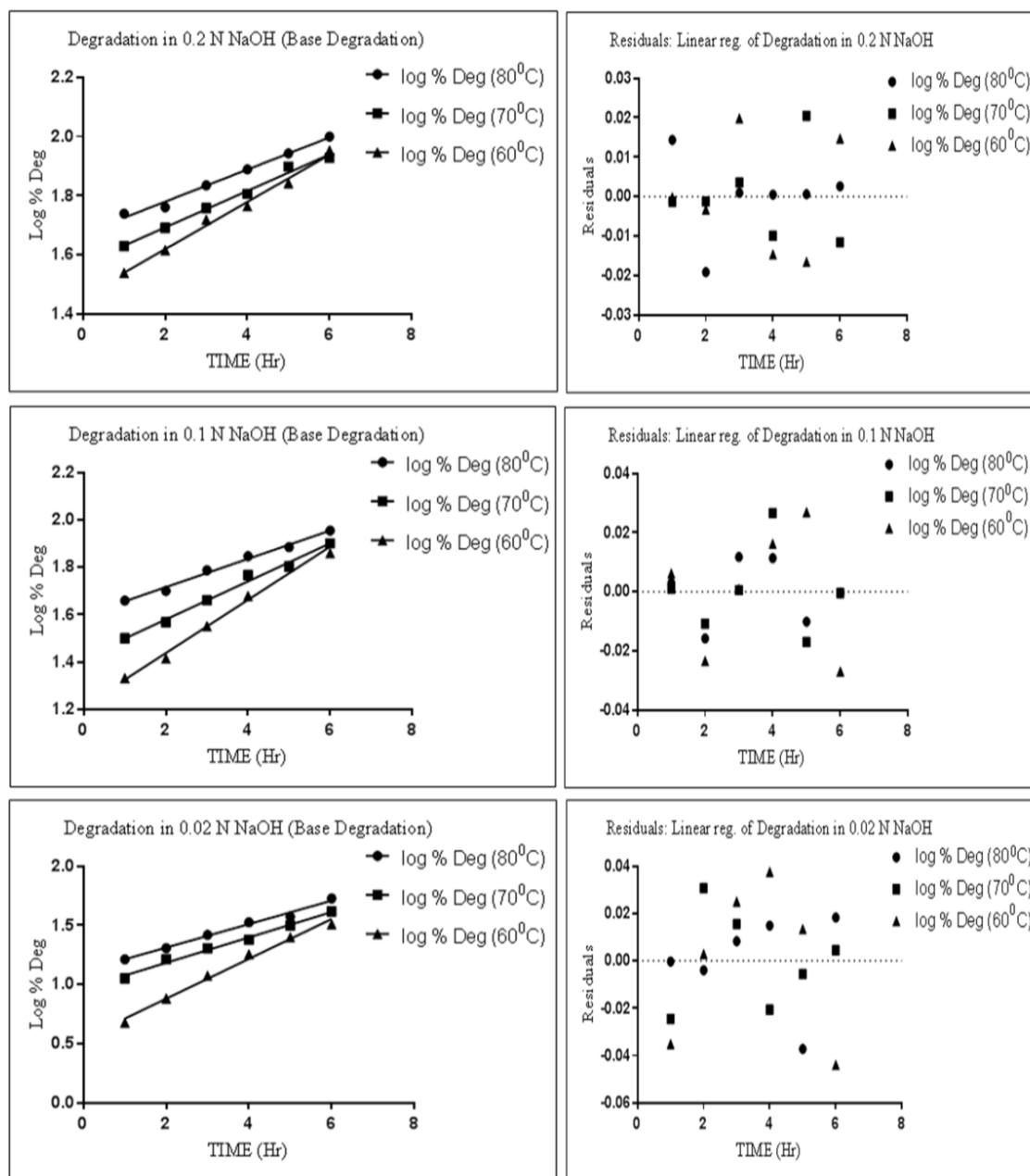


Figure 3.32: First order reaction kinetic and residual plots for base degradation

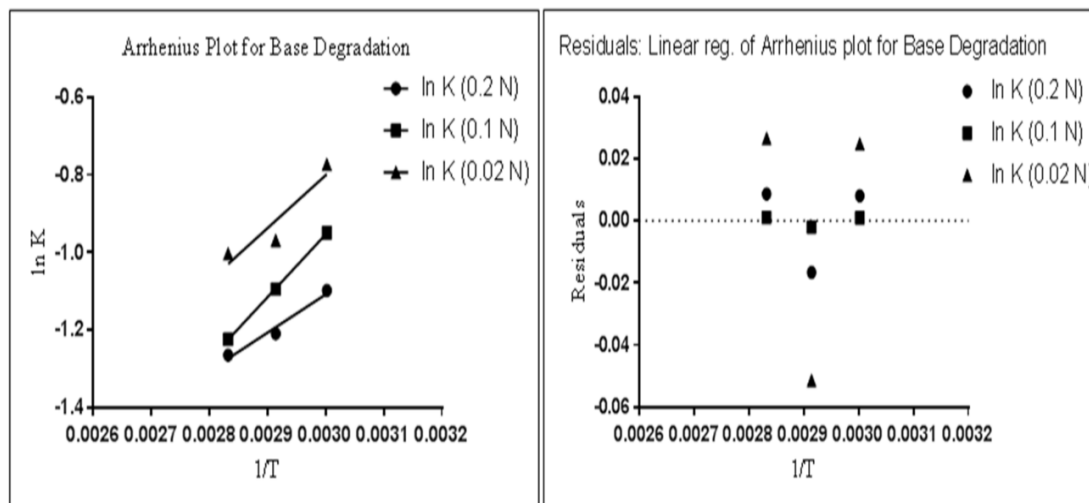


Figure 3.33: Arrhenius plot and residual plot for base degradation

Table 3.29: Regression equation and r^2 value for zero, first and second order reaction for oxidative degradation

S. No	Conc. (H ₂ O ₂)	Te mp.	r ² Value			Regression Equation		
			Zero Order	First Order	Second Order	Zero Order	First Order	Second Order
1	0.1%	60	0.9671	0.9889	0.9624	0.8636x + 7.552	0.0074x + 1.293	-0.0004x + 0.0425
		80	0.9742	0.9884	0.9683	0.8247x + 13.616	0.0065x + 1.3801	-0.0003x + 0.036
		100	0.9767	0.9904	0.979	0.6947x + 27.655	0.0048x + 1.5381	-0.0002x + 0.0265
2	0.01%	60	0.9668	0.9899	0.9094	0.7557x - 6.3704	0.0111x + 0.8501	-0.0011x + 0.1033
		80	0.9556	0.9887	0.9292	0.8007x - 3.3161	0.0098x + 1.0047	-0.0008x + 0.0758
		100	0.974	0.99	0.9563	0.8348x + 5.897	0.0077x + 1.247	-0.0004x + 0.0469
3	0.001%	60	0.9021	0.9641	0.9489	0.1137x +	0.0076x +	-0.003x +

				0.5662	0.3708	0.3468
80	0.9636	0.9894	0.9418	$0.3476x + 0.704$	$0.0085x + 0.7805$	$-0.0013x + 0.1334$
100	0.9841	0.9904	0.9254	$0.6072x + 2.986$	$0.0082x + 1.0643$	$-0.0007x + 0.0712$

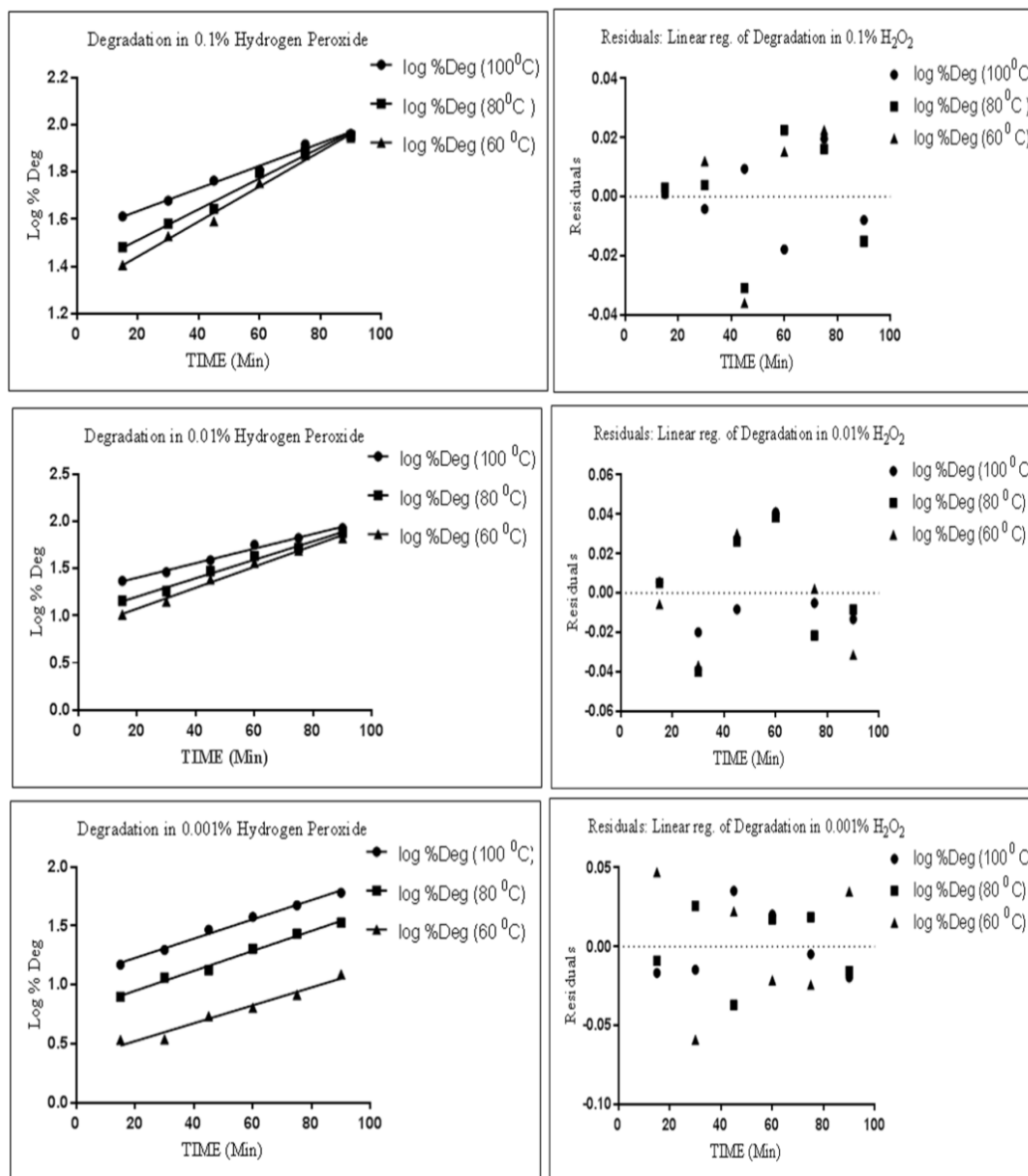


Figure 3.34: First order reaction kinetic and residual plots for oxidative degradation

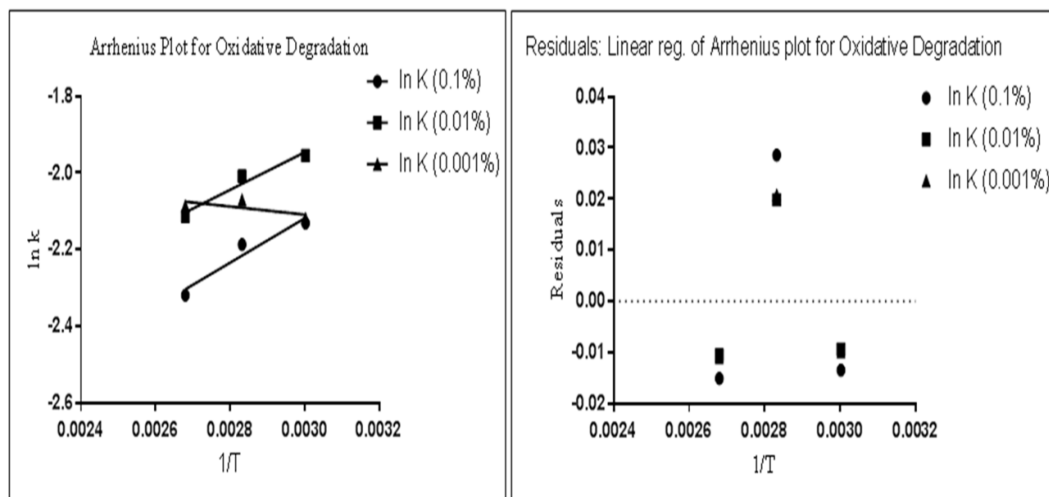


Figure 3.35: Arrhenius plot and residual plot for oxidative degradation

Table 3.30: Half- life ($t_{1/2}$) and activation energy (E_a) for first order reaction kinetic of acid degradation

S. No	Conc. (HCl)	Temp.	$t_{1/2}$ (Hr.)	E_a (kJ/mol)
1	1.5 N	60	6.6189	6.5423
		70	8.5874	
		80	8.9883	
2	0.8 N	60	5.95361	1.5030
		70	6.63158	
		80	6.38121	
3	0.1 N	60	4.11520	1.4225
		70	4.41120	
		80	4.39721	

Table 3.31: Half- life ($t_{1/2}$) and activation energy (E_a) for first order reaction kinetic of base degradation

S. No	Conc. (NaOH)	Temp.	$t_{1/2}$ (Hr.)	Ea (kJ/mol)
1	1.5 N	60	8.6951	8.1755
		70	11.2327	
		80	12.7624	
2	0.8 N	60	6.1709	13.4253
		70	8.6194	
		80	11.6080	
3	0.1 N	60	4.1176	11.3027
		70	6.4645	
		80	6.9859	

Table 3.32: Half- life ($t_{1/2}$) and activation energy (Ea) for first order reaction kinetic of oxidative degradation

S. No	Conc. (H ₂ O ₂)	Temp.	$t_{1/2}$ (min)	Ea (kJ/mol)
1	0.1%	60	93.6486	4.8158
		80	106.6153	
		100	144.375	
2	0.01% N	60	62.4324	4.0752
		80	70.7143	
		100	90	
3	0.001%	60	91.18421	0.8830
		80	81.52941	
		100	84.5122	

3.5.2.2 Kinetics of neutral and photolytic degradation

The r^2 values for neutral and photolytic degradation indicate that these conditions followed zero order degradation kinetics as r^2 values are highest (almost near to one) for zero order degradation reaction. The regression equation and r^2 value for zero, first and second order

reaction for neutral and photolytic degradation conditions are presented in Table 3.33 and 3.34 respectively. Finally after studying different parameters that affected the rate of the reaction it was concluded that the rate of degradation increases with the increase in temperature for neutral degradation and time for photolytic degradation.

In order to demonstrate the effect of temperature on the rate constant the arrhenius plot was constructed for neutral degradation. The zero order reaction kinetic plot and arrhenius plot along with residual plots for neutral degradation are presented in figure 3.36 and 3.37 respectively. Similarly zero order reaction kinetic plot with residual plot for photolytic degradation is presented in figure 3.38. The half- life and activation energy at different concentration and temperature was also calculated for neutral degradation and is shown in table 3.35.

Table 3.33: Regression equation and r^2 value for zero, first and second order reaction for neutral degradation

S. No	Tem p.	r^2 Value			Regression Equation		
		Zero Order	First Order	Second Order	Zero Order	First Order	Second Order
1	60	0.9993	0.9764	0.9208	1.202x + 2.8547	0.0785x + 0.5542	-0.0288x + 0.2566
	80	0.999	0.9908	0.9556	1.192x + 3.2047	0.073x + 0.5947	-0.0249x + 0.2343
	100	0.9991	0.9927	0.9631	1.3406x + 4.2313	0.0675x + 0.6994	-0.0187x + 0.1859

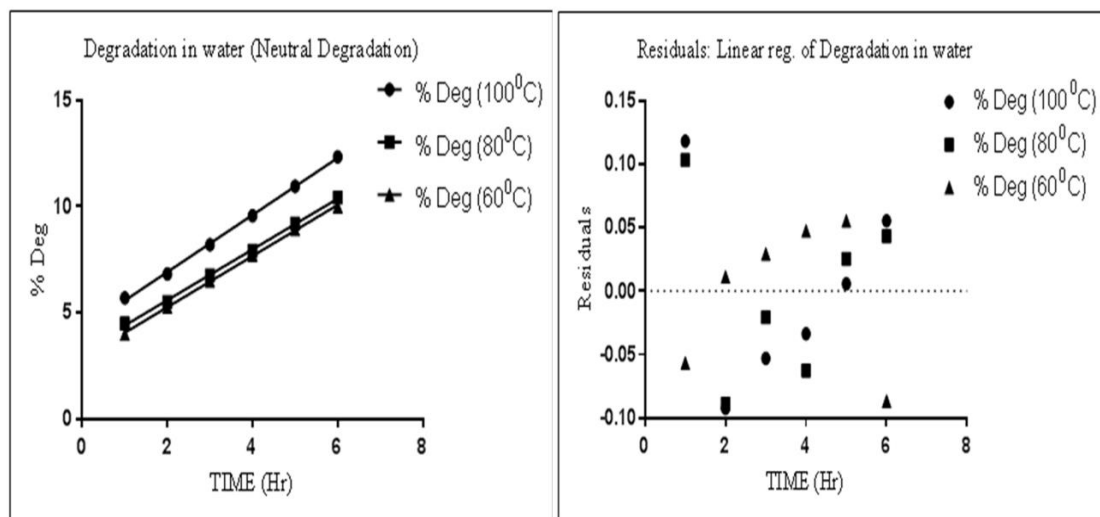


Figure 3.36: Zero order reaction kinetic plot for neutral degradation

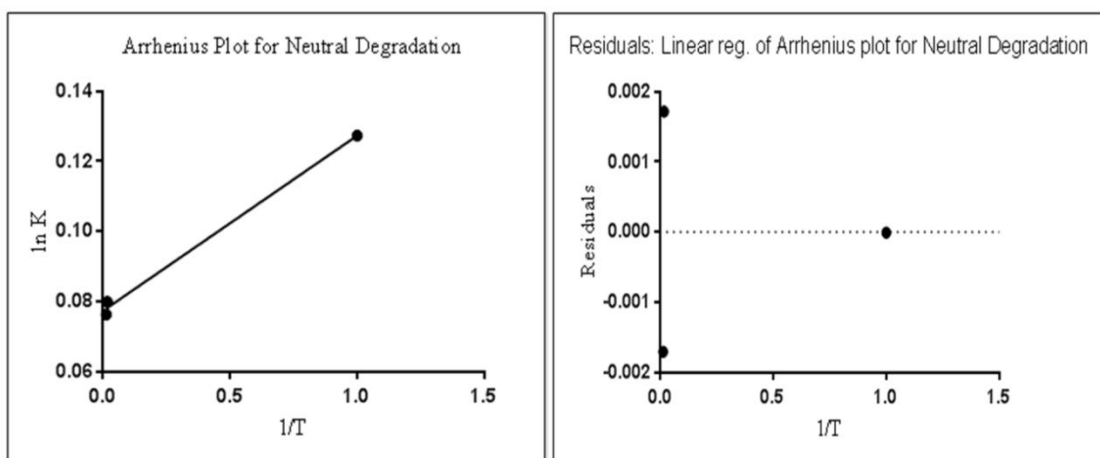


Figure 3.37: Arrhenius plot and residual plot for neutral degradation

Table 3.34: Regression equation and r^2 value for zero, first and second order reaction for photolytic degradation

S. No	r^2 Value			Regression Equation		
	Zero Order	First Order	Second Order	Zero Order	First Order	Second Order
1	0.9899	0.9827	0.9068	$0.4371x - 1.0698$	$0.0435x + 0.0423$	$-0.0266x + 0.6284$

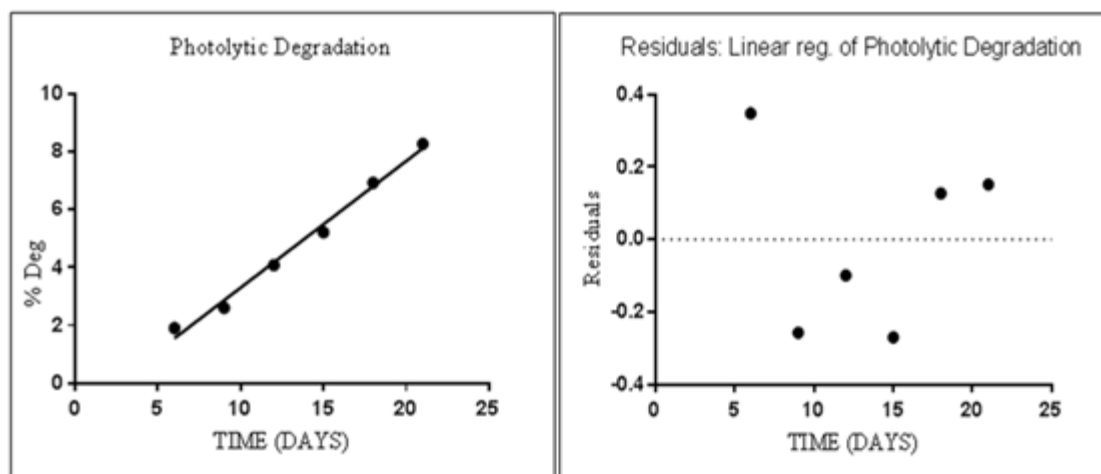


Figure 3.38: Zero order reaction kinetic for Photolytic Degradation

Table 3.35: Half- life ($t_{1/2}$) and activation energy (E_a) for zero order reaction kinetic of neutral degradation

S. No	Stressor	Temp.	$t_{1/2}$ (Hr.)	E_a (kJ/mol)
1	Neutral Degradation	60	67.03	0.0668
		80	60.1	
		100	59.6	

3.6 SECTION-C

ISOLATION AND CHARACTERIZATION OF MAJOR DEGRADATION PRODUCTS OF PIDOTIMOD

3.6.1 EXPERIMENTAL

3.6.1.1 Chemicals and Reagents

The PDM bulk drug was purchased from Swapnaroop drugs, Aurangabad, India. Analytical grade ethyl acetate, methanol (MeOH), n-butanol, dichloromethane (DCM), acetone, ninhydrine, iodine and glacial acetic acid (GAA) were procured from Spectrochem Pvt. Ltd., Mumbai. Silica gel-G for TLC was procured from Spectrochem Pvt. Ltd., Mumbai. Other chemicals and reagents utilized in present section were same as described in section 3.4.1.1.

3.6.1.2 Equipments and Chromatographic Conditions

The preparative TLC was performed on 20 cm X 20 cm (length X diameter) glass plate and 20cm X 20 cm (length X diameter) twin trough glass chamber. Other equipments and chromatographic conditions used to check % degradation and purity of isolated degradation products (DPs) were same as described in section 3.4.1.2.

3.6.1.3 Preparation of Stock, Sample and Buffer solutions

Stock, sample and buffer solutions were prepared in same way with similar dilutions as described in section 3.4.1.3.

3.6.1.4 Isolation and Characterization of Degradation Products (DPs)

Two major DPs (DP-2 and DP-4) formed during acid degradation were selected for isolation and characterization. These DPs were formed in almost all degradation condition (except neutral and thermal-humidity degradation for DP-2 and except oxidative degradation for DP-4) and were formed in higher percentage as compared to other DPs, based on HPLC peak area. The appropriate quantities of the DPs were prepared for structure elucidation studies. The stress condition producing optimum yields of DPs were chosen based on the degradation profile and kinetic studies using same chromatographic condition and column. The % degradation and purity of isolated DPs were analyzed by HPLC.

3.6.1.4.1 Isolation of DPs

DP-2 (Rt-3.3)

Degradant enrichment

For enrichment of DP-2 about 500 mg of PDM bulk drug was dissolved in 50 mL of 1.5 N HCl and refluxed in thermostatically controlled oil bath at 100⁰C for 6 hours. The solution was then neutralized with saturated solution of sodium bicarbonate and the % degradation was checked by HPLC. The above mentioned acid degradation condition of PDM showed formation of various DPs and the same is summarized in table 3.36 with their HPLC percentage area and Rt.

Isolation and purification

DP-2 was isolated by liquid-liquid extraction (LLE) and was further purified by preparative TLC and recrystallization using suitable solvent.

Liquid-liquid extraction (LLE)

The sample containing approximately 90% of DP-2 was subjected to LLE using half of the volume of n-butanol. The residue obtained was further dissolved in one volume of n-butanol and three volumes of water and mixed well (repeated two times). The n-butanol layers were then separated. The n-butanol fractions were combined and evaporated on rotary evaporator at 90°C under reduced pressure to get the crude residue of DP-2.

Table 3.36: HPLC percentage area of DPs in sample after degradant enrichment (for DP-2)

S. No	DP	Retention Time	% Area
1	DP-1	2.8	1.14
2	DP-2	3.27	90.35
3	DP-3	3.72	1.43
4	PDM	8.74	2.97
5	DP-4	11.48	4.11

Preparative TLC

A preparative TLC was optimized to purify the crude residue obtained after LLE. Preparative TLC plates were prepared by slurry of Silica gel G. Plates were dried in air and activated in hot air oven at 100°C for 30 min. 5 mg/ml of solution was prepared from crude extract in methanol. After sample application the plates were developed in pre-saturated 20 X 20 cm twin trough glass chamber using mobile phase, n-Butanol- ethyl acetate- GAA (08:02:0.05). The bands were visualized with ninhydrine solution as both PDM and DP-2 gives purple colour. The desired band was scrapped and extracted with mixture of ethyl acetate- methanol (08:02). The combined organic layer after extraction was evaporated in rotary evaporator under reduced pressure.

Recrystallization

Finally the residue obtained after preparative TLC was recrystallized with hot ethyl acetate to get pure DP-2.

DP-4 (*Rt* 12.25)

Degradant enrichment

For enrichment of DP-4 about 500 mg of PDM bulk drug was dissolved in 50 mL of 0.8 N HCl and refluxed in thermostatically controlled oil bath at 80°C for 5 hours. The solution was then neutralized with saturated solution of sodium bicarbonate and the % degradation was checked by HPLC. The above mentioned acid degradation condition of PDM showed formation of various DPs which are summarized in table 3.37 alongwith it's HPLC percentage area and *Rt*.

Isolation and purification

The sample containing approximately 40% of DP-4 was subjected to LLE using half of the volume of ethyl acetate and ethyl acetate layer was separated. The residue obtained was further dissolved in one volume of ethyl acetate and three volumes of water and mixed well (repeated two times). The ethyl acetate layer was then separated. The ethyl acetate fractions were combined and evaporated with the help of rotary evaporator at 55°C under reduced pressure to get the crude residue of DP-4.

Table 3.37: HPLC percentage area of DPs in sample after degradant enrichment (for DP-4)

S. No	DP	Retention Time	% Area
1	DP-1	2.902	6.47
2	DP-2	3.442	14.12
3	DP-3	3.695	8.61
4	PDM	9.180	31.57
5	DP-4	12.703	39.23

Preparative TLC

A preparative TLC was optimized to purify the crude residue obtained after LLE. Preparative TLC plates were prepared by slurry of Silica gel G and activated as discussed above. 5 mg/ml

of solution was prepared from crude extract in methanol. After sample application the plates were developed in pre saturated 20 X 20 cm twin trough glass chamber using mobile phase, n-butanol- ethyl acetate (08:02). The band were visualized in ninhydrine solution and in iodine chamber as PDM gives purple colour in ninhydrine and DP-4 gives yellow colour in iodine vapour. The desired band was scrapped and extracted with ethyl acetate. The combined organic layer after extraction was evaporated in rotary evaporator under reduced pressure.

Recrystallization

Finally the residue obtained after preparative TLC was recrystallized with hot dichloromethane to get pure DP-4.

3.6.1.4.2 Structural elucidation of isolated degradation products (DPs)

Based on LC-MS/MS, FT-IR and NMR studies, the probable structure of isolated DPs were proposed.

3.6.2 RESULTS AND DISCUSSION

3.6.2.1 Isolation and Purification of DPs

3.6.2.1.1 DP-2 (*Rt* 3.3)

The analytical chromatogram during isolation which involves sequential conversion of DP-2 from other DPs are illustrated in figure 3.39. The analytical chromatogram of crude and purified DP is given in figure 40. The HPLC purity of recrystallized DP was 99.4%. The peak purity study of isolated DP-2 is shown in table 3.38 and figure 3.41.

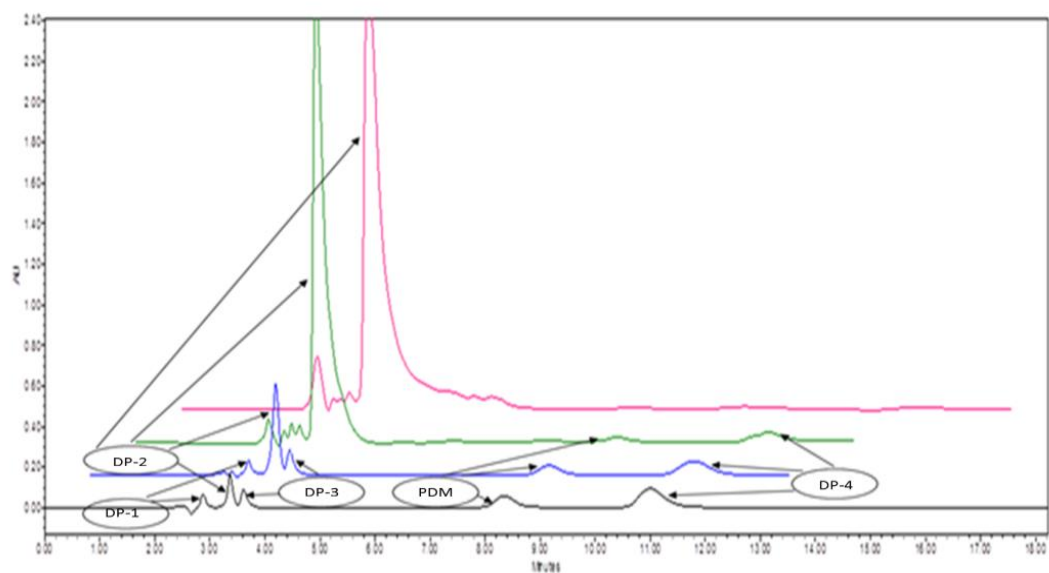


Figure 3.39: Chromatogram showing formation of DP-2

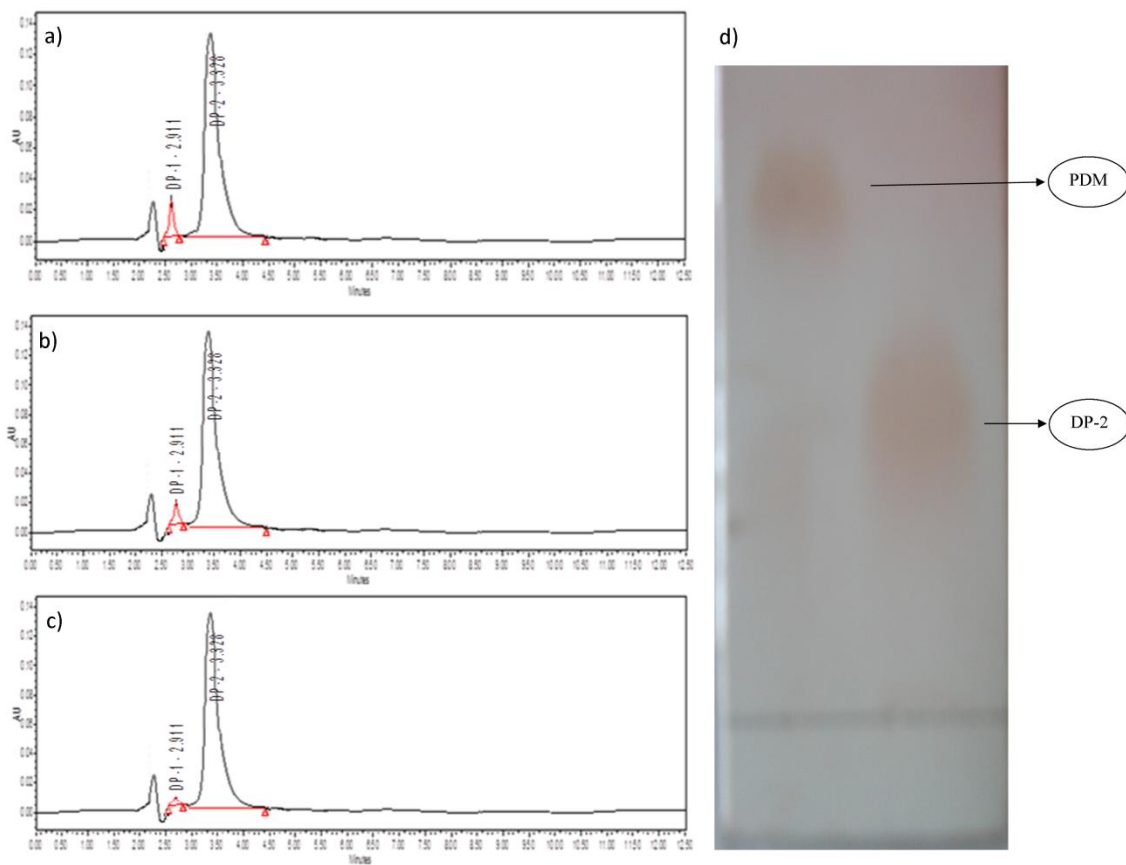


Figure 3.40: Analytical chromatogram of DP-2 a) after extraction b) after preparative TLC c) after Recrystallization d) TLC showing resolution of PDM and DP-2

Table 3.38: Peak purity study of isolated DP-2 and DP-4

S. No.	Peaks	Rt	Peak purity Angle	Peak purity Threshold
1.	DP-2	3.402	0.555	0.606
2.	DP-4	12.225	0.433	0.479

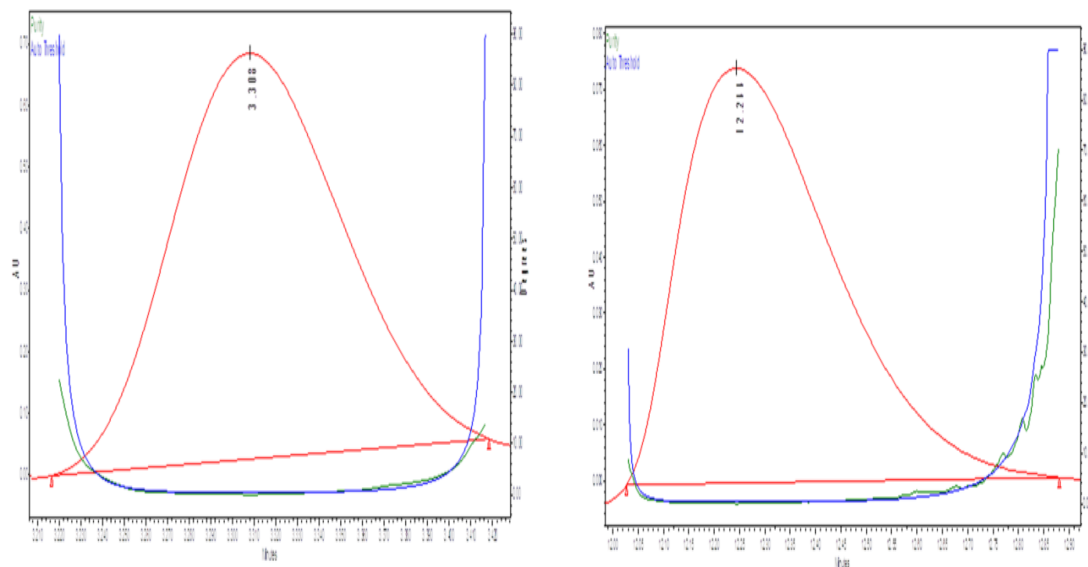


Figure 3.41: Peak purity plot for DP-2 and DP-4

3.6.2.1.2 DP-4 (Rt 12.25)

The analytical chromatogram for optimum degradation during isolation of DP-4 and analytical chromatogram of crude and purified DP is given in figure 3.42. The HPLC purity of recrystallized DP was 99.6%. The peak purity study of isolated DP-4 is shown in table 3.38 and figure 3.41.

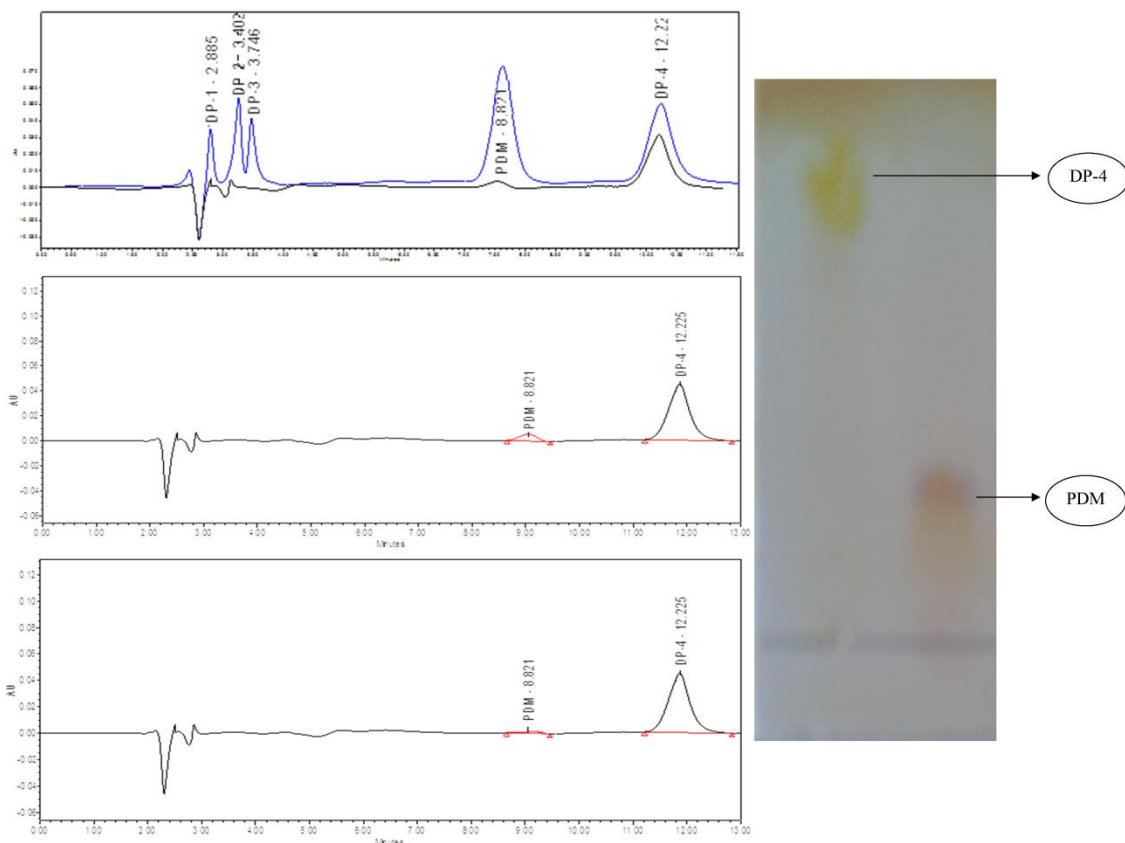


Figure 3.42: Analytical chromatogram of DP-4 a) overlay chromatogram during Isolation and after extraction b) after preparative TLC c) after Recrystallization d) TLC showing resolution of PDM and DP-4

3.6.2.2 Structural characterization of DPs

3.6.2.2.1 Characterization of DP-2

MS/MS Spectra

The molecular mass of PDM and isolated DP-2 was determined by the LC-MS/MS in positive ion mode and is shown in figure 3.43 and 3.44. The molecular weight of DP-2 is 262 which is 18 amu more as compared to the PDM. The fragmentation pattern of PDM and DP-2 are illustrated in figure 3.45.

MS/MS of PDM (m/z 245): The ESI-MS/MS spectrum of $[M+H]^+$ ion of PDM showed most abundant product ions at m/z 227 due to the loss of H_2O . The spectrum also include abundant product ions at m/z 134 corresponding to INH-2 (inherent impurity-2) (21)

Thiazolidine carboxylic acid, which further fragment to give product ions at m/z 88 due to the loss of $-\text{COO}+\text{H}_2$. In addition, the spectrum showed low abundant product ions that correspond to m/z 187.

MS/MS of DP-2 and DP-2 (e) (m/z 263): The ESI-MS/MS spectrum of the ion at m/z 263 showed two different fragmentation patterns that was observed as shouldered peak in LC-MS/MS while it was observed as single peak in LC-PDA. This may be due to presence of isomeric peak which was further confirmed by chiral separation of DP-2 in chiral column (CHIRADEX) after isolation and purification in section 3.5.5. Both showed abundant product ion at m/z 245, which correspond to either PDM or DP-4 reported by Crimella T (21), since both have same m/z . Further DP-2 showed abundant product ion at m/z 148 and DP-2 (e) at 227.

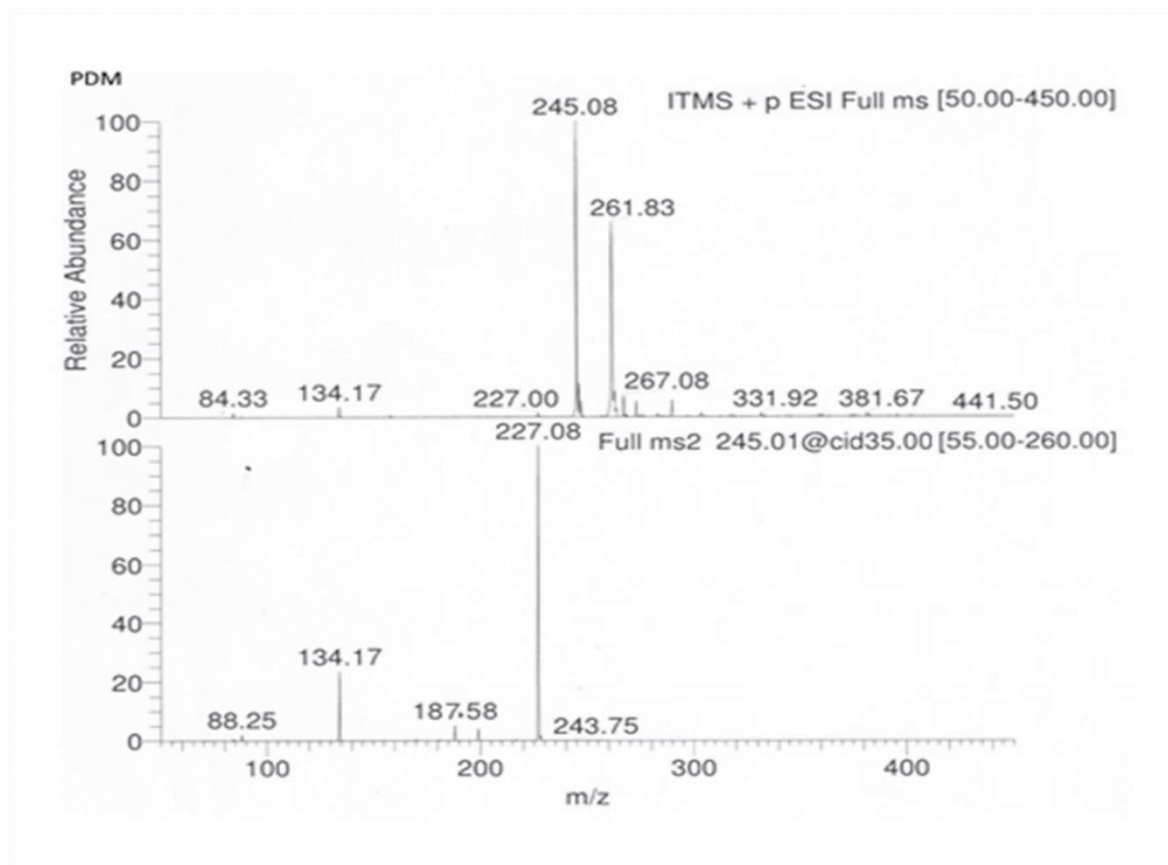


Figure 3.43: ESI-MS/MS Spectra of PDM Standard

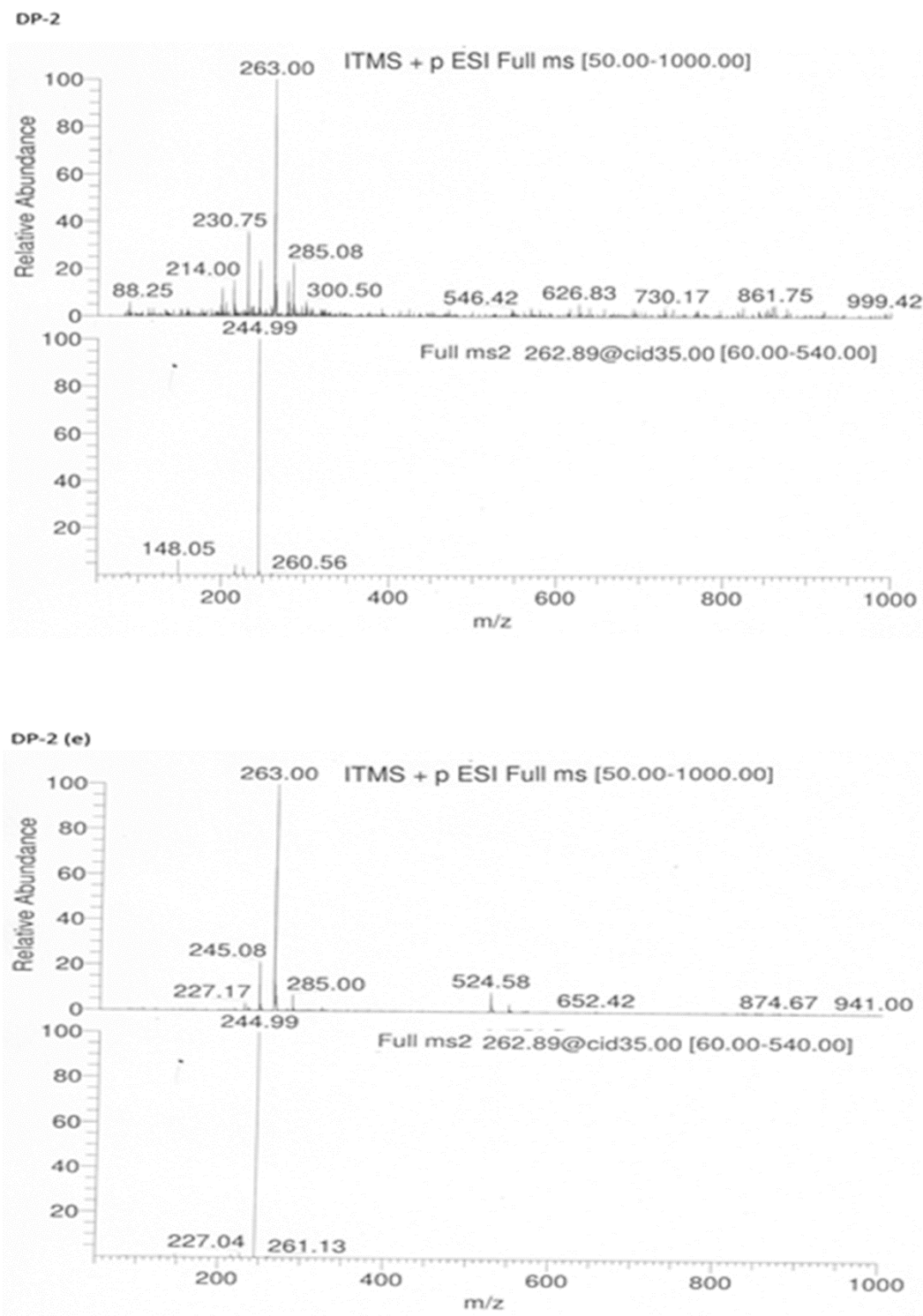


Figure 3.44: ESI-MS/MS Spectra of DP-2 and DP-2 (e)

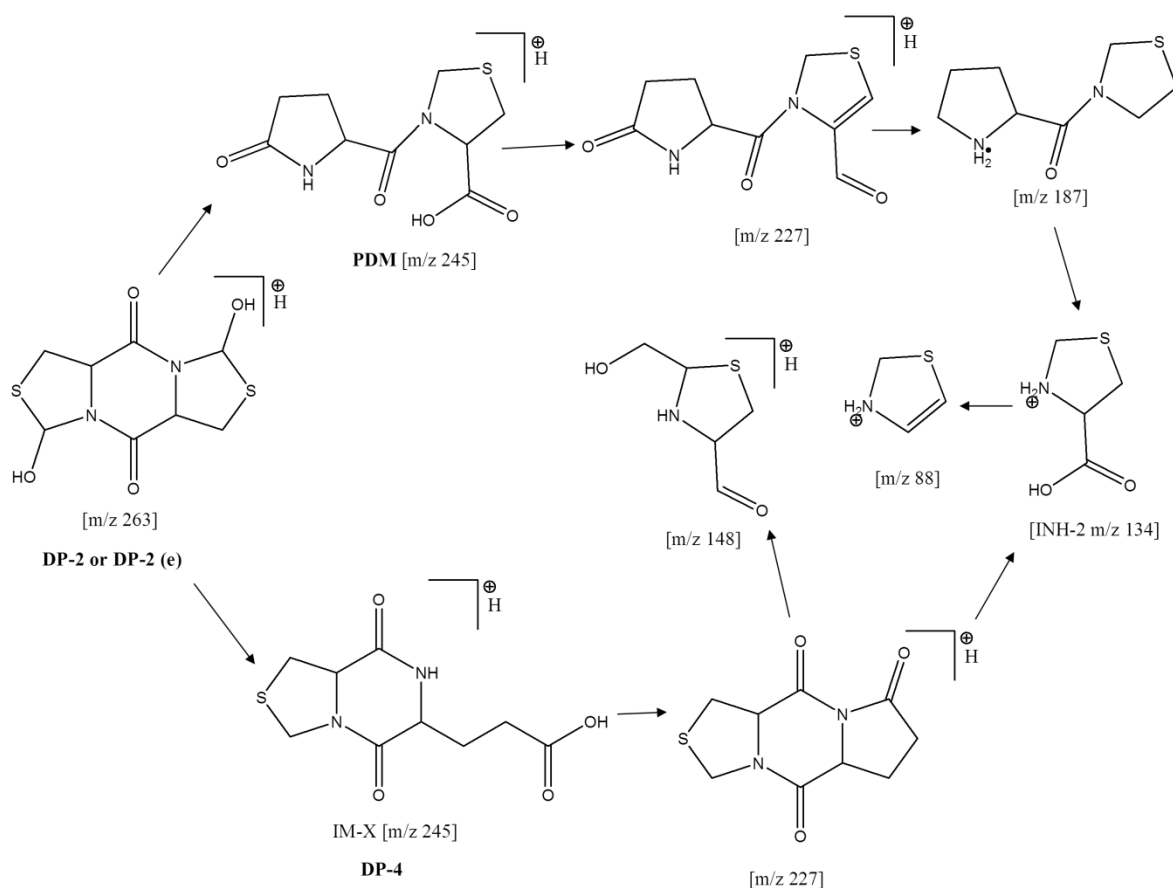


Figure 3.45: Proposed fragmentation pathway of PDM, DP-2 and DP-2 (e)

IR Spectra

In IR spectra it was observed that --OH stretching vibration at 3431 cm^{-1} in PDM standard was not changed and observed at 3447 cm^{-1} in DP-2. Similarly the C(6)O stretching vibration at 1659 was not changed and observed at 1654 cm^{-1} in DP-2. While C(12)O stretching vibration at 1705 and --NH stretching vibration at 3275 were disappeared in DP-2. The IR spectral assignment for DP-2 is presented in table 3.39. The IR Spectra of PDM standard, and DP-2 are illustrated in figure 3.46 and 3.47 respectively.

Table 3.39: IR Spectral assignments for PDM Standard, DP-2 and DP-4

Standard (PDM)		DP-2		DP-4	
Wave No (cm^{-1})	Assignments	Wave No (cm^{-1})	Assignments	Wave No (cm^{-1})	Assignments

3431.74	Stretching - OH	3447.37	Stretching - OH	3438.05	Stretching - OH
3275.00	Stretching - NH	3275.00	Stretching - NH (disappeared)	3275.00	Stretching - NH (disappeared)
1705.36	Stretching - C(12)O	1705.36	Stretching - C(12)O (disappeared)	1716.25	Stretching - C(12)O
1659.39	Stretching - C(6)O	1654.46	Stretching - C(6)O	1660.16	Stretching - C(6)O
1625.79	Stretching - C(2)O	1625.79	Stretching - C(2)O (disappeared)	1625.79	Stretching - C(2)O (disappeared)

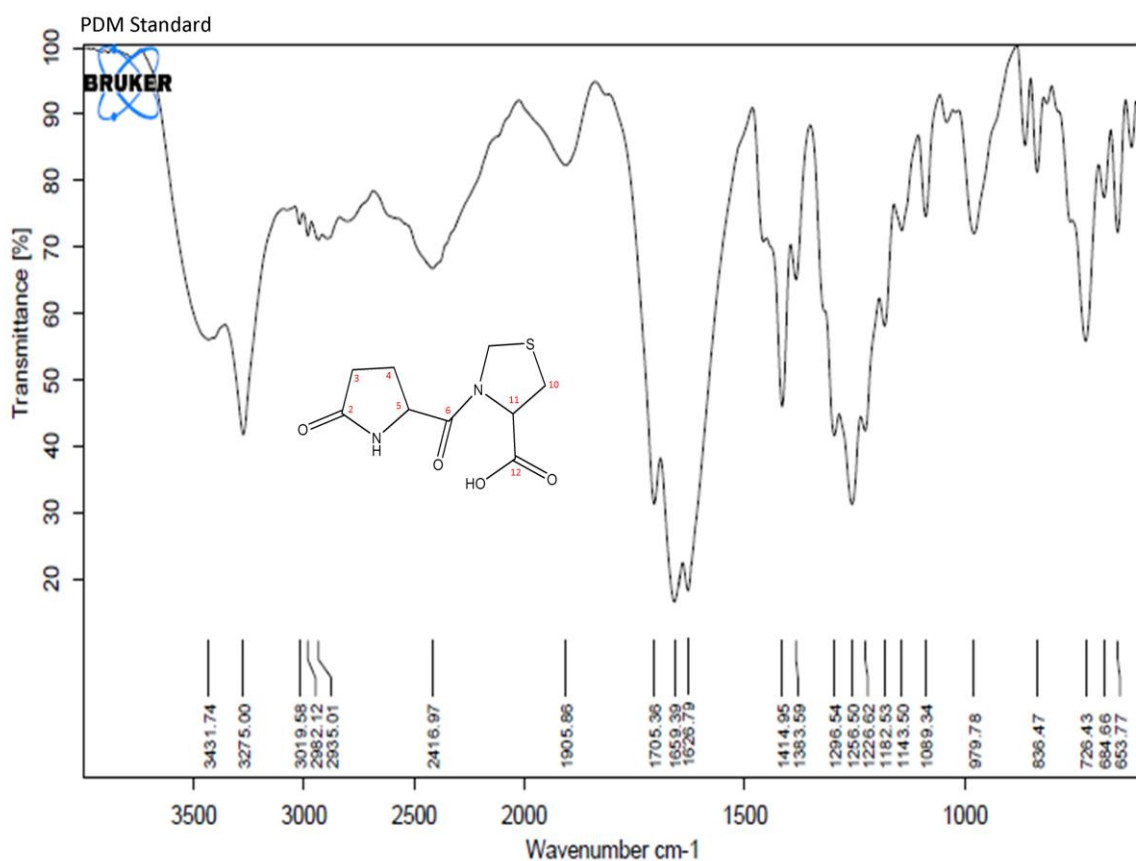


Figure 3.46: IR spectra of PDM Standard

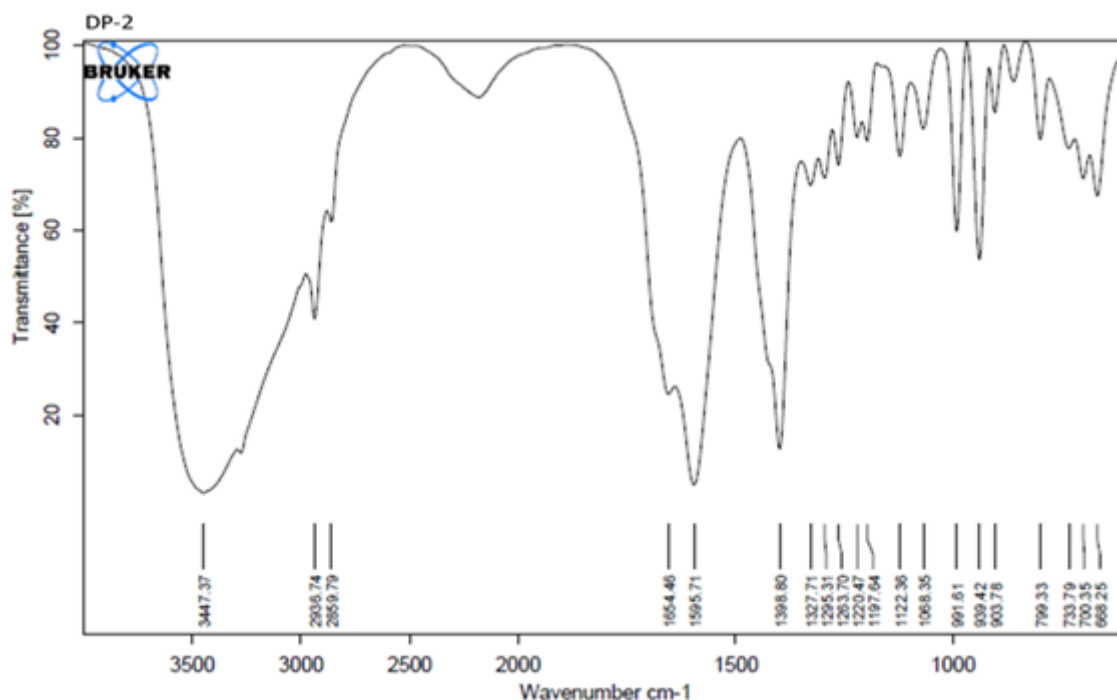


Figure 3.47: IR Spectra of DP-2

NMR Spectra

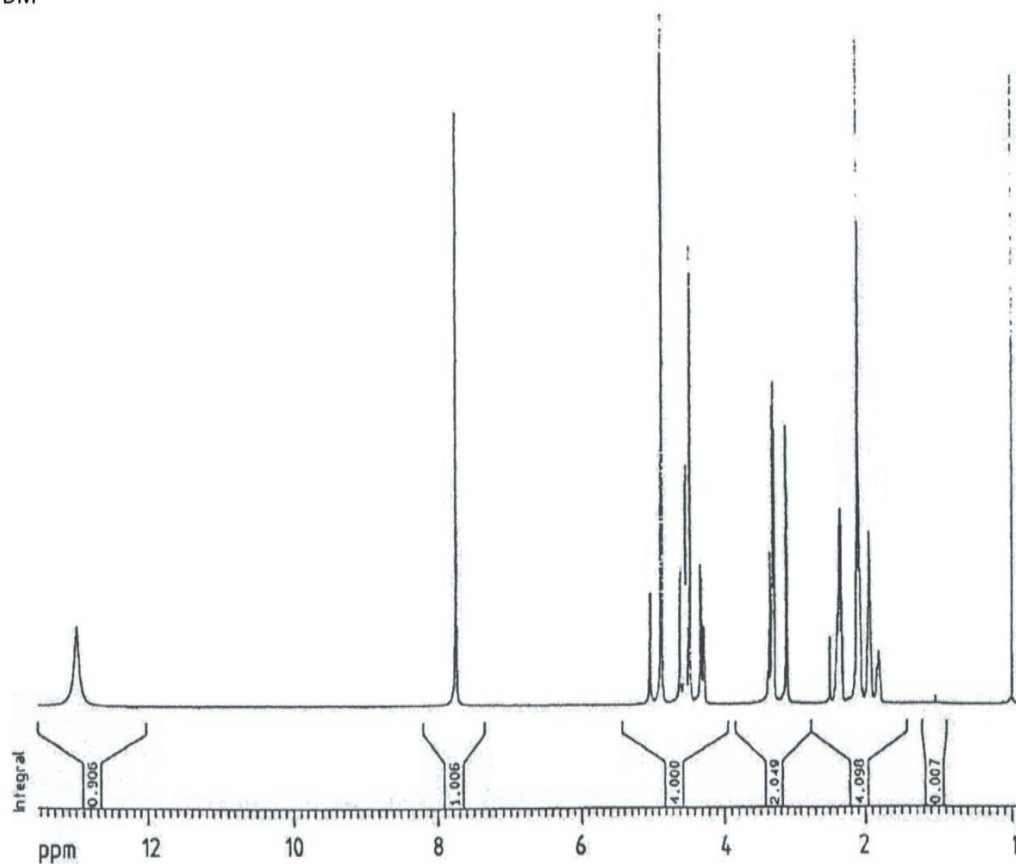
The ^1H spectrum of DP-2 indicates presence of four identical pair of carbon atom (as indicated by chemical shift value) while in PDM standard identical carbons are not present. ^{13}C NMR spectrum of DP-2 indicates the presence of four different carbon atom while in PDM nine different carbon atoms are present. This may be due to presence of identical carbon atoms since the mass spectrum shows increment in mol. wt by 18 amu. The ^1H and ^{13}C spectral assignments for DP-2 and PDM are illustrated in table 3.40 and 3.41. The ^1H spectra of PDM and DP-2 are shown in figure 3.48 and 3.49. The ^{13}C spectra of PDM and DP-2 are shown in figure 3.50 and 3.51.

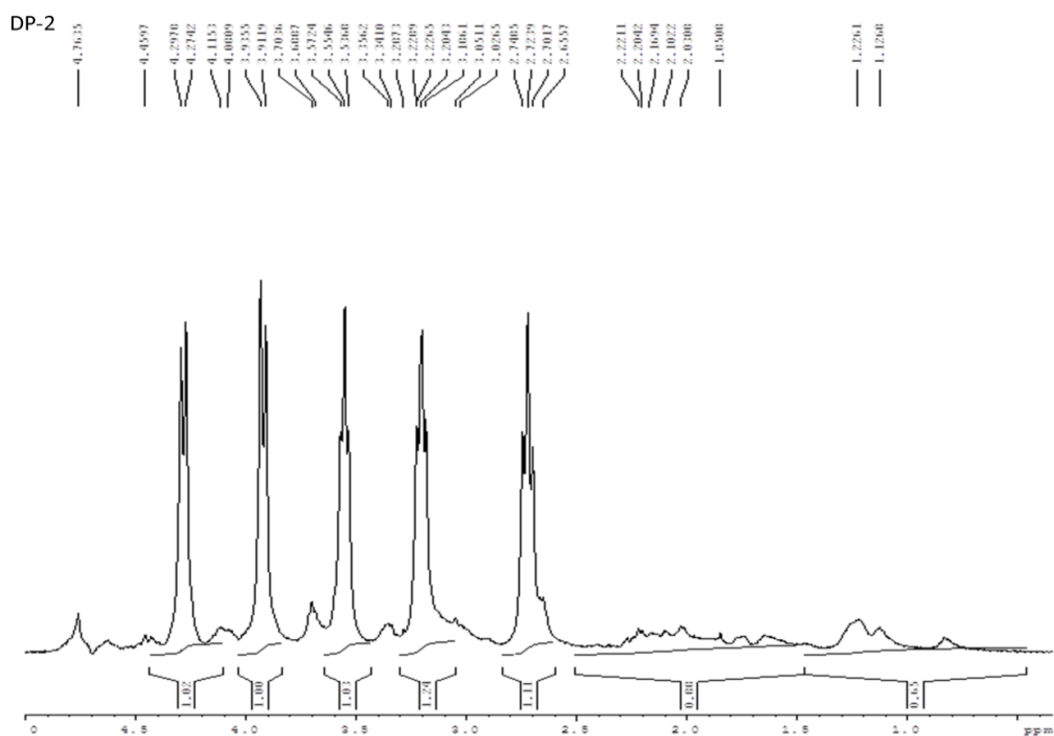
Table 3.40: ^1H - NMR Data of PDM standard and DP-2

PDM (Standard)			DP-2		
Position	Chemical Shift (δ , ppm)	Multiplicity	Position	Chemical Shift (δ , ppm)	Multiplicity
1	7.76	Broad	1	4.76	s

3	2.12	m	2	3.93,3.91	d
4	2.36/1.95	m	3	3.53, 3.55, 3.57	t
5	4.53	dd	4	4.29,4.11	d
8	4.87	m	5	4.76	s
10	3.32/3.12	dd/m	6	3.93,3.91	d
11	4.87	m	7	3.53, 3.55, 3.57	t
12	13.00	broad	8	4.29,4.11	d
			-OH	2.03	s

PDM

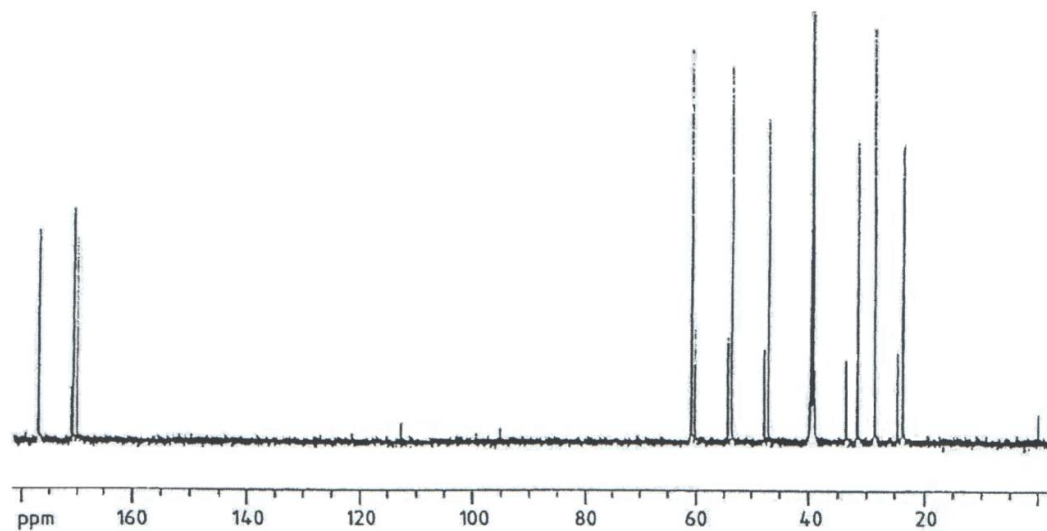
Figure 3.48: ^1H NMR spectra of PDM Standard

Figure 3.49: ^1H NMR Spectra of DP-2Table 3.41: ^{13}C - NMR Data of PDM standard and DP-2

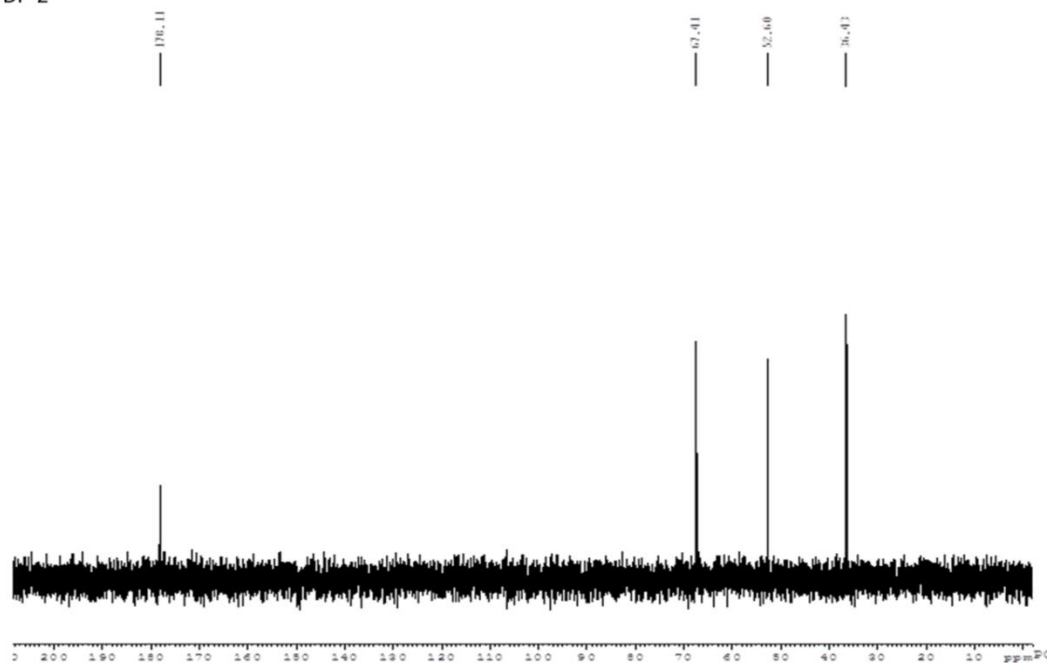
Standard (PDM)		DP-2	
Position	Chemical Shift (δ , ppm)	Position	Chemical Shift (δ , ppm)
2	177.10,170.85,170.17	1,5	67.41
3	28.75	2,6	36.43
4	23.80	3,7	52.60
5	53.76	4,8	178.11
6	177.10,170.85,170.17		
8	47.20		
10	31.69		
11	61.06		

*DP-2 GIVES ONLY 4 PEAKS IN SPECTRA SINCE IDENTICAL CARBONS ARE PRESENT

PDM

Figure 3.50: ^{13}C NMR Spectra of PDM

DP-2

Figure 3.51: ^{13}C NMR Spectra of DP-2

DSC Thermogram

DSC thermogram of both API and DP-2 are shown in figure 3.52 and 3.53. The DSC thermogram of PDM showed an endothermic peak at 191.08 °C which indicates that it melts

at this temperature and releases energy. Similarly in DP-2 one endothermic peak was observed at 128.3 °C so it can be concluded that DP-2 melts at this temperature and releases its energy. DP-2 is also showing a broad endotherm at around 80°C which may be due to loss of moisture or water molecule.

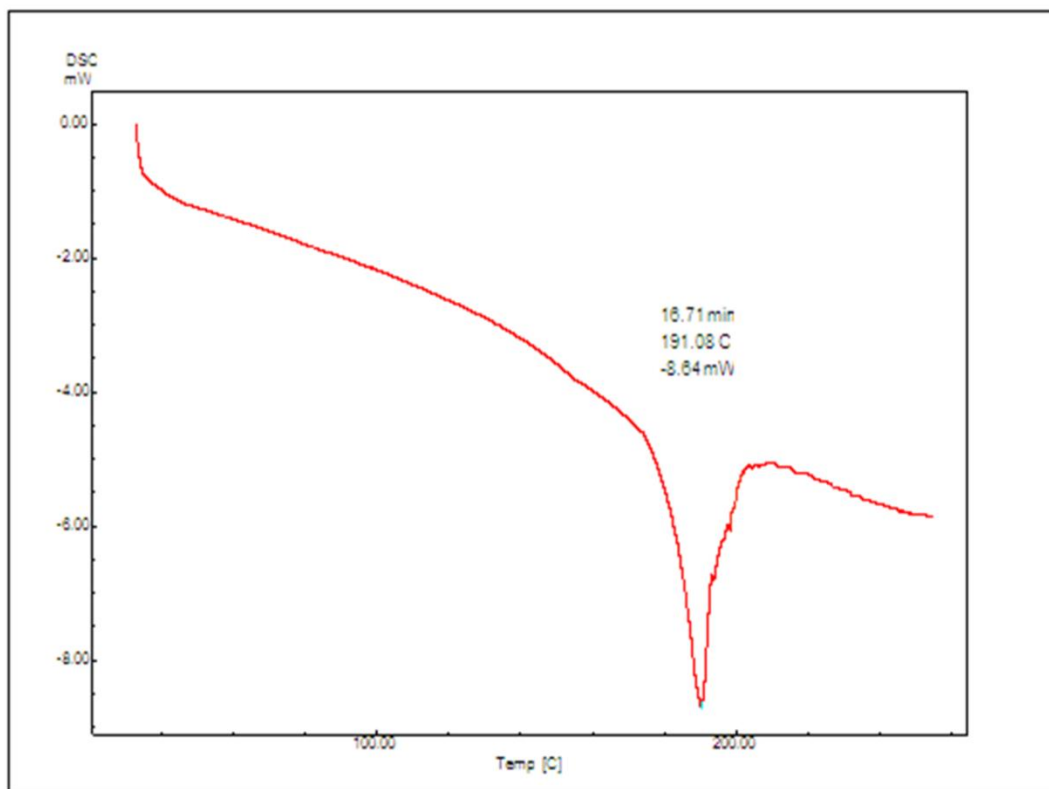


Figure 3.52: DSC Thermogram of PDM

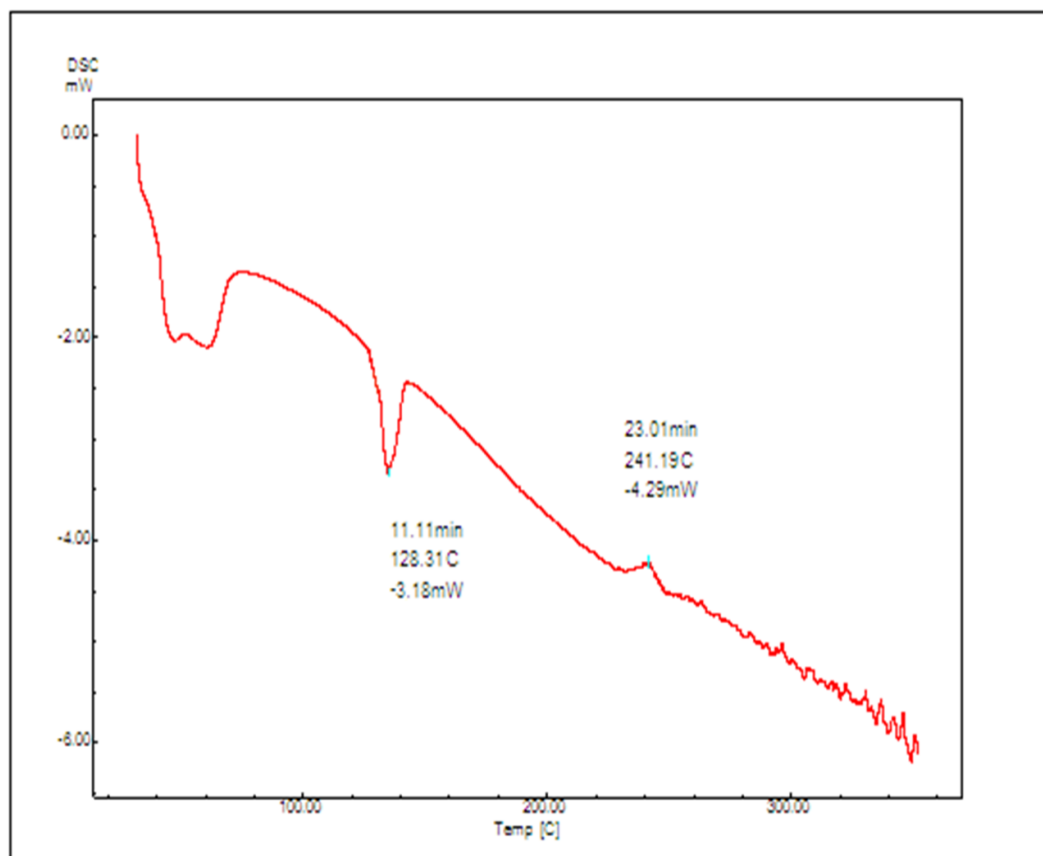


Figure 3.53: DSC thermogram of DP-2

Based on observations retrieved from various spectral data as mentioned and discussed above, DP-2 was assigned a bisthiazolopyrazine structure, chemically named as 3,8-Dihydroxy-tetrahydro-bisthiazolo[3,4,4a,3',4'-d]pyrazine-5,10-dione. The thio group may be incorporated in DP-2 from INH-2. The compound is chiral in nature with presence of two chiral centers at position 1 and 5. The comparative structures of PDM and DP-2 is shown in figure 3.54 with their assigned positions used in interpretation.

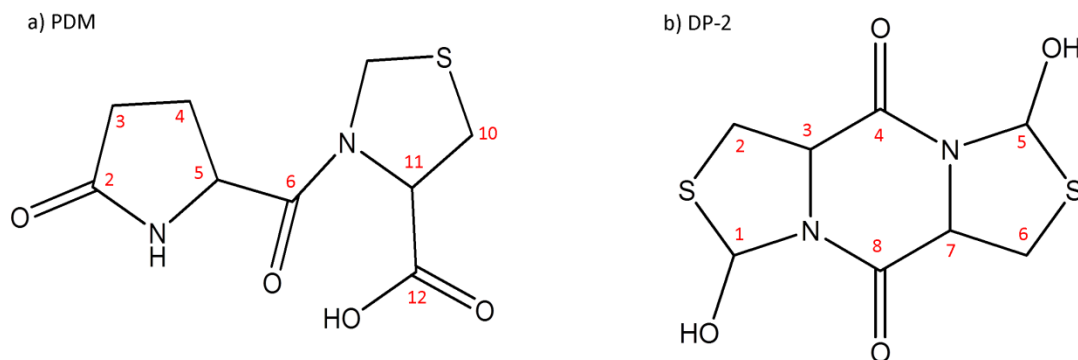


Figure 3.54: Structure of a) PDM and b) DP-2 with their assigned numbers

3.6.2.2.2 Characterization of DP-4

The molecular mass of isolated DP-4 is 244 as determined by the LC-MS/MS in positive ion mode. The molecular weight of DP-4 is same as PDM. The positive ion ESI-MS of DP-4 showed abundant $[M+H]^+$ ion at m/z 245. The ESI-MS/MS spectrum of $[M+H]^+$ ion of DP-4 showed most abundant product ions at m/z 227 due to the loss of H_2O . The spectrum also includes abundant product ions at m/z 134 corresponding to INH-2 thiazolidine carboxylic acid. The MS/MS spectra and proposed fragmentation pathway of DP-4 is shown in figure 3.55 and 3.56.

In IR spectra it was observed that $-OH$ stretching vibration at 3431 in PDM standard was not changed and was observed at 3438 cm^{-1} . Similarly the $C(12)O$ stretching vibration at 1705 and $C(6)O$ stretching vibration at 1659 were not changed and observed at 1716 and 1660 cm^{-1} respectively while $-NH$ stretching vibration at 3275 and $C(12)O$ stretching vibration at 1625 cm^{-1} were disappeared in DP-4. The IR spectral assignment for DP-4 is presented in table 3.40 and the IR Spectra is illustrated in figure 3.57.

Effort for further structural assignment of DP-4 was not done since the molecular weight and IR spectra matched the reported degradation related impurity; IM-X (21).

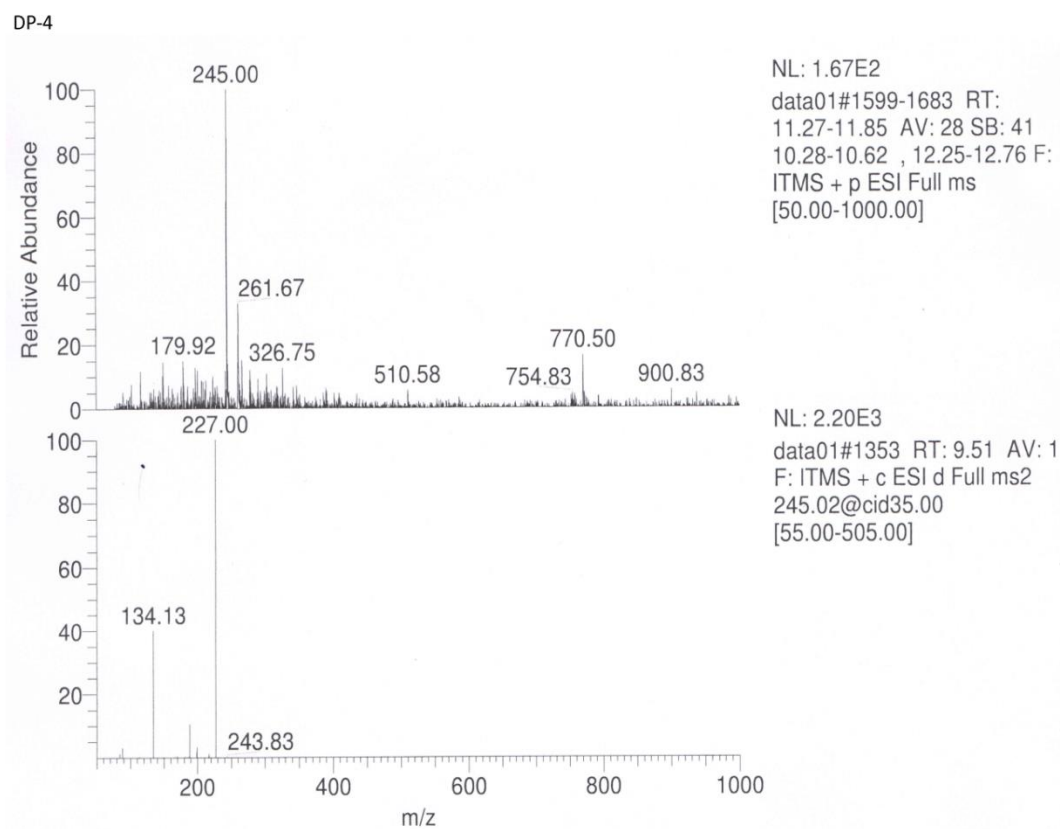


Figure 3.55: ESI-MS/MS spectra of DP-4

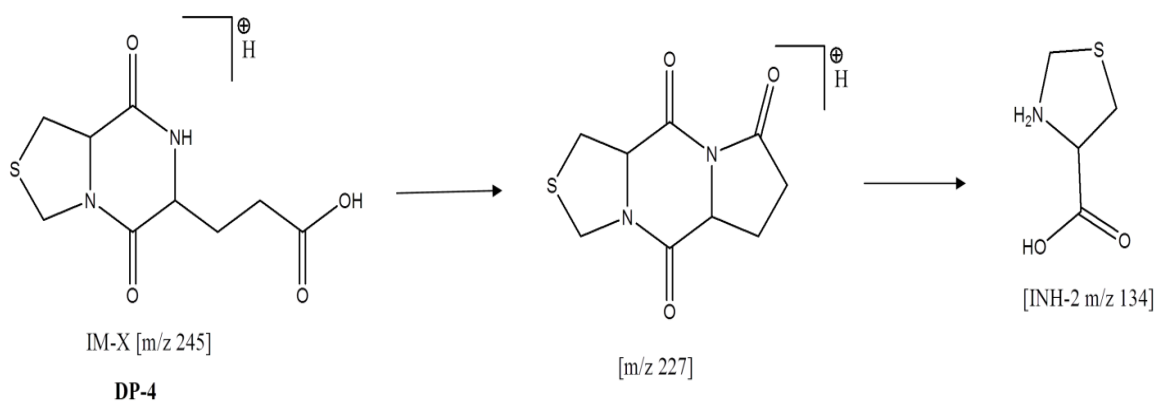


Figure 3.56: Proposed fragmentation pathway of DP-4

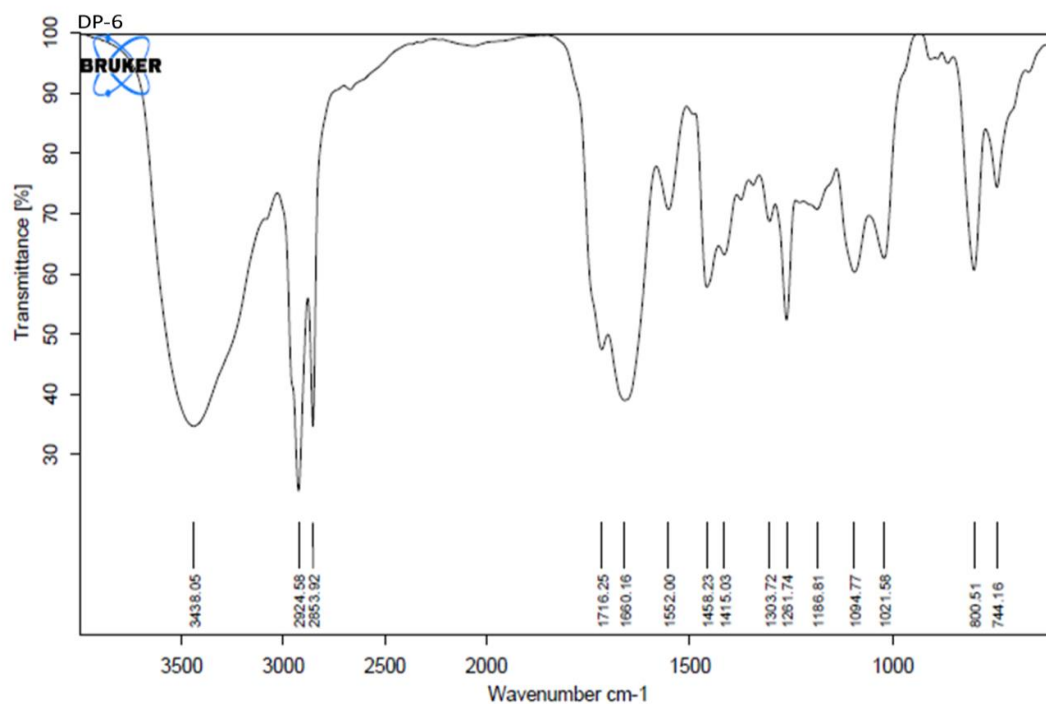


Figure 3.57: IR Spectra of DP-4

3.7 SECTION-D

IMPURITY PROFILING AND DEGRADATION STUDY OF PIDOTIMOD

3.7.1 EXPERIMENTAL

3.7.1.1 Chemicals and Reagents

The chemicals and reagents used in present section were same as described in section 3.4.1.1.

3.7.1.2 Equipments and Chromatographic Conditions

The instruments and chromatographic conditions utilized for impurity profiling and degradation study were same as described in section 3.4.1.2.

For LC-MS/MS analysis PDM degradation samples were subjected to similar chromatographic conditions as mentioned in section 3.4.1.2. The m/z values were recorded in both positive and negative ESI mode and were compared to the molecular weights

(MW) of the known inherent or process related impurities and degradation products (DPs) reported in literature. The fragmentation patterns were investigated. On the basis of MW and fragmentation pattern, the presence of known process related impurity and DPs were confirmed and structures were proposed for the unknowns and the degradation pathways were also outlined.

3.7.1.3 Preparation of Stock, Sample and Buffer solutions

Stock, sample and buffer solutions were prepared in same way with similar dilutions as described in section 3.4.1.3.

3.7.2 RESULTS AND DISCUSSION

The stress degradation behavior of PDM was studied as per ICH guidelines. Two process related impurities (INH-1 and INH-2) were reported by Crimella T. (21), they had also reported two other impurities named IM-X and IM-Y in industrial lot of PDM bulk drug but not specified whether these are process related or degradation related impurity. The structures of reported process related impurities and related substances of PDM are provided in figure 3.58.

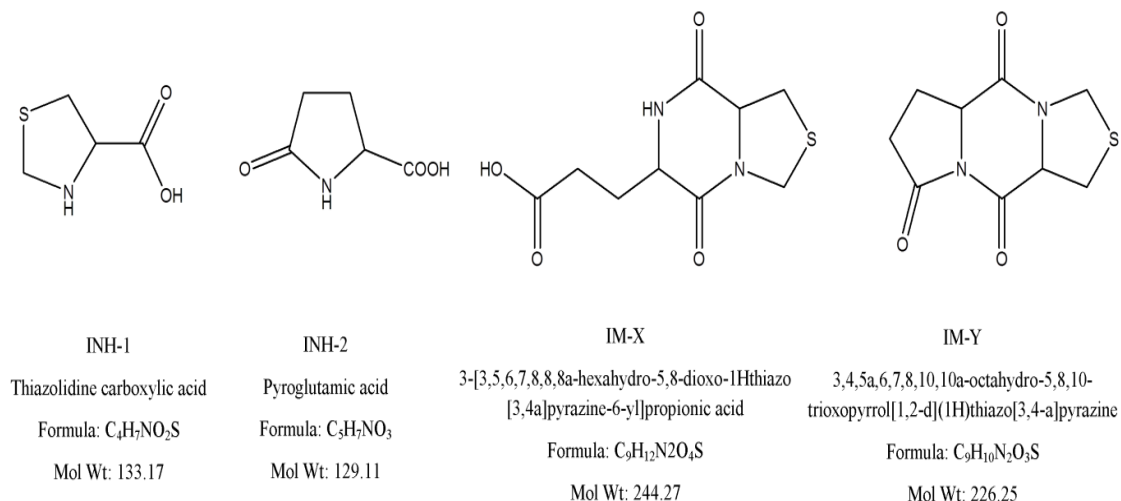


Figure 3.58: Molecular structures of PDM related compounds

3.7.2.1 LC-PDA Study

Six DPs were formed under stress conditions as detected by LC-PDA (described in section 3.4.2, table 3.20 and in figure 3.16). Two process related impurities (INH-1 and INH-2) were observed at Rt of 2.95 and 3.79 and are shown in figure 3.59. These processes related impurities were also formed during stress degradation and were identified as DP-1 and DP-3 respectively. After LC-MS/MS study the MW of INH-1 was found to be 129 that correspond to process related impurity Pyroglutamic acid whereas the MW of INH-2 was found to be 133 that correspond to process related impurity Thiazolidine carboxylic acid.

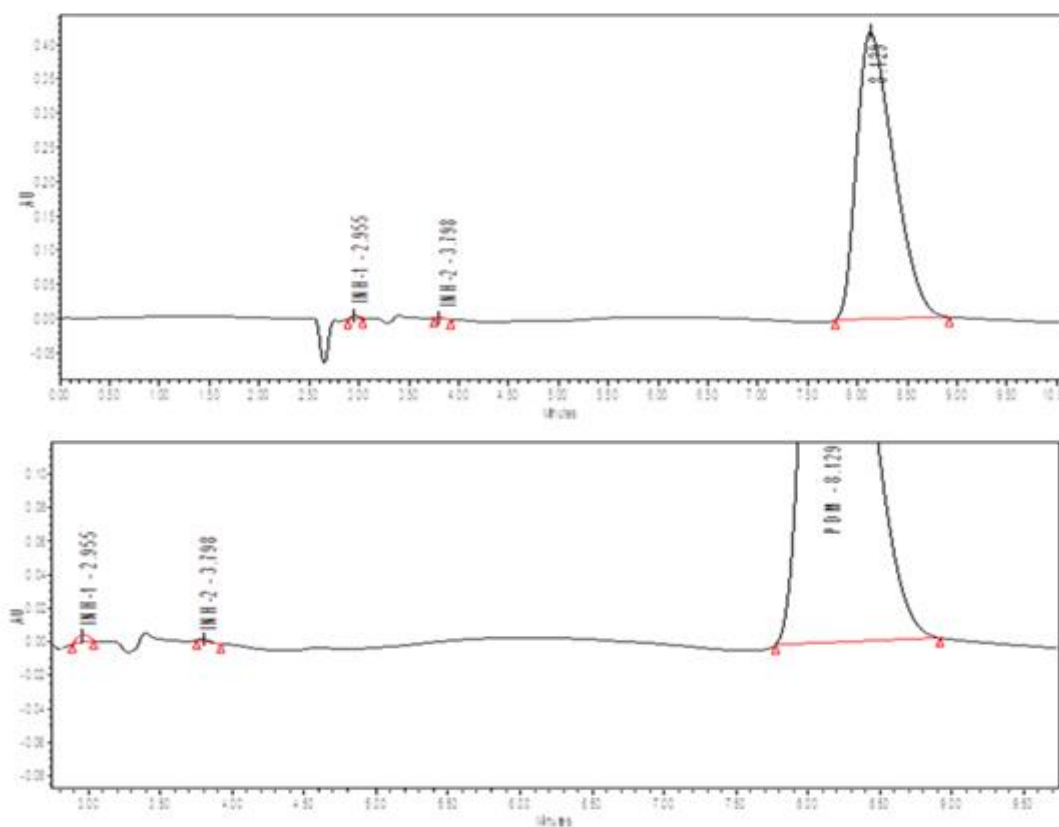


Figure 3.59: Chromatogram showing two process related impurity (INH-1 and INH-2)

3.7.2.2 LC-MS/MS study and characterization of DPs

The LC-MS/MS analysis illustrated total 11 DPs including DP-1 and DP-3. Different masses were observed in LC-MS/MS for individual stress degradation condition which gives same retention time in LC-PDA when the mixtures of DPs are injected. Neutral and

oxidative degradation showed different masses of peaks that had same retention time in LC-PDA as acid, base, photolytic and thermal-humidity induced degradation. Hence for degradants observed in LC-MS/MS different nomenclature have been used for DPs. For neutral degradation it was named DP-7 and for oxidative degradation these were named DP-8, DP-9 and DP-10. Peak that was observed at 2.9 in oxidative degradation was identified as ACN adduct of DP-8 and named DP-11. The modified nomenclatures of DPs used in LC-MS/MS are shown in table 3.42.

Also the peak of DP-2 that was observed as single pure peak in LC-PDA (in case of acid, base, photolytic degradation) and was observed as bifurcated peak in LC-MS/MS with same MW hence two different nomenclature DP-2 and DP-2 (e) was used during explanation. The availability of enantiomeric forms of DP-2 was further confirmed by LC-MS/MS after isolation and chiral separation in Lichrocart CHIRADEX column.

Table 3.42: Modified nomenclature of DPs in LC-MS/MS

Stressor Type	DPs nomenclature with Rt (LC-PDA)	Modified nomenclature of DPs in LC-MS/MS
Acid degradation	DP-1(2.88), DP-2(3.40), DP-3(3.74), DP-4(12.22)	DP-2 was observed as bifurcated peak so named DP-2 and DP-2 (e)
Base degradation	DP-5(2.36) DP-1(3.01), DP-2(3.43), DP-3(3.82), DP-4(12.86)	DP-2 was observed as bifurcated peak so named DP-2 and DP-2 (e)
Neutral degradation	DP-5(2.48), DP-1(2.91), DP-4(12.22)	DP-1 with Rt 2.91 was named DP-7
Oxidative degradation	DP-1(2.94), DP-2(3.24), DP-3(3.79), DP-6(6.19)	DP-1 with Rt 2.94 named DP-11, DP-2 with Rt 3.24 named DP-8, DP-3 with Rt 3.79 named DP-9, DP-6 with Rt 6.19 named DP-10

Photolytic degradation	DP-1(2.90), DP-2(3.28), DP-3(3.86), DP-4(12.36)	No change
Dry Heat induced degradation	No degradation	
Thermal Humidity induced degradation	DP-1(2.91), DP-3(3.84), DP-4(11.98)	No change

LC-MS/MS spectra were recorded in positive ion ESI-MS but for some DPs it was recorded in negative mode (DP-1, DP-6, DP-7 and DP-11). According to the m/z values and fragmentation pattern in MS/MS the structures and degradation pathways for PDM and DPs were proposed and are as follows:

PDM (m/z 245)

MS/MS of PDM standard is explained in section 3.6.2.2.1 and ESI-MS/MS spectra is shown in figure 3.43.

DP-1 (m/z 128)

The negative ion ESI-MS of DP-1 shows abundant $[M-H]^-$ ion at m/z 128 corresponding to MW of INH-1 Pyroglutamic acid. The ESI-MS/MS spectrum of $[M+H]^+$ of DP-1 could not be generated due to low sensitivity and absence of ionization. ESI-MS/MS spectra is provided in figure 3.60.

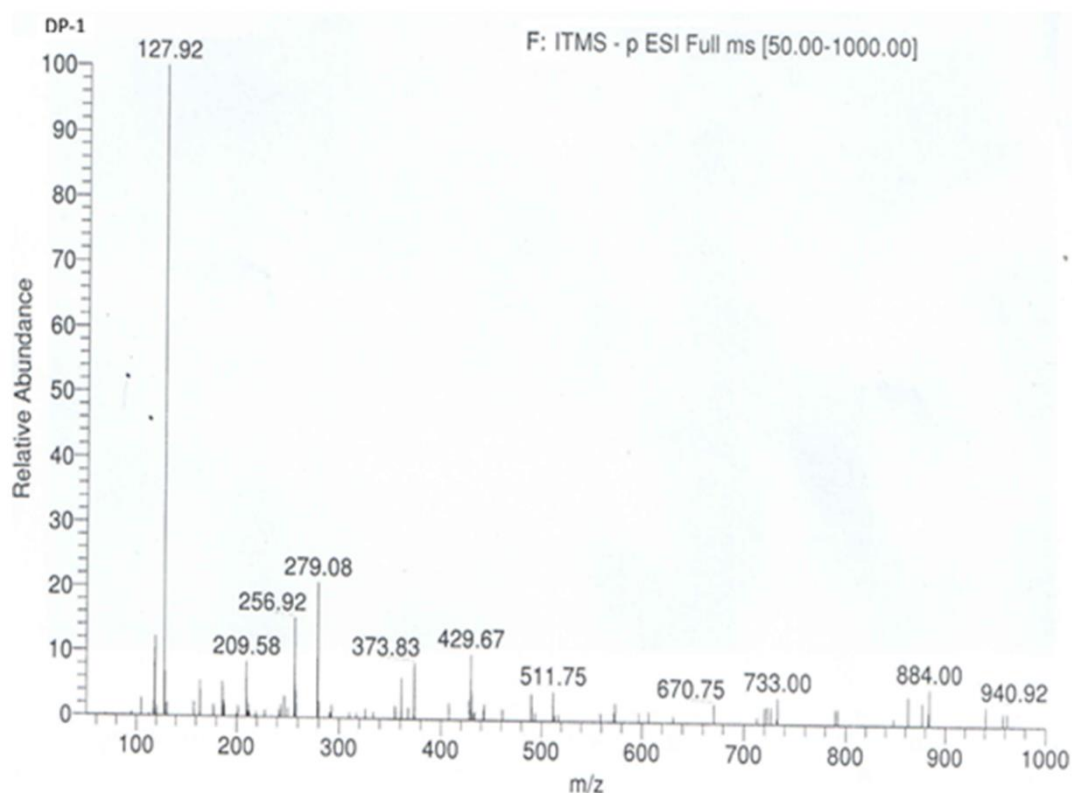


Figure 3.60: ESI-MS/MS spectra of DP-1

DP-2 and DP-2 (e) (m/z 263)

MS/MS of DP-2 and DP-2 (e) is explained in section 3.6.2.2.1 and ESI-MS/MS spectra is provided in figure 3.44.

DP-3 (m/z 134)

The positive ion ESI-MS (figure 3.61) of DP-3 showed abundant $[M+H]^+$ ion at m/z 134, that did not show protonated ions. The MW of the parent ion confirmed the proposed structure for DP-3 (table 3.44), which is one of the process related impurity (INH-2) of PDM i.e. Thiazolidine carboxylic acid.

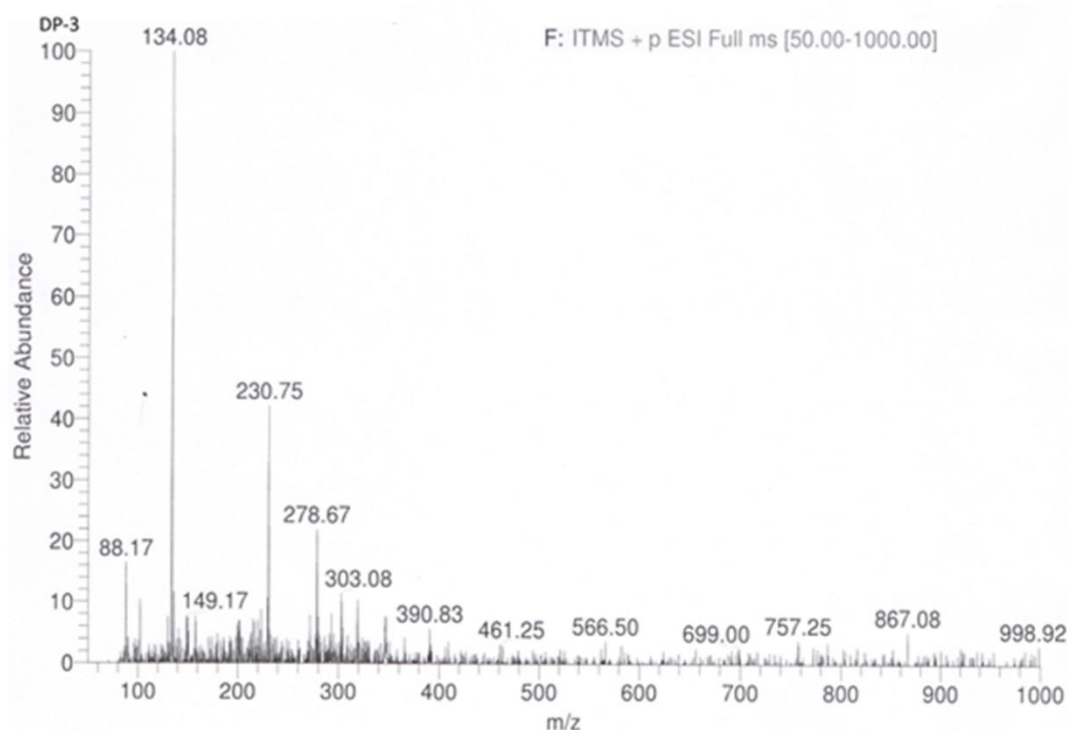


Figure 3.61: ESI-MS/MS spectra of DP-3

DP-4 (m/z 245)

MS/MS of DP-4 is explained in section 3.6.2.2.2 and ESI-MS/MS spectra is provided in figure 3.55. The spectrum also includes abundant product ions at m/z 134 corresponding to INH-2 thiazolidine carboxylic acid i. e DP-3.

DP-5 (m/z 148)

The positive ion ESI-MS/MS (figure 3.62) of DP-5 showed abundant $[M+H]^+$ ion at m/z 148, that showed abundant product ions at m/z 130.

DP-6 (m/z 119)

The negative ion ESI-MS (figure 3.63) spectrum of DP-6 showed abundant $[M-H]^-$ ion at m/z 119, that did not show protonated ions.

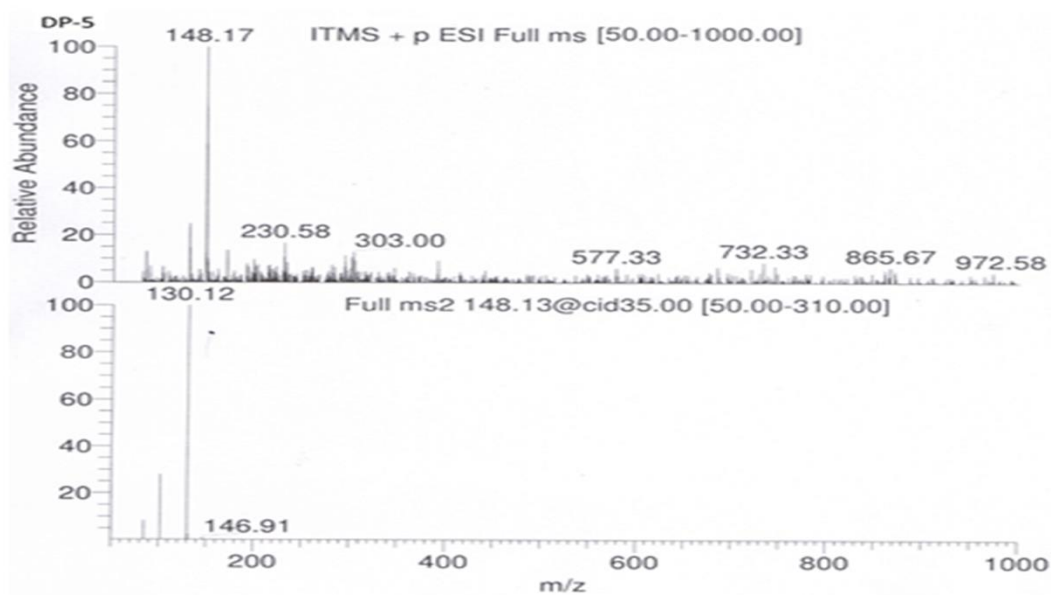


Figure 3.62: ESI-MS/MS spectra of DP-5

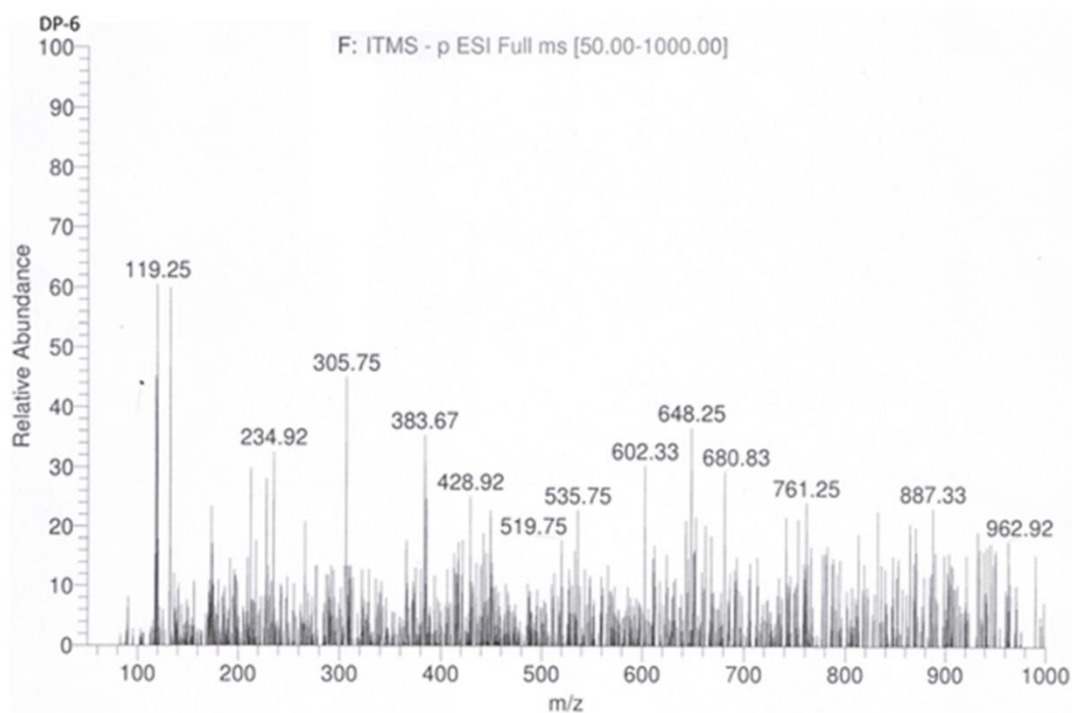


Figure 3.63: ESI-MS/MS spectra of DP-6

DP-7 (m/z 197)

The negative ion ESI-MS spectrum (figure 3.64) of DP-7 showed abundant $[M-H]^-$ ion at m/z 197, that did not show protonated ions.

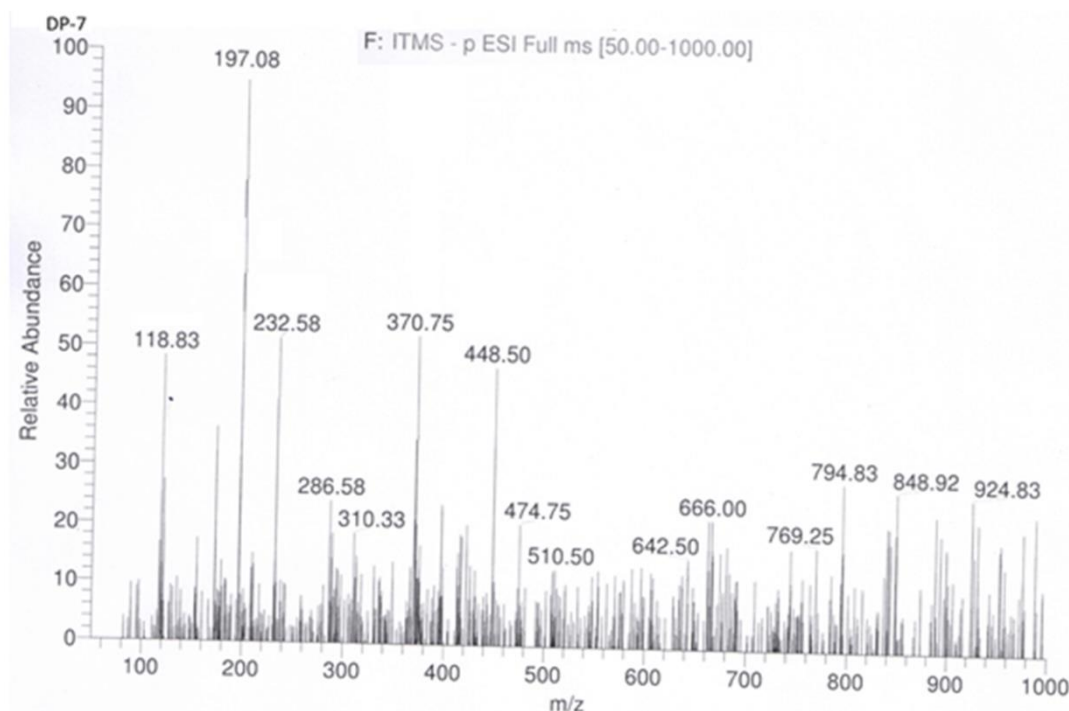


Figure 3.64: ESI-MS/MS spectra of DP-7

DP-8 (m/z 261)

The positive ion ESI-MS/MS spectrum (figure 3.65) of DP-8 showed abundant $[M+H]^+$ ion at m/z 261. The ESI-MS/MS spectrum of $[M+H]^+$ ion of DP-8 showed most abundant product ions at m/z 245 that correspond to either PDM or DP-4 which further fragment to give product ions at m/z 132.

DP-9 (m/z 267)

The positive ion ESI-MS/MS (figure 3.66) spectrum of DP-9 showed abundant $[M+H]^+$ ion at m/z 267. The spectrum of DP-9 showed abundant product ions at m/z 261 that correspond DP-8 which further fragment to give most abundant product ions at m/z 245 that correspond to either PDM or DP-4. m/z 245 further fragment to give m/z of 148 that correspond to DP-5 which fragment to give m/z of 132.

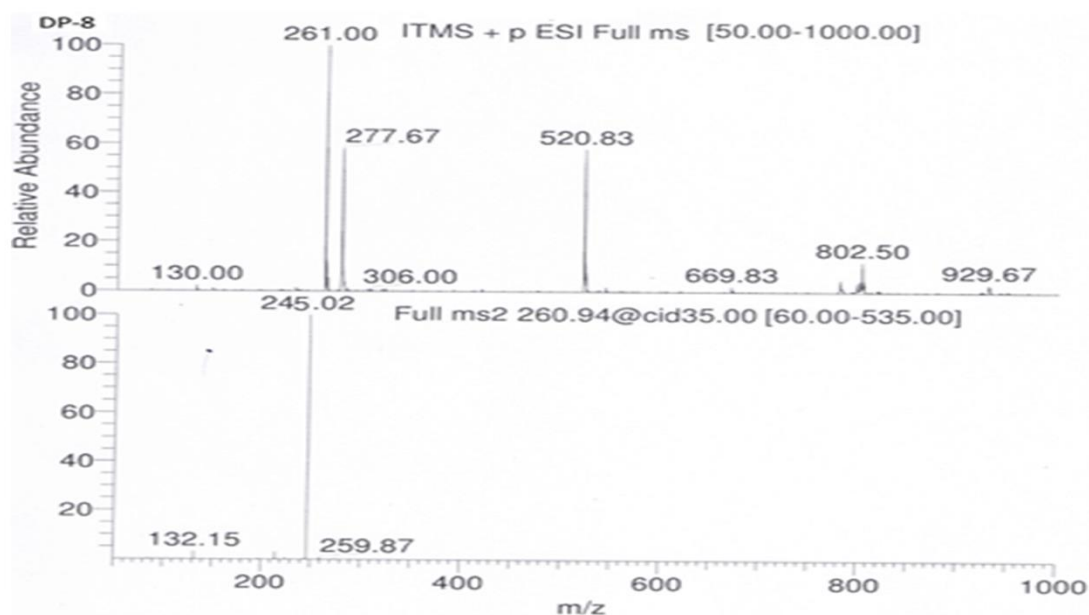


Figure 3.65: ESI-MS/MS spectra of DP-8

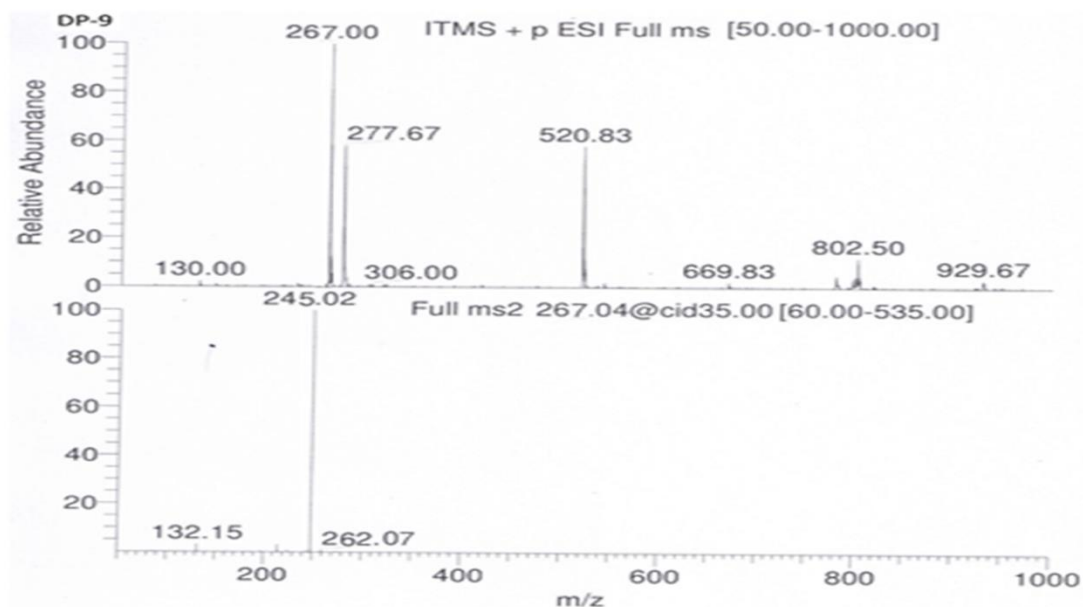


Figure 3.66: ESI-MS/MS spectra of DP-9

DP-10 (m/z 521)

The positive ion ESI-MS/MS (figure 3.67) spectrum of DP-10 shows abundant $[M+H]^+$ ion at m/z 521 that may be due to formation of dimer of DP-8 (m/z 261). The ESI-MS/MS spectrum of $[M+H]^+$ ion of DP-10 showed product ions at m/z 485 and 243.

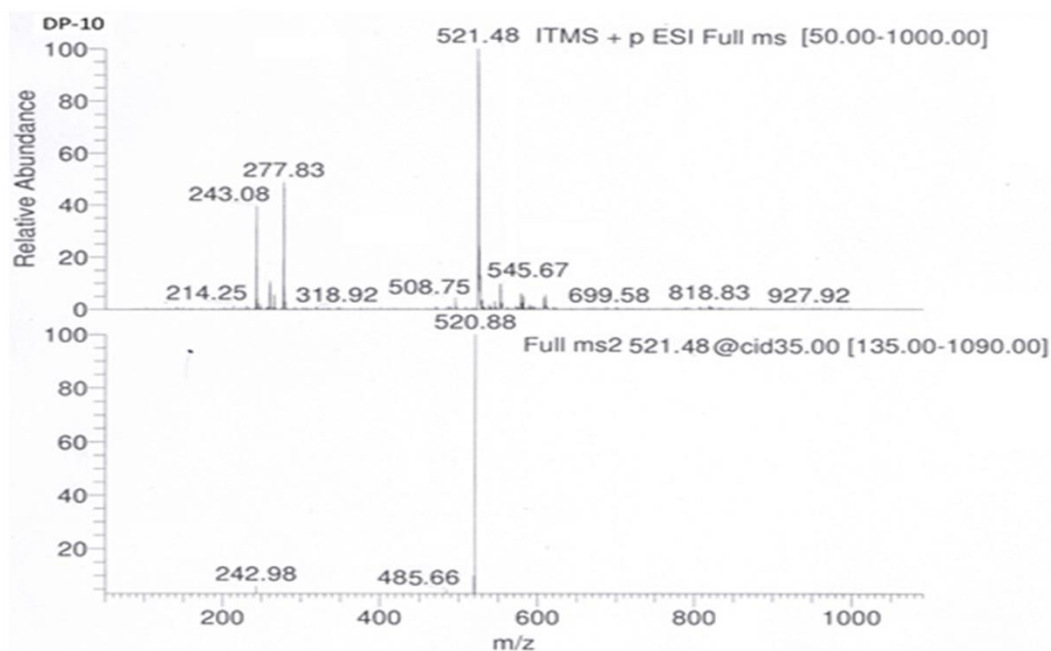


Figure 3.67: ESI-MS/MS spectra of DP-10

DP-11

The ACN adduct of DP-8 was observed at Rt 2.9 in oxidative degradation that gives [M-H]⁺ ion at m/z 306 in negative ion ESI-MS spectrum (figure 3.68).

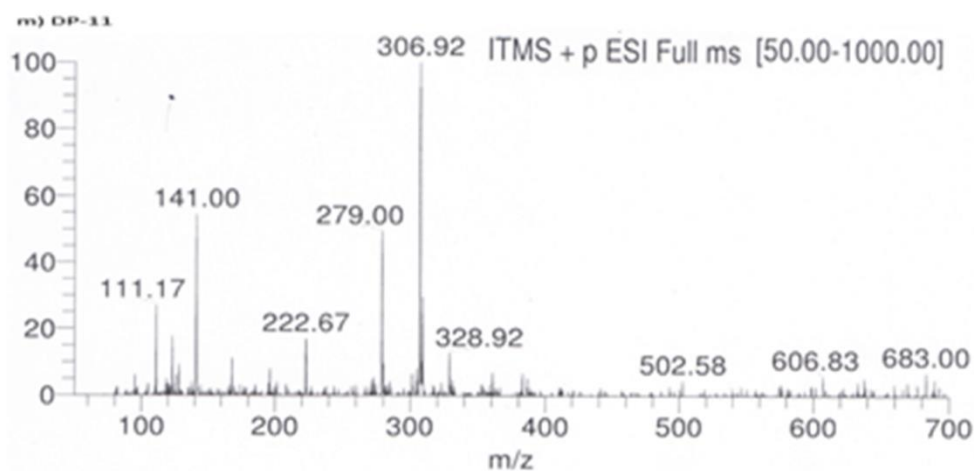


Figure 3.68: ESI-MS/MS spectra of DP-11

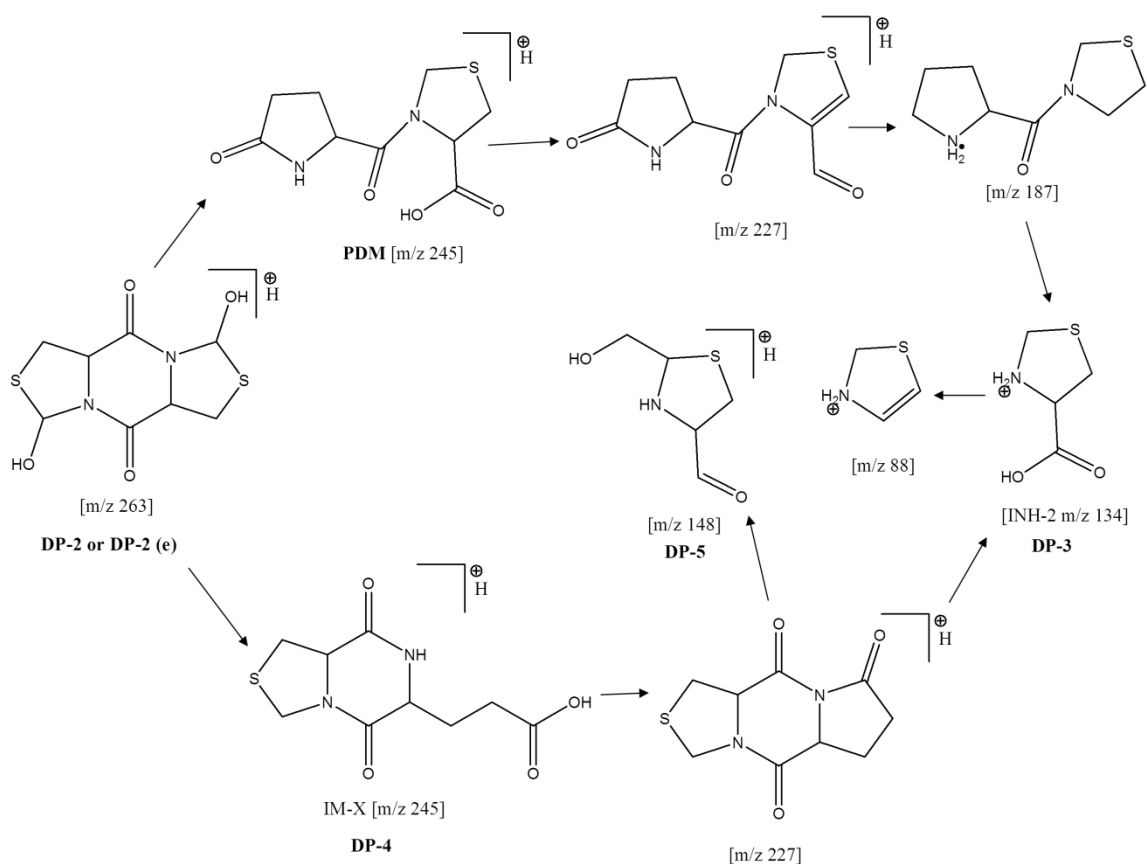


Figure 3.69: (a) Proposed fragmentation pathway of DP-2, DP-2 (e) DP-3 and DP-4

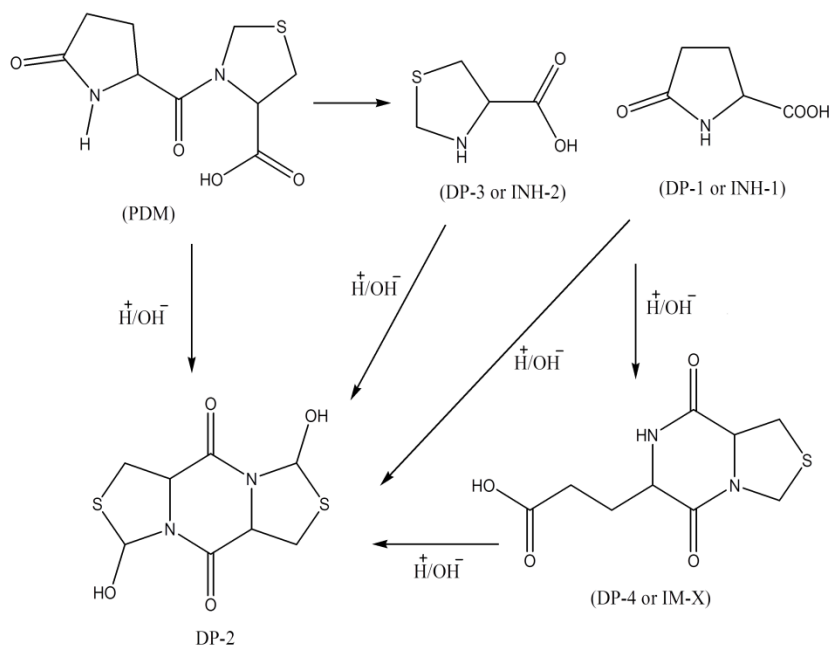


Figure 3.69: (b) Mechanism of formation of DP-4 and DP-2

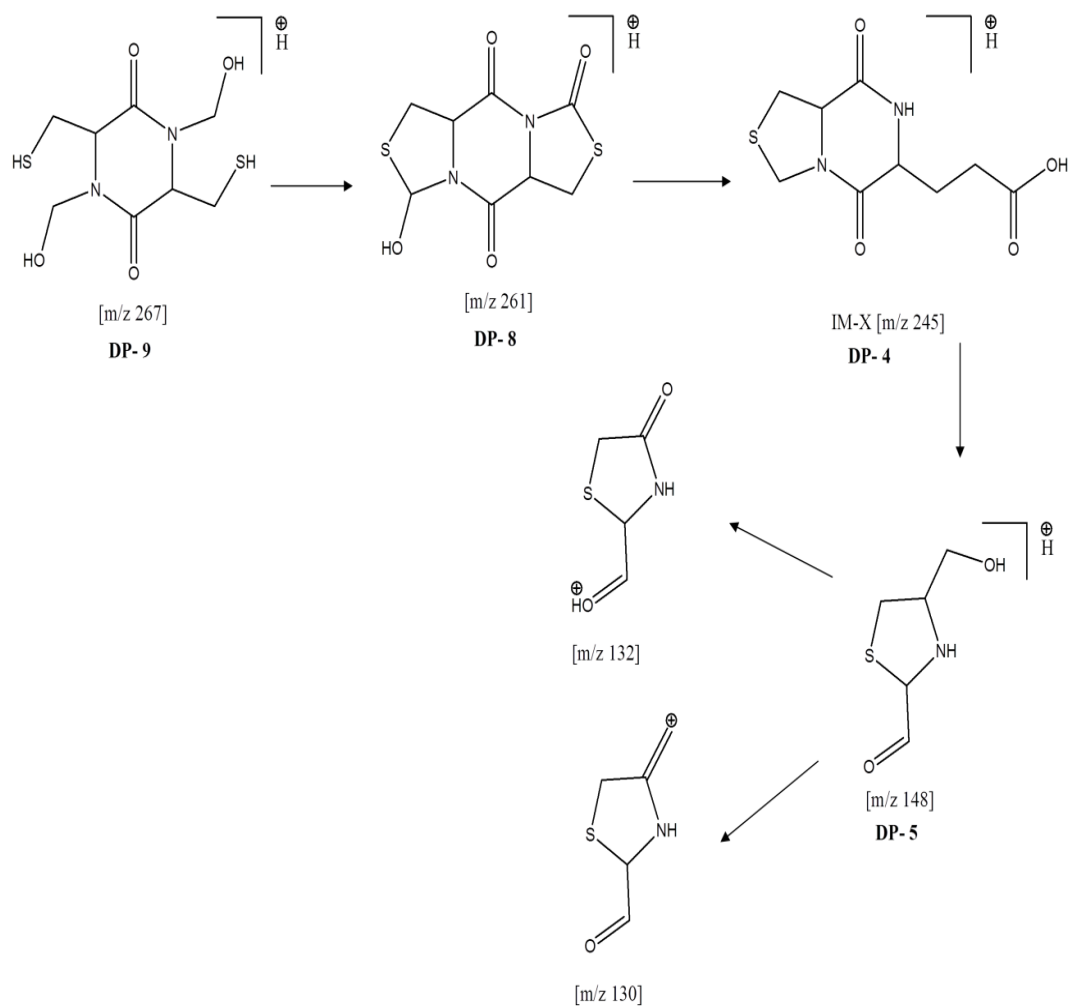


Figure 3.70: Proposed fragmentation pathway of DP-9, DP-8 and DP-5

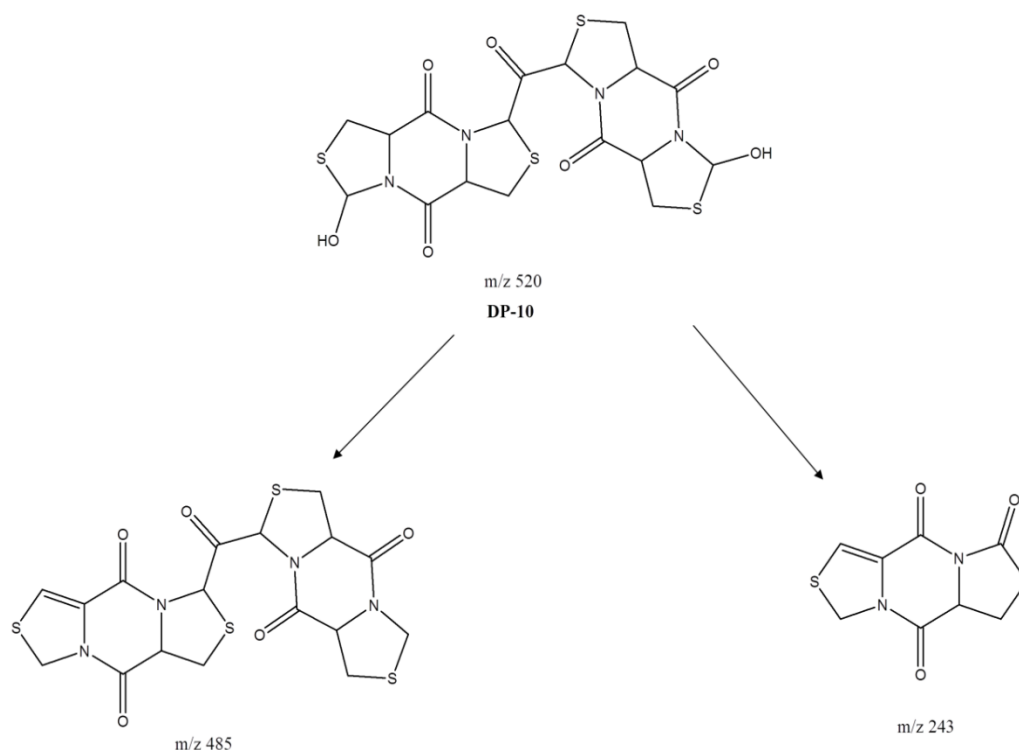


Figure 3.71: Proposed fragmentation pathway of DP-10

Finally based on above observations, schematic flow chart of PDM degradation showing formation of all DPs was prepared and is shown in figure 3.72. Chemical structure of PDM and all the related compounds already reported or unknown along with their origin, degradation route, R_t and observed m/z values for major fragments are shown in table 3.43.

It is clear from the table that PDM may contain 11 impurities which may be inherent (or process related) or degradation related. Out of 11 impurities identified, eight impurities are not reported in literature.

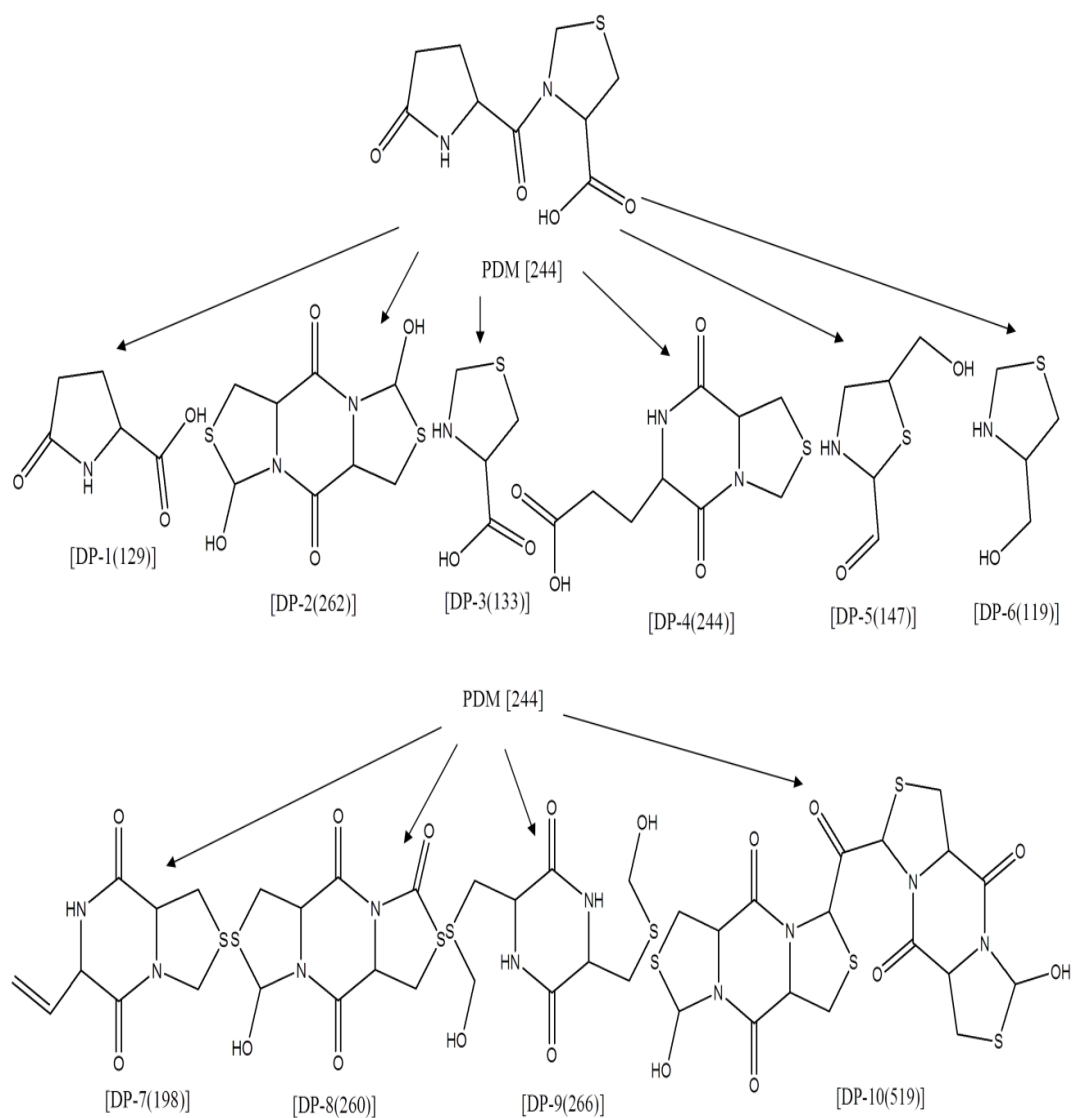
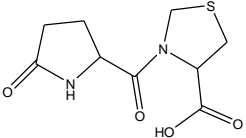
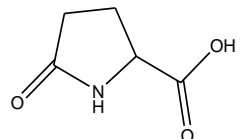
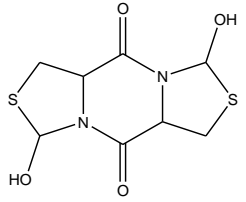
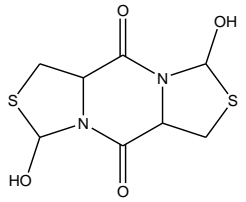
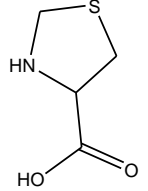
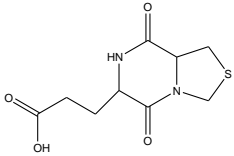
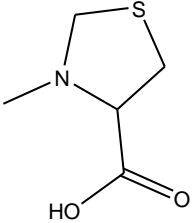
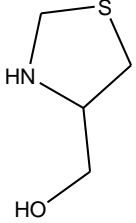
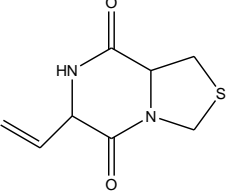
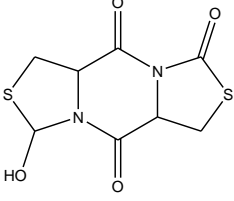
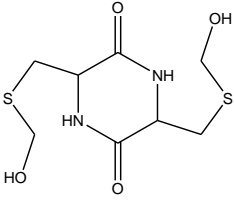
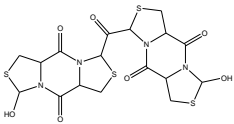
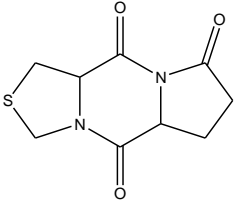


Figure 3.72: A schematic representation of PDM degradation

Table 3.43: Chemical structures of PDM and related compounds, their origin, degradation route, Rt and observed m/z values for major fragments.

Analyte	Structure	Molecular formula molecular weight Fragments (m/z)	Origin	Degradation route	Rt (LC-PDA)
PDM		$C_{19}H_{12}N_2O_4S$ 244.27 (227.08, 187.58, 134.17, 88.25)	API	--	8.821
INH-1 and DP-1		$C_5H_7NO_3$ 129.11	Process related	Acid, Base, photolytic, thermal-humidity induced Degradation	2.88
DP-2		$C_8H_{10}N_2O_4S_2$ 262.31 (244.99, 227.04)	Degradation product (unk)	Acid, Base, photolytic, Degradation	3.4
DP-2 (e)		$C_8H_{10}N_2O_4S_2$ 262.31 (244.99, 148.05)	Degradation product (unk)	Acid, Base, Degradation	3.4
INH-2 and DP-3		$C_4H_7NO_2S$ 133.17	Process related (Known)	Acid, Base, photolytic, thermal-humidity induced Degradation	3.8

DP-4 and IM-X		$C_9H_{12}N_2O_4S$ 244.27 (227.00, 134.13)	Degradation product (Known)	Acid, Base, neutral Photolytic and thermal-humidity induced Degradation	12.25
DP-5		$C_5H_9NO_2S$ 147.20 (130.13)	Degradation product (unk)	Base and neutral degradation	2.4
DP-6		C_4H_9NOS 119.19	Degradation product (unk)	oxidative degradation	6.22
DP-7		$C_8H_{12}N_2O_2S$ 198.24	Degradation product (unk)	Neutral Degradation	2.91
DP-8		$C_8H_8N_2O_4S_2$ 260.29 (245.02, 132.15)	Degradation product (unk)	Oxidative Degradation	3.12
DP-9		$C_8H_{14}N_2O_4S_2$ 266.34 (262.07, 245.02, 132.15)	Degradation product (unk)	Oxidative Degradation	3.71

DP-10		$C_{17}H_{18}N_4O_7S_4$ 518.61 (485.66, 242.98)	Degradation product (unk)	Oxidative Degradation	6.22
DP-11	ACN adduct of DP-8	307	Degradation product (unk)	Oxidative Degradation	2.9
IM-Y		$C_9H_{10}N_2O_3S$ 226.25	Degradation product (Known)	Not observed	--

3.8 SECTION-E

CHIRAL SEPARATION OF PIDOTIMOD, ISOLATED DEGRADATION PRODUCT-2 AND DEVELOPMENT OF STABILITY INDICATING CHIRAL RP-HPLC ASSAY METHOD

Pidotimod (PDM) isolated degradation product (DP-2) were chiral in nature, hence a stability indicating chiral RP-HPLC assay method was developed and validated as per ICH Q2(R1) guideline for separation of PDM enantiomers and its quantification in presence of degradation products (DPs) formed under stress condition.

3.8.1 EXPERIMENTAL

3.8.1.1 Chemicals and Reagents

The chemicals and reagents utilized in present study were same as described in section 3.4.1.1.

3.8.1.2 Equipments and Chromatographic Conditions

Same instruments were utilized as described in section 3.4.1.2. The separation was achieved on Lichrocart CHIRADEX RP column (150 × 4.6 mm, 5 μm) at wavelength of 215 nm. The mobile phase consisted of ammonium acetate buffer (10 mM, pH adjusted to 5.8 with glacial acetic acid) and methanol in the ratio of 80:20 at flow rate of 0.8 ml/min.

The analysis was performed at ambient temperature with isocratic elution and injection volume of 20 μ L. The mobile phase was filtered using 0.2 μ m disposable filters (Ultipore, PALL lifesciences, 40 mm) and degassed by ultrasonic vibrations prior to use.

3.8.1.3 Preparation of Stock, Sample and Buffer solutions

The stock solutions containing 1 mg/ml of R form of PDM was prepared in double distilled water. Aliquots of 50-250 μ g/ml of PDM with respect to R-enantiomer were prepared in the mobile phase for analysis. The powder equivalent to 5 mg of PDM from synthetic mixture was accurately weighed and transferred into a 5 mL volumetric flask. To this 2 mL of mobile phase was added and mixed well by ultra-sonication for 5 minutes. The resulting solution was made up to volume with mobile phase and filtered using 0.2 μ membrane filter. The standard and sample solutions were analyzed by the chromatographic conditions described below and the chromatograms were recorded.

Ammonium acetate buffer (10 mM) was prepared in same way as described in section 3.4.1.3.

3.8.1.4 Preparation of Degradation Products (DPs)

DPs were prepared in same way using same stress degradation condition as described in section 3.4.1.4 to develop chiral stability indicating assay method.

3.8.1.5 Preparation of synthetic mixture

Synthetic mixture was prepared using same formula as described in section 3.4.1.5 for assay and stress degradation study of formulation.

3.8.1.6 Method Development

Selection of detection wavelength

Solution of 50 μ g/ml of PDM was prepared in water and scanned in the UV region of 200-400 nm. The spectrum was recorded and shown in figure 3.73 (a). The UV spectrum of PDM and its chiral degradation related impurities were extracted in PDA from 200-400 nm and is shown in figure 3.73 (b). The wavelength of 215 nm was chosen for estimation since, PDM and DPs show sufficient absorbance at this wavelength.

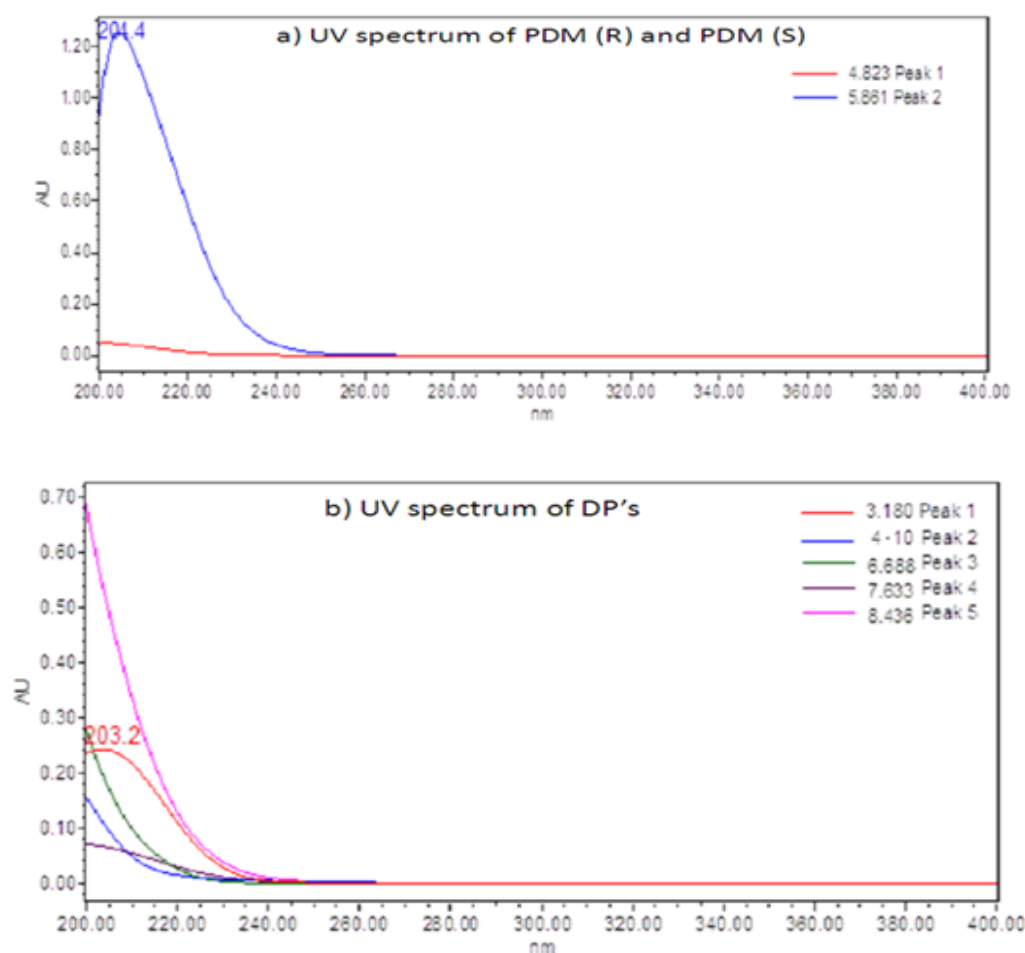


Figure 3.73: UV spectra extracted from PDA a) PDM (R) and (S) b) chiral DPs

The effects of different chromatographic variables such as composition, pH and flow rate of mobile phase, column oven temperature were studied to optimize the chromatographic method. The chromatograms obtained were recorded and the chromatographic parameters such as resolution, asymmetric factor, and theoretical plates were calculated to optimize the chromatographic conditions.

3.8.1.7 Method Validation

The developed method was validated as per ICH Q2(R1) guideline.

3.8.1.8 LC-MS/MS Study of PDM, DP-2 and their enantiomers

LC-MS/MS study was conducted to identify the enantiomeric peaks of PDM, DP-2 and their enantiomers.

3.8.1.9 Application of developed HPLC method

The developed SIAM was applied for the analysis of PDM in synthetic mixture. Stress degradation was carried out in synthetic mixture and % degradation was calculated as described in 3.4.2.5 and 3.4.2.6.

3.8.2 RESULTS AND DISCUSSION

3.8.2.1 Selection and Optimization of suitable chromatographic conditions

The conditions that gave the best resolution, theoretical plate and peak symmetry were selected for analysis. The results of some of these trials are presented in Table 3.44.

Table 3.44: Optimization of chromatographic conditions

Mobile phase	flow rate ml/min	PDM		
		Rt (min)	Asymmetry	
Column – Lichrocart CHIRADEX RP (150mm X 4.6mm i.d., 5μ particle size)				
Water: Methanol	70:30	1	No peak up to 20 min	
Water: ACN	70:30	1	No peak up to 18 min	
MeOH: 0.1 M Ammonium Formate Buffer (pH 3 adjusted with GAA)	70:30	1	3.290	1.927
MeOH: 0.1 M Ammonium Formate Buffer (pH 3.5 adjusted with GAA)	70:30	1	4.157	2.57
MeOH: 0.1 M Ammonium Acetate Buffer (pH 3 adjusted with GAA)	70:30	1	3.43	1.527
MeOH: 0.1 M Ammonium Acetate Buffer (pH 4 adjusted with GAA)	70:30	1	3.6	2.44

MeOH: 0.1 M Ammonium Acetate Buffer (pH 4.5 adjusted with GAA)	70:30	1	3.00	2.04
MeOH: 0.1 M Ammonium Acetate Buffer (pH 5.0 adjusted with GAA)	70:30	1	3.17	1.32
MeOH: 0.1 M Ammonium Acetate Buffer (pH 5.8 adjusted with GAA)	70:30	1	3.27	1.02
MeOH: 0.05 M Ammonium Acetate Buffer (pH 5.8 adjusted with GAA)	70:30	1	6.53	1.52
MeOH: 0.15 M Ammonium Acetate Buffer (pH 5.8 adjusted with GAA)	70:30	1	3.03	0.84
MeOH: 0.1 M Ammonium Acetate Buffer (pH 5.8 adjusted with GAA)	80:20	1	4.42	1.00
MeOH: 0.1 M Ammonium Acetate Buffer (pH 5.8 adjusted with GAA)	90:10	1	5.05	0.98
MeOH: 0.1 M Ammonium Acetate Buffer (pH 5.8 adjusted with GAA)	80:20	0.8	4.86	0.90

To analyze PDM along with its possible degradation products, reverse phase chiral separation in combination with PDA detector was optimized, developed and validated because besides determination of PDM enantiomer, determination of possible enantiomer of degradation products is as important as quantification of PDM in pharmaceutical formulations. To optimize the HPLC parameters, several mobile phase compositions with different flow rate and pH were tried. The studies suggested that a mobile phase containing ammonium acetate at acidic pH value might favor the peak shape of PDM, its enantiomer and DPs on column to achieve a reasonable resolution and retention but too acidic pH distorted the peak shape and increased the tailing. Temperature did not have much effect on resolution, peak symmetry and theoretical plates, hence it was kept ambient. A composition of MeOH: 10 mM Ammonium Acetate buffer (pH adjusted to 5.8 with GAA)

at flow rate of 0.8 ml/min showed good peak symmetry at ambient temperature. A satisfactory separation and peak symmetry for DPs were also obtained with same mobile phase. So the quantitation was achieved using this mobile phase based on peak area, with UV detection at 215 nm. The chromatogram of PDM along with its enantiomer and PDM spiked with isolated DP-2 is shown in figure 3.74 and 3.75. Three different and resolved peaks of DP-2 were observed and were labeled DP-2(e1), DP-2(e2) and DP-2(e3).

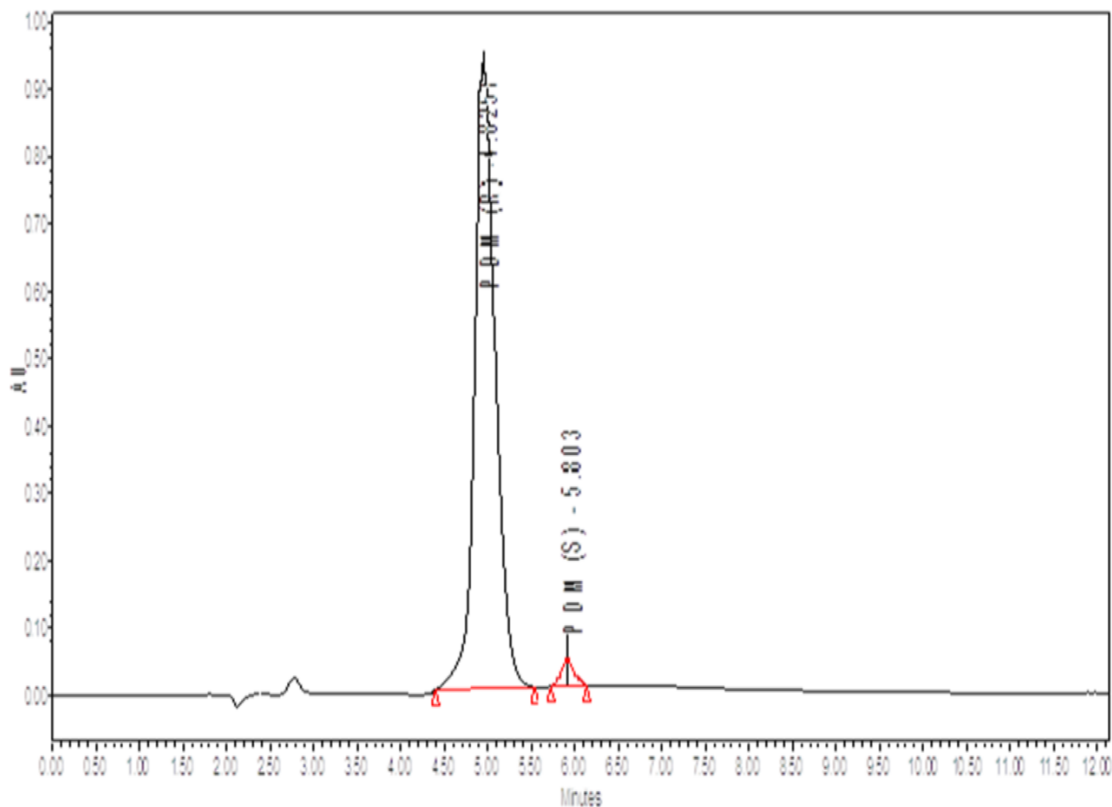


Figure 3.74: Chromatogram of PDM and its enantiomer

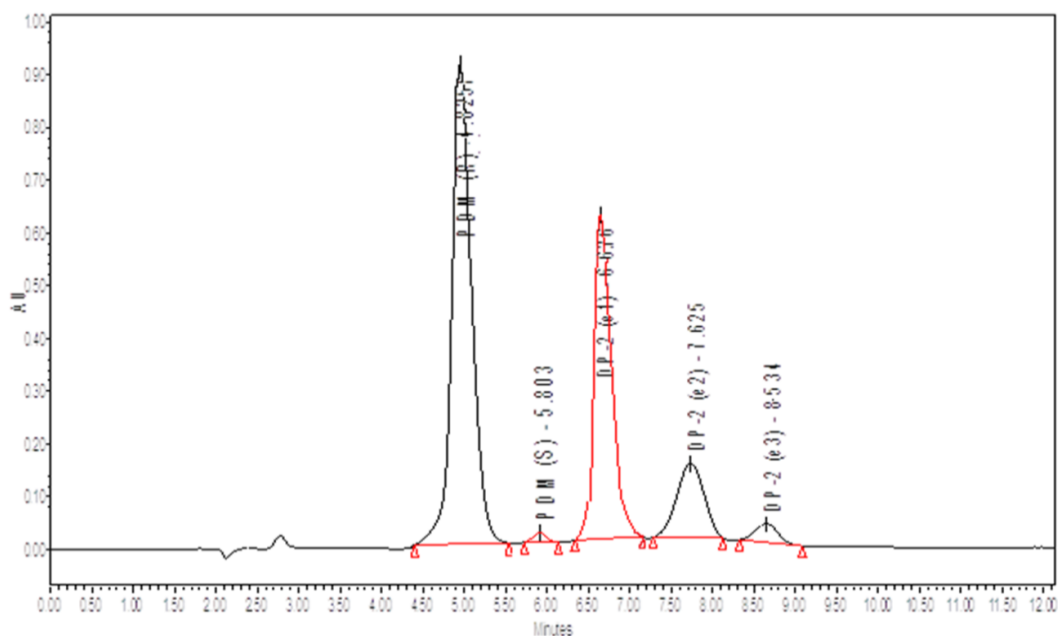


Figure 3.75: PDM enantiomers spiked with DP-2

3.8.2.2 Method Validation

3.8.2.2.1 Linearity and Range

To study linearity of the method five different concentrations were selected and the calibration curve was constructed with respect to R-PDM and was linear over the concentration range of 50-250 µg/ml. The correlation co-efficient was 0.9989 with regression equation $y = 23066x + 180512$. The overlain chromatogram and calibration curve is shown in figure 3.76. The linearity data is shown in table 3.45.

Table 3.45: Linearity data for PDM (R-enantiomer)

S.No.	Conc.(µg/ml)	PDM (R enantiomer)
		Peak Area (mV.s) (Mean±%RSD)
1	50	1397155±0.1407
2	100	2389671±0.7973
3	150	3655832±0.4305
4	200	4724476±1.3870
5	250	935.764±0.0156

* Average of three determinants

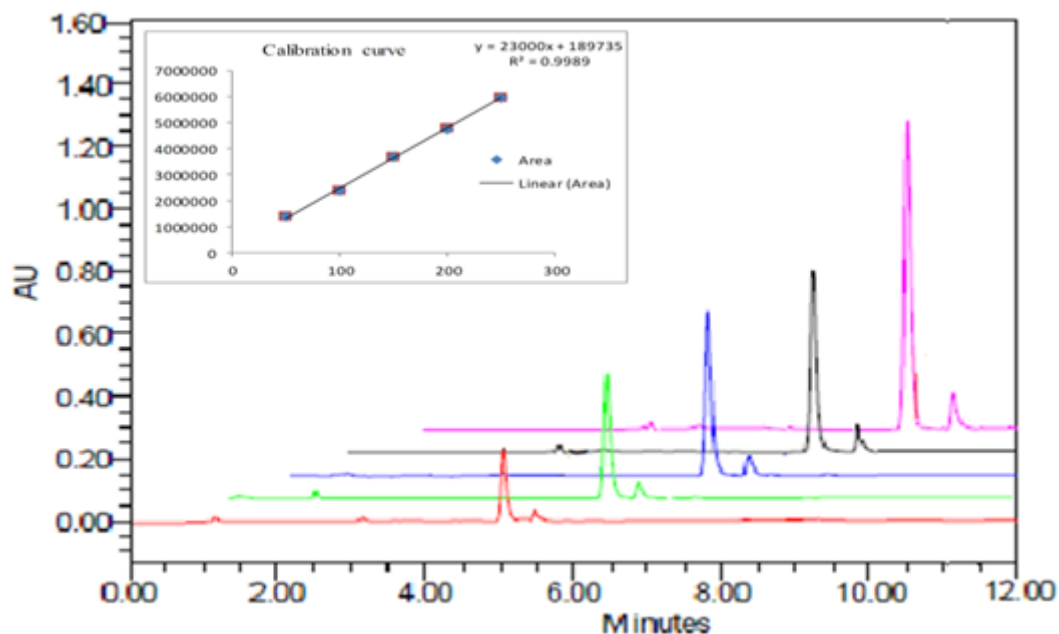


Figure 3.76: Overlain chromatogram of PDM (R) and PDM (S) and calibration curve

3.8.2.2.2 Precision

For intra-day precision (table 3.46) the experiment was repeated 3 times in a day and for inter-day (table 3.47) precision on 3 different days. The average % RSD of both intra-day and inter-day measurements were found to be 0.5303 and 0.9422 respectively. The low value of %RSD obtained confirms the precision of the method.

Table 3.46: Intra-day precision for estimation of PDM (R)

S. No ($\mu\text{g/ml}$)	Peak Area (mV.s)			MEAN	%RSD
	Set 1	Set 2	Set 3		
50	1391987	1397042	1407400	1398810	0.5616
100	2368021	2389041	2377972	2378345	0.4421
150	3640582	3667206	3668061	3658616	0.4270
200	4699894	4746705	4769039	4738546	0.7446
250	5996930	5990994	5944905	5977610	0.4764
Average %RSD					0.5303

Table 3.47: Inter-day precision for estimation of PDM

S. No (µg/ml)	Peak Area(mV.s)			MEAN	%RSD
	Set 1	Set 2	Set 3		
50	1402920	1397195	1379392	1393169	0.8807
100	2359183	2409017	2392007	2386736	1.0613
150	3633061	3706175	3668204	3669147	0.9965
200	4752047	4773091	4690814	4738651	0.9020
250	5917450	5991455	5892037	5933647	0.8704
Average %RSD					0.9422

3.8.2.2.3 LOD and LOQ

The LOD and LOQ were found to be 1.2072 and 3.6583.

3.8.2.2.4 Accuracy

Accuracy of the method was confirmed by recovery study from laboratory prepared synthetic mixture at 3 level of standard addition (80 %, 100% and 120 %). The results are shown in table 3.48. Low SD and recovery greater than 99%, justifies the accuracy of the developed method.

Table 3.48: Recovery study from synthetic mixture

Excess drug added to analyte (%)	Theoretical Content (µg/ml)	*Amount Found (µg/ml)	Recovery (%) ± S.D.
0	100	99.85	99.855±0.1895
80	180	179.82	99.907±0.0890
100	200	199.78	99.894± 0.0633
120	220	219.55	99.797±0.0424

*Average of three determinants.

3.8.2.2.5 Robustness

For robustness study few parameters were deliberately varied, these are variation of mobile phase composition, flow rate and pH of buffer. The low average value of % RSD for determination of PDM less than 2% revealed the robustness of the developed method (Table 3.49).

Table 3.49: Robustness of HPLC method

Factor	Level	Retention time
Mobile Phase composition (Ratio of MeOH)		
18	-0.1	5.83
20	0	4.805
22	0.1	3.98
Mean \pm % RSD		4.871 \pm 0.1902
Flow Rate		
0.7	-0.1	5.04
0.8	0	4.8
0.8	0.1	4.47
Mean \pm % RSD		4.77 \pm 0.0599
pH		
5.6	-0.2	5.58
5.8	0	4.813
6.0	0.2	3.85
Mean \pm % RSD		4.74 \pm 0.1825

3.8.2.2.6 Selectivity

The results of stress degradation studies indicated a high degree of selectivity of developed method for PDM. Slight variation was found in degradation of PDM for API and synthetic mixture.

3.8.2.2.7 Specificity

As illustrated in figure 3.77 the developed method is specific since complete separation of PDM, its enantiomer and other DPs were observed. The peaks of PDM, its enantiomer and

DPs were well resolved. The resolutions for the separating peaks were more than 1.5 from the nearest resolving peak. Also it was justified by peak purity plots as shown in figure 3.78. The peak purity studies of resolved peaks are presented in table 3.52.

3.8.2.2.8 Stability in sample solutions

Solutions containing different concentrations of PDM and stressed samples were prepared from standard stock solution and stored at ambient temperature for 24hrs. No additional peaks were found in chromatogram indicating the stability of PDM in the sample solution.

3.8.2.2.9 System Suitability Parameters (SST)

System suitability testing was carried out on six replicate solutions that were freshly prepared (n=6). SST parameters obtained with 20 μ L injection volumes are summarized in table 3.50.

Table 3.50: System Suitability Parameters for PDM

Parameter	Data Obtained	
	PDM (R)	PDM (S)
Retention time (min) \pm SD	4.82 \pm 0.0357	5.80 \pm 0.0432
Theoretical plate \pm SD	6288 \pm 13.31	4592 \pm 79.33
Tailing factor \pm SD	1.04 \pm 0.0449	1.18 \pm 0.0843
Resolution \pm SD	2.66 \pm 0.1383	

*Data shown is the average of six replicates. SD= Standard Deviation

3.8.2.3 Applicability of the developed SIAM method

The Developed SIAM method was successfully applied for the estimation of PDM (R) and PDM (S) in its Synthetic mixture. The chromatograms of stressed samples are shown in figure 3.77.

3.8.2.4 Stress Degradation Study

Stress degradation was performed in the same way as discussed in section 3.3.10.4 and given in table 3.51. The optimized chromatograms of stressed samples in mixture of degradants are illustrated in figure 3.77 and their peak purity plots are shown in figure 3.78. The chromatograms of individual stress conditions are shown in figure 3.79. There was slight difference in % degradation of PDM in RP C-18 and chiral column, some peaks of DPs were not retained in chiral column.

Table 3.51: Summary of stress degradation of PDM bulk drug and synthetic mixture

Stressor Type	Stressor Conc.	Time	DPs formed with Rt	% Deg (API)	% Deg (Formulation)
Acid degradation	0.8 N, 80 ⁰ C	3 Hrs	DP-3(3.24), DP-2e1(6.57), DP-2e2(7.62), DP-2e3(8.48)	44.65	44.10
Base degradation	0.1 N, 80 ⁰ C	3 Hrs	DP-3(3.44), DP-2e1(6.63), DP-2e2(7.54), DP-2e3(8.55)	60.32	60.00
Neutral degradation	80 ⁰ C	6 Hrs	---	9.15	8.91
Oxidative degradation	0.01 %, 80 ⁰ C	1.5 Hrs	DP-8(4.25)	73.98	73.54
Photolytic degradation	--	21 days	DP-2e1(6.66), DP-2e2(7.54)	7.94	7.40
Dry Heat induced degradation	80 ⁰ C	21 days	No degradation		
Thermal Humidity induced degradation	40 ⁰ C±2 ⁰ C and 75 ⁰ C±5 ⁰ C	21 days	--	4.11	4.00

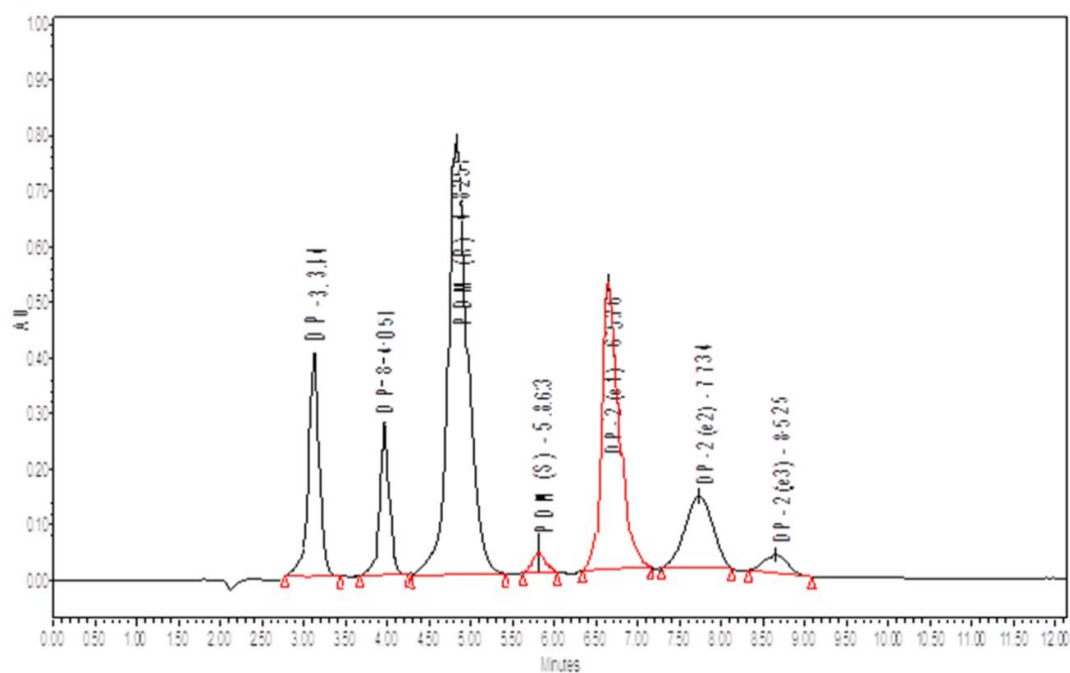
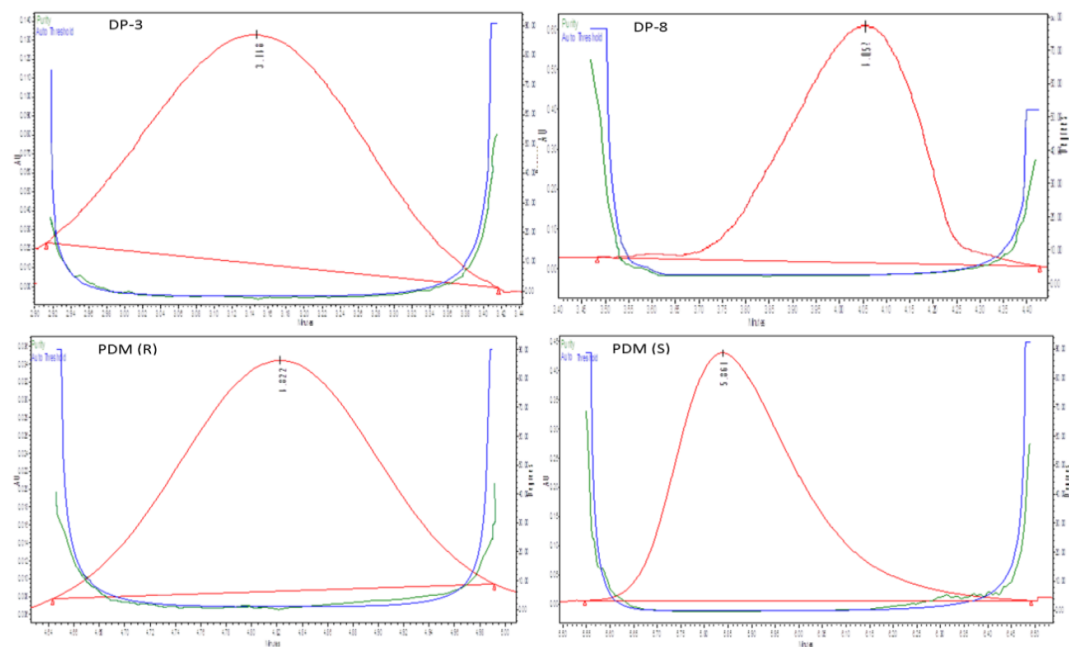


Figure 3.77: Chromatogram of mixture of degradants



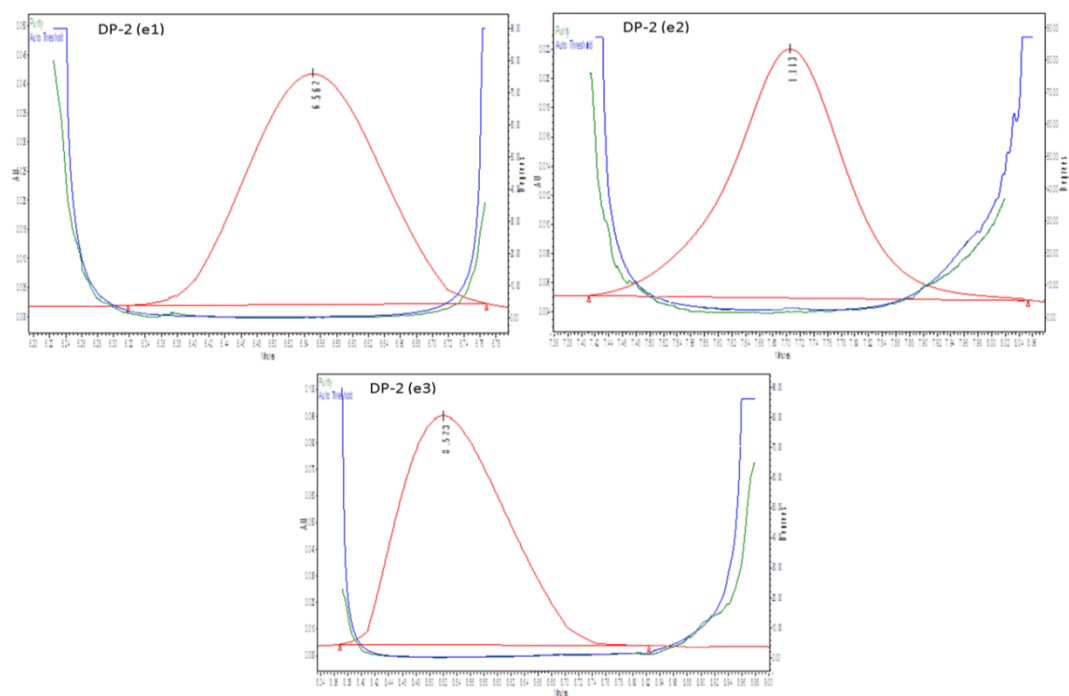
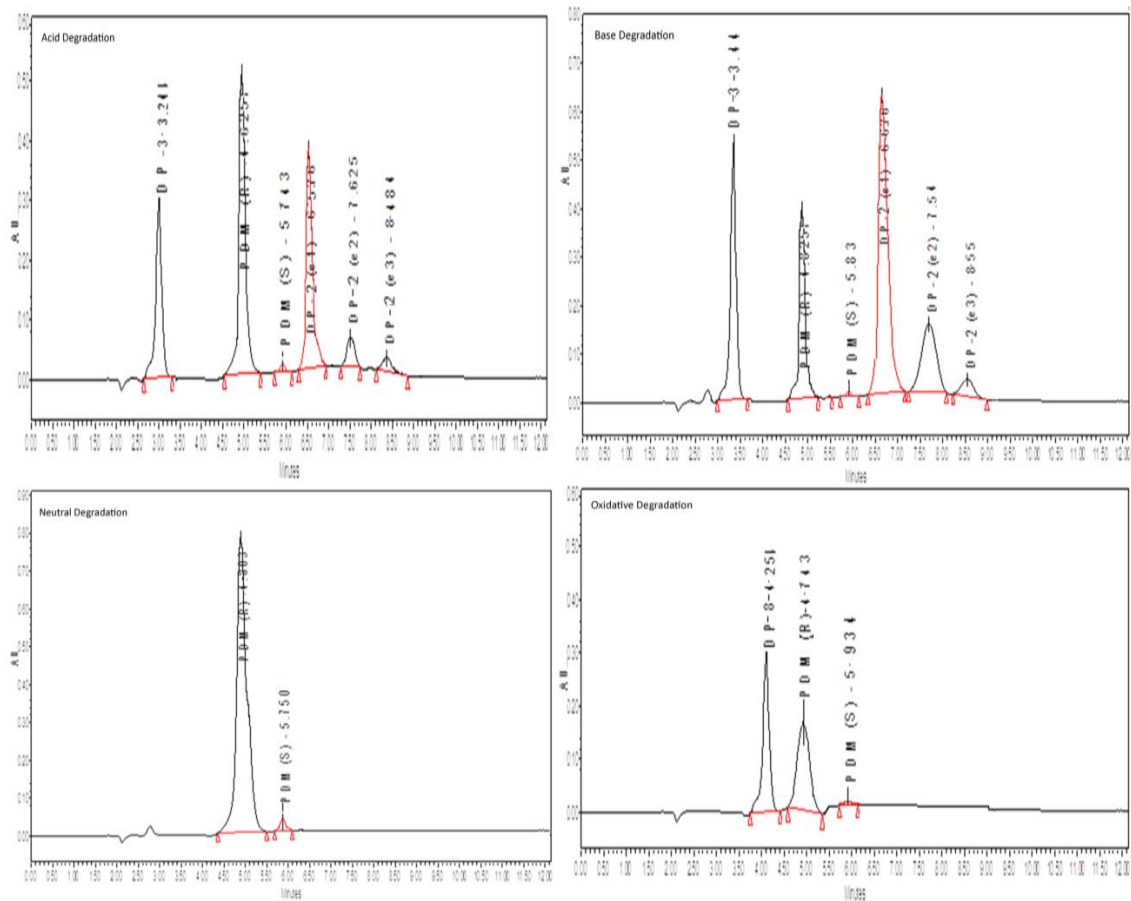


Figure 3.78: Peak purity plots of resolved peaks

Table 3.52: Peak purity studies of resolved peaks

S. No.	Peaks	Rt	Peak purity Angle	Peak purity Threshold
1.	DP-3	3.14	0.337	0.810
2.	DP-8	4.051	1.209	1.286
3.	PDM (R)	4.82	0.098	0.307
4.	PDM (S)	5.86	1.552	1.747
5.	DP-2 (e1)	6.57	0.257	0.301
6.	DP-2 (e2)	7.73	0.951	1.070
7.	DP-2 (e3)	8.52	1.550	1.589



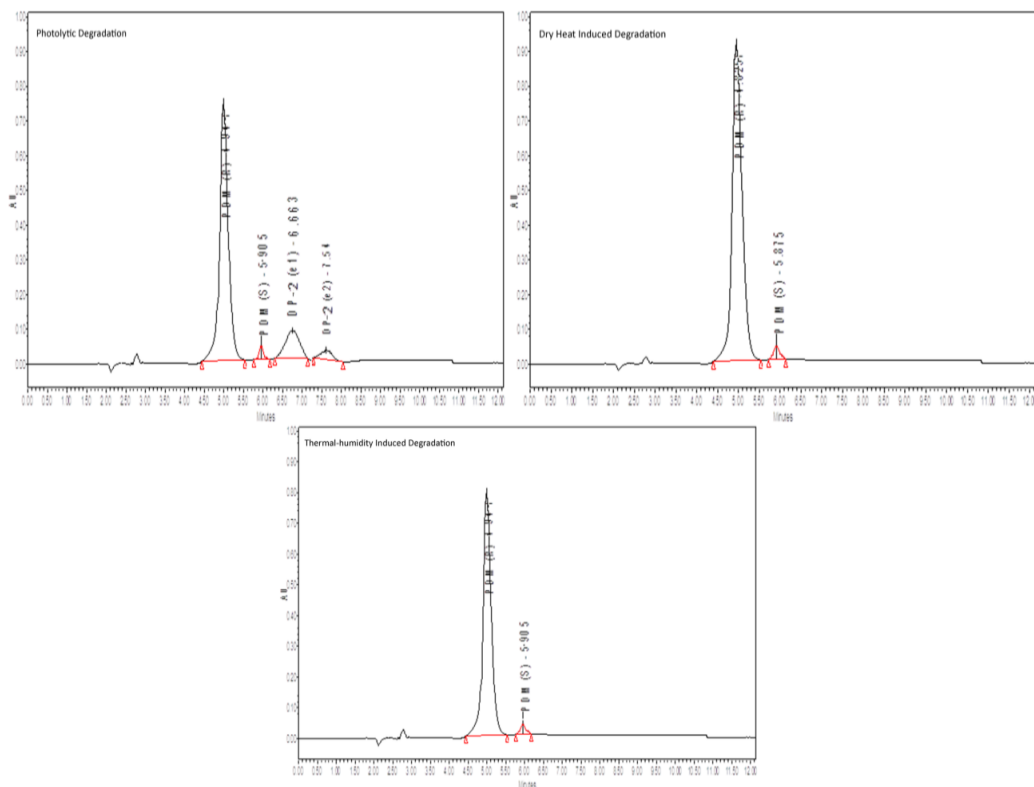


Figure 3.79: Chromatograms of different stress degradation condition

3.8.2.5 LC-MS/MS study of PDM, DP-2 and their enantiomers

The LC-MS/MS was taken on positive ESI mode (figure 3.80 and 3.81). The mass spectrum of PDM at retention time 4.86 confirms the structure of PDM as it has same molecular weight (MW) and fragmentation pattern. The ESI-MS spectrum at Rt 5.86 did not show protonated ions, but the $[M+H]^+$ ion at 245 confirms the enantiomeric forms of PDM. Similarly the ESI-MS spectrum of DP-2 (e1) at Rt 6.57 shows the abundant $[M+H]^+$ ion at m/z 263. The spectrum of DP-2 showed most abundant product ions at m/z 245 corresponds to PDM or DP-4 and it also include abundant product ions at m/z 148. Protonated ions could not be generated for the ESI-MS spectra of DP-2 (e2) and DP-2 (e3) at Rt 7.73 and 8.5, but the $[M+H]^+$ ion at 263 confirms the enantiomeric forms of DP-2.

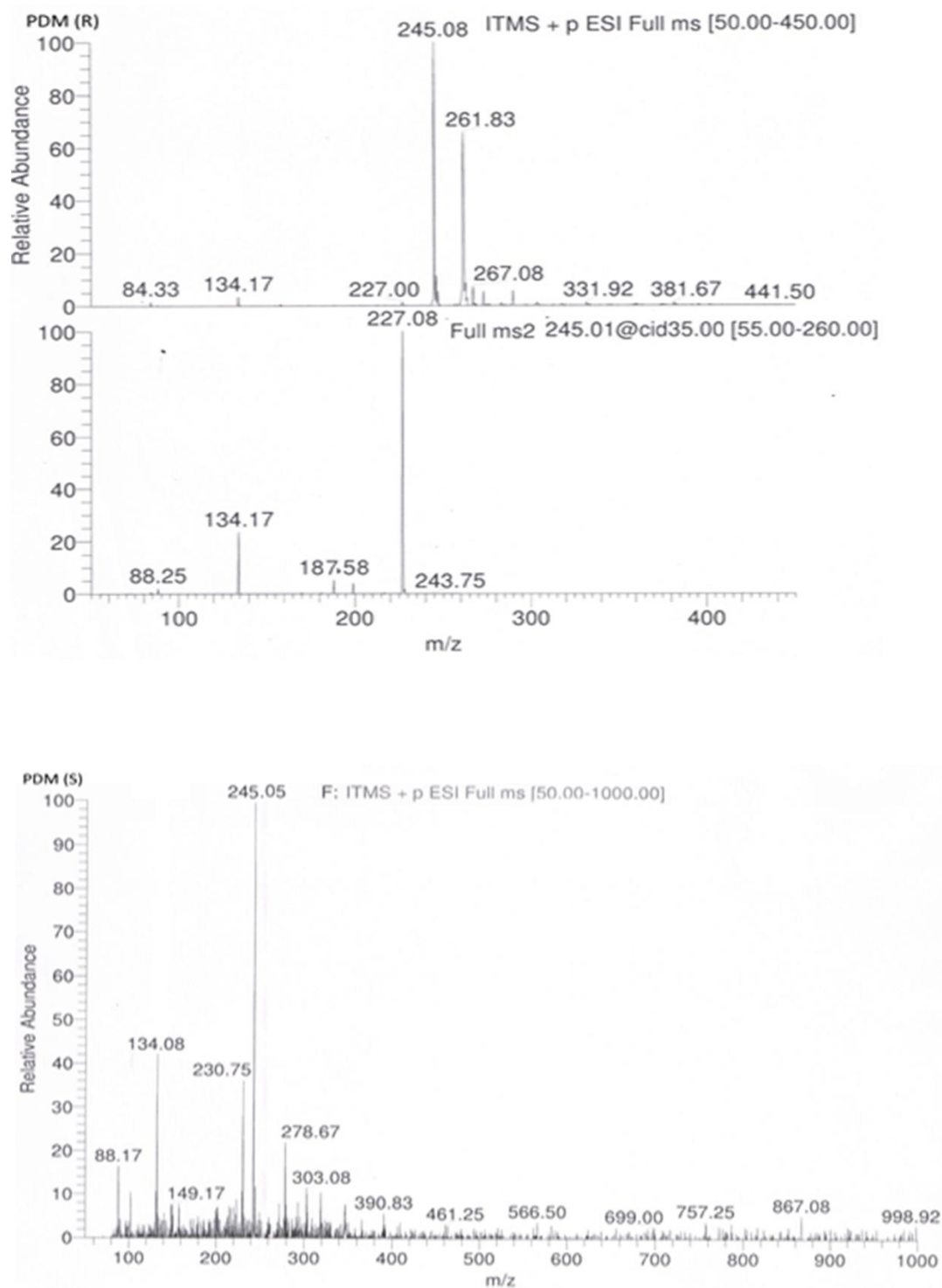
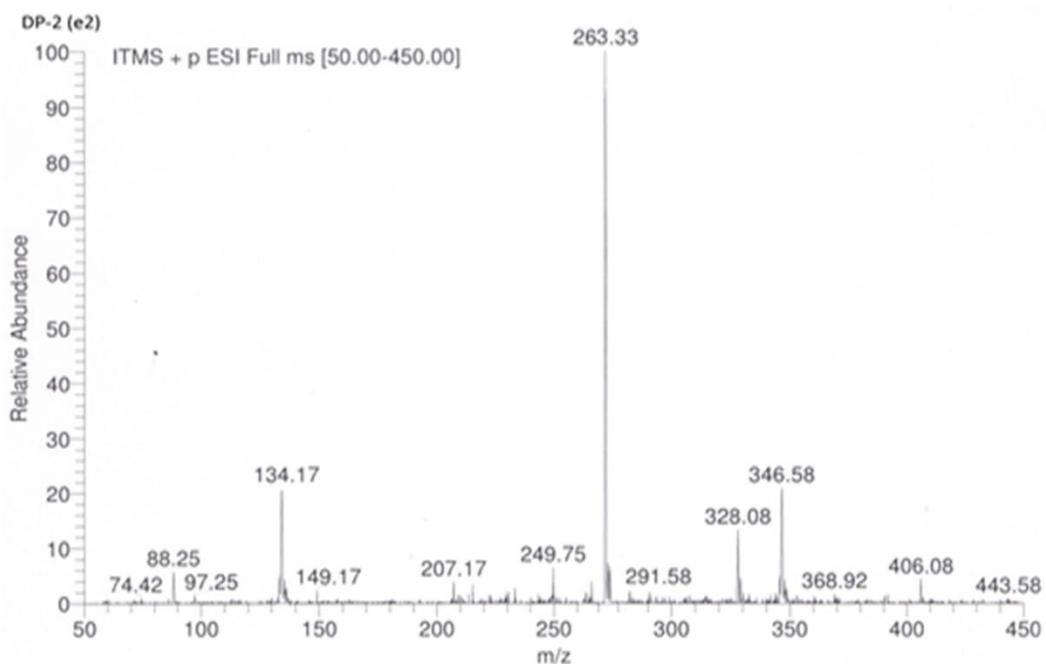
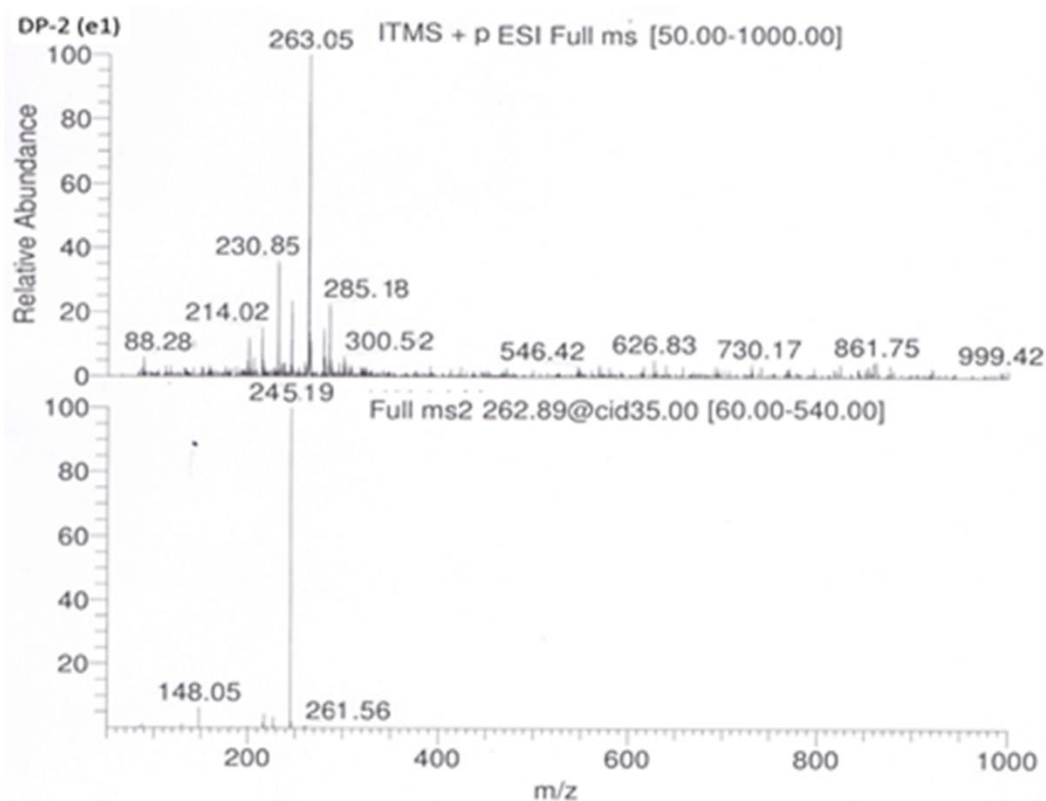


Figure 3.80: ESI-MS/MS spectra of PDM and its enantiomers



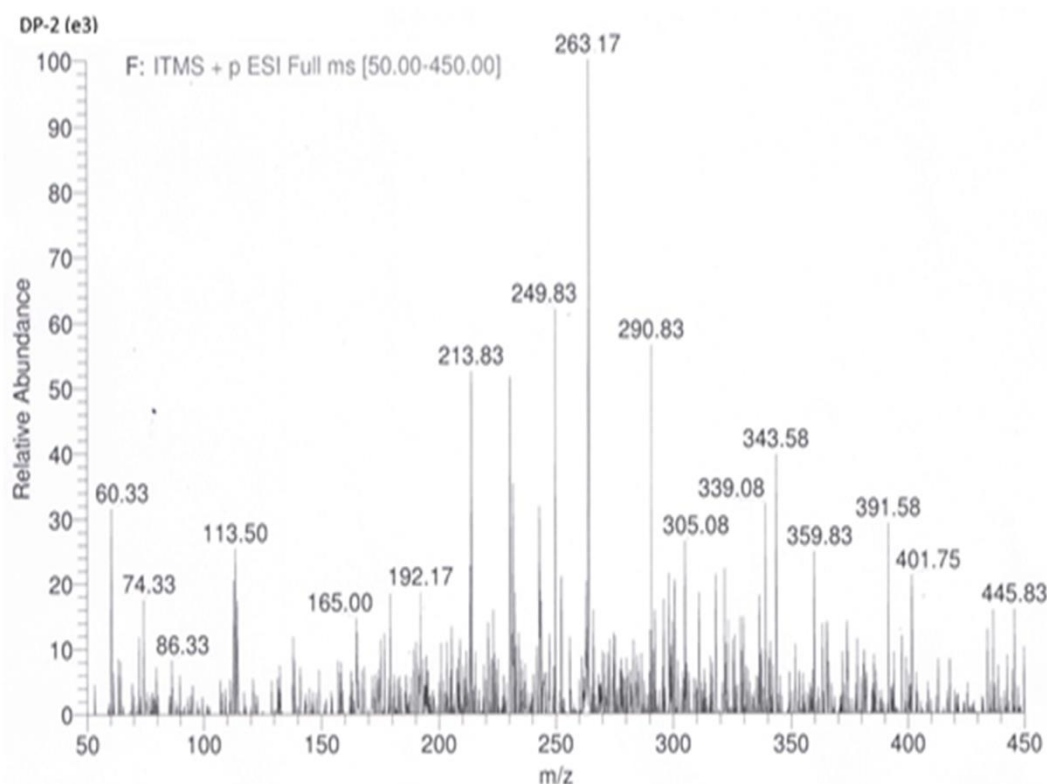


Figure 3.81: ESI-MS/MS spectra of DP-2 and its enantiomers

3.9 CONCLUSION

Impurity profiling and degradation study of Pidotimod was carried out systematically with LC-PDA detection and LC-MS/MS throughout the profiling. Total six impurities including degradation related and process related or inherent impurity was observed in LC-PDA while 11 impurities were observed in LC/MS-MS. Two degradation products formed under stress degradation were identified as inherent/process related impurities INH-1 and INH-2. Two Major degradation products DP-2 and DP-4 (based on HPLC peak area) formed from acid degradation condition were isolated and successfully characterized by IR, LC-MS/MS and NMR studies. The chemical names of isolated degradation product at Rt 3.3 (DP-2) is 3,8-Dihydroxy-tetrahydro-bisthiazolo[3,4,4a,3',4'-d]pyrazine-5,10-dione and at Rt 12.2 (DP-4) is 3-[3,5,6,7,8,8a-hexahydro-5,8-dioxo-1H-thiazolo[3,4a]pyrazine-6-yl]propionic acid. The isolated degradation product DP-4 was known. The molecular structure of DP-2 showed the presence of two chiral centers. Also Pidotimod is chiral in nature hence chiral

separation of the enantiomeric forms of Pidotimod and isolated DP-2 was successfully carried out in Lichrocart CHIRADEX chiral column and were further confirmed by mass study. The structures and degradation pathway of degradation products were proposed on the basis of LC-MS/MS analysis. Pidotimod was susceptible to almost all stress degradation condition hence degradation kinetic study was carried out for acid, base, neutral, oxidative and photolytic degradation by RP-HPLC method. Acid, base and oxidative degradation followed linear first order degradation kinetic while neutral and photolytic degradation followed linear zero order degradation kinetic. A QbD based stability indicating HPLC method for Pidotimod was developed and validated as per ICH Q2(R1) guideline and total error approach. Also stability indicating chiral HPLC method was developed for estimation of chiral impurities of Pidotimod and validated. Both the methods are simple, sensitive, accurate and fast which is applicable to assay and estimation of impurities and degradation products of Pidotimod in bulk drug and formulation.

3.10 REFERENCES

1. Zuccotti GV, Mameli C. Pidotimod: the past and the present. *International Journal of Pediatrics*. 2013;39(75):2-3.
2. Mailland F, Coppi G, Signorelli G. Pidotimod. *Drugs of the Future*. 1991;16:1096.
3. Mameli C, Pasinato A, Picca M, Bedogni G, Pisanelli S, Zuccotti GV, et al. Pidotimod for the prevention of acute respiratory infections in healthy children entering into daycare: a double blind randomized placebo-controlled study. *Pharmacological Research*. 2015;97:79-83.
4. Giagulli C, Noerder M, Avolio M, Becker PD, Fiorentini S, Guzman CA, et al. Pidotimod promotes functional maturation of dendritic cells and displays adjuvant properties at the nasal mucosa level. *International immunopharmacology*. 2009;9(12):1366-73.
5. Masihi K. Immunomodulatory agents for prophylaxis and therapy of infections. *International journal of antimicrobial agents*. 2000;14(3):181-91.

6. Riboldi P, Gerosa M, Meroni P. Pidotimod: a reappraisal. *International journal of immunopathology and pharmacology*. 2009;22(2):255-62.
7. Ye L, Luo Y, Ou X. Improvement of the Synthesis Technology of Pidotimod. *China Pharmacy*. 2012;1:017.
8. Parfitt K, Martindale W. The complete drug reference. Pharmaceutical Press, London. 1999;31:51.
9. Brayfield A. Martindale: The Complete Drug Reference. Drug Monographs 2014.
10. Auteri A, Pasqui A, Bruni F, Saletti M, Di Renzo M, Bova G. Effect of Pidotimod, a new immunostimulating agent, on some aspects of immune response. In vitro study. *Pharmacological Research*. 1992;26:196-7.
11. Migliorati G, D'adamio L, Coppi G, Nicoletti I, Riccardi C. Pidotimod stimulates natural killer cell activity and inhibits thymocyte cell death. *Immunopharmacology and immunotoxicology*. 1992;14(4):737-48.
12. Migliorati G, Nicoletti I, Riccardi C. Immunomodulating activity of pidotimod. *Arzneimittel-Forschung*. 1994;44(12A):1421-4.
13. Carta S, Silvestri M, Rossi GA. Modulation of airway epithelial cell functions by Pidotimod: NF-kB cytoplasmatic expression and its nuclear translocation are associated with an increased TLR-2 expression. *Italian Journal of Pediatrics*. 2013;39(8):29.
14. Coppi G, Barchielli M. Simple high-performance liquid chromatographic method for the determination of PGT/1A, a new immunostimulating drug, in biological fluids. *Journal of Chromatography B: Biomedical Sciences and Applications*. 1991;563(2):385-91.
15. Zhang Y, Xiong Z, Qin F, Lu S, Liu W, Li F. High-performance liquid chromatography–tandem mass spectrometry for the determination of pidotimod in human plasma and its application to a pharmacokinetic study. *Journal of Chromatography B*. 2009;877(24):2566-70.
16. Lou H, Ruan Z, Jiang B. Quantitative determination of pidotimod in human plasma by liquid chromatography tandem mass spectrometry: application to a bioequivalence study. *Arzneimittel-Forschung*. 2012;62(2):99-104.

17. Chen H, Shen M, Chen L. HILIC-MS-MS for the Quantification of Pidotimod in Human Plasma. *Chromatographia*. 2011;73(7-8):767-73.
18. Huang J-H, Huang X-H, Wang K, Li J-C, Xie X-F, Shen C-L, et al. Bioequivalence evaluation of two formulations of pidotimod using a limited sampling strategy. *Biomedicine and Pharmacotherapy*. 2013;67(6):475-80.
19. Jun-fang L. Determination of Residual Organic Solvents in Pidotimod Tablets by GC. *China Pharmacy*. 2009;31:028.
20. Magni A, Signorelli G, Bocchiola G. Synthesis and preliminary pharmacological evaluation of pidotimod, its enantiomer, diastereomers and carboxamido derivatives. *Arzneimittel-Forschung*. 1994;44(12A):1402-4.
21. Crimella T, Orlandi R, Bocchiola G, Anders U, Stradi R. Analytical and chemical profile of pidotimod. *Arzneimittel-Forschung*. 1994;44(12A):1405-10.
22. Zhang LX, Yin T-J, Shen W-Y, Cheng Y, Jiang C-P, Zhang X-Y. enantiomeric separation of Pidotimod by HPLC using chiral stationary phase. *Journal of china pharmaceutical university*. 2011;42(3):238-41.
23. Dou X, Su X, Wang Y, Chen Y, Shen W. Studies on Pidotimod Enantiomers With Chiralpak-IA: Crystal Structure, Thermodynamic Parameters and Molecular Docking. *Chirality*. 2015;27(11):802-8.
24. Caruso A, Fiorentini S. Pidotimod for use in the treatment of inflammation-associated diseases. Google Patents WO2015036370A1; 2015.
25. Schweitzer M, Pohl M, Hanna-Brown M, Nethercote P, Borman P, Hansen G, et al. Implications and opportunities of applying QbD principles to analytical measurements. *Pharmaceutical Technology*. 2010;34(2).
26. Ermer J. A lifecycle concept for pharmaceutical analysis. *European Pharmaceutical Review*. 2011;16(3):16-24.
27. Rozet E, Lebrun P, Hubert P, Debrus B, Boulanger B. Design spaces for analytical methods. *Trends In Analytical Chemistry*. 2013;42:157-67.
28. Guideline ICH Q8 (2R) Pharmaceutical development., in: International Conference on harmonization, IFPMA, Geneva (Switzerland) August, 2009.

29. Vogt FG, Kord AS. Development of quality-by-design analytical methods. *Journal of pharmaceutical sciences*. 2011;100(3):797-812.
30. Ishikawa K. What is total quality control? The Japanese way.(Translated by David J. Lu). Englewood Cliffs. NJ: Prentice-Hall; 1985.
31. Zhou L, Socha JM, Vogt FG, Chen S, Kord AS. A systematic method development strategy for water determinations in drug substance using Karl Fischer titrations. *American Pharmaceutical Review*. 2010;13(1):74-84.
32. Panda SS, Beg S, Kumar R, Bera VV, Singh P. Analytical Quality-By-Design Compliant Ultrafast Liquid Chromatographic Method for Determination of Paliperidone in Extended Release Tablet Dosage Form. *Journal of Bioanalysis and Biomedicine*. 2015;7(4):116.
33. Guideline ICH Q2B Validation of Analytical Procedures: methodology. European Agency for the Evaluation of Medicinal Products, International Commission on Harmonisation, London (CPMP/ICH/281/95). 1996.
34. Guideline IEC 17025: General Requirements for the Competence of Calibration and Testing Laboratories International Organization for Standardization. Geneva. 1999.
35. Hubert P, Nguyen-Huu JJ, Boulanger B, Chapuzet E, Cohen N, Compagnon P-A, et al. Harmonization of strategies for the validation of quantitative analytical procedures: A SFSTP proposal: Part IV. Examples of application. *Journal of pharmaceutical and biomedical analysis*. 2008;48(3):760-71.